5-2013

Control of Solar Photovoltaic (PhV) Power Generation In Grid-connected and Islanded Microgrids

Sarina Adhikari
sadhikar@utk.edu

To the Graduate Council:

I am submitting herewith a dissertation written by Sarina Adhikari entitled "Control of Solar Photovoltaic (PhV) Power Generation In Grid-connected and Islanded Microgrids." I have examined the final electronic copy of this dissertation for form and content and recommend that it be accepted in partial fulfillment of the requirements for the degree of Doctor of Philosophy, with a major in Electrical Engineering.

Fangxing Li, Major Professor

We have read this dissertation and recommend its acceptance:

Leon M. Tolbert, Yilu Liu, Yanfei Gao

Accepted for the Council:

Carolyn R. Hodges

Vice Provost and Dean of the Graduate School

(Original signatures are on file with official student records.)

Control of Solar Photovoltaic (PhV) Power Generation In Grid-connected and Islanded Microgrids

A Dissertation Presented for the
Doctor of Philosophy
Degree
The University of Tennessee, Knoxville

Sarina Adhikari
May 2013

DEDICATION

I dedicate my work to my beloved parents, loving husband, dearest son, my wonderful brother, caring sister-in-law and my entire family.

ACKNOWLEDGEMENTS

First and the foremost, I would like to express my gratitude to my advisor, Dr. Fangxing (Fran) Li for his continuous guidance and support for this and all other research and course works during my PhD study at the University of Tennessee.

I am very thankful to Dr. Yan Xu of Oak Ridge National Laboratory (ORNL) who always provided me with very valuable suggestions for my research. I would also like to express my sincere thanks to Mr. D. Tom Rizy of ORNL for being so supportive to my work and in providing kind advices in the course of my research. I would really like to appreciate and acknowledge very friendly, yet useful advices from Dr. Huijuan Li of ORNL while conducting all the research works during my PhD study.

My heartfelt thanks go to Dr. Leon M. Tolbert, Dr. Yilu Liu and Dr. Yanfei Gao for their time and effort in serving as the members of my dissertation committee.

I would also like to thank all the professors and friends of CURENT center for their encouragement in my research.

I would also like to acknowledge the US Department of Energy (DOE) and ORNL in providing financial support to conduct this and other research during my study period.

Last but not the least, I would like to thank my beloved parents, my wonderful husband, my loving brother and sister in law for their unconditional love and moral support without which I would not be able to conduct my research smoothly.

ABSTRACT

With the ever increasing electricity demand, fast depletion of fossil fuel and the growing trend towards renewable energy resources, the integration of green distributed energy resources (DERs) such as solar photovoltaic (PhV) generation and wind power in the utility grid is gaining high popularity in the present years. The capability of these modular generators needs to be harnessed properly in order to achieve the maximum benefit out of such integrated systems. Most DERs are connected to the utility grid or microgrids with the help of power electronics interface. They are capable of producing both active and reactive power with the proper control of the inverter interface.

This dissertation focuses on examination of the capability of the renewable energy based DERs, such as solar PhV array and battery energy storage system (BESS) in providing voltage support in grid connected low-voltage microgrids and both voltage and frequency support in islanded microgrids. In addition, active and reactive (a.k.a. nonactive) power control capability of the PhV generators to supply the local loads assigned by the microgrid central operator in grid connected mode is also investigated. The control methods are developed by using a Proportional and Integral (PI) controller. A new method of Maximum Power Point Tracking (MPPT) of solar array including the MPPT at solar PhV array side and a new control method of transferring this MPP power to the inverter side insuring the DC voltage stability by using the concept of power balance at various conversion stages is proposed and studied. The dissertation also proposes a new coordinated control method for voltage and frequency regulation of microgrid with solar

PhV generator operating at MPP and backed up by battery energy storage systems. A coordinated active and reactive power control for solar PhV generator with MPPT control and battery storage is also proposed and investigated. Various case studies are presented to validate the proposed methods. The simulation results clearly prove the effectiveness of the proposed control methods.

TABLE OF CONTENTS

LIST OF TABLES

LIST OF FIGURES

CHAPTER 1

INTRODUCTION AND GENERAL INFORMATION

1.1 BACKGROUND

The traditional power systems comprise of the generation system which consists of large central power stations, the transmission and sub-transmission systems to deliver power from remote generating plants to the site near load centers, and the distribution system to serve all end users such as residential, commercial and industrial loads. The power flow is hence, unidirectional, that is, from generation to the load centers.

With the ever increasing demand of electricity that has been raising important power system operational issues like voltage and frequency instability, the integration of distributed energy resources into the modern power systems have become very popular since last few decades. The fast depletion of fossil fuel reserves and environmental concerns have provided greater incentive to integrate renewable energy based DERs like solar, wind and biomass in modern power systems.

DERs are usually connected to the power distribution system. DER includes distributed generation (DG), energy storage systems and demand response. DGs are defined as small generators located in close proximity of load with the size ranging from 10kW- 10MW [1, 2]. Though the standard definition of DG has not been agreed upon far, there are

several other definitions proposed by several power system working groups and institutions like CIGRE[1], IEEE[2], IEA[3], etc [3].

DERs, in general, provide several technical, operational, environmental and market benefits when integrated to the modern deregulated power systems and hence, these act as important driving factors for their integration into the grid and in formation of micro-grid [4-6]. DERs can act as an emergency back-up power supply for the customers where the power outages cannot be accepted such as hospitals and manufacturing industries. Due to the flexibility of DERs in terms of size, expandability, they have wider range of operation either as a base load generator or a peak shaving generators. This helps to cope with the rapid electricity price fluctuations when they participate in the deregulated market environment. Power system reliability and power quality are of major concerns when it comes to the liberalized power market. DERs can help in maintaining the power quality problems like voltage sags and harmonics and also in maintaining reliability of the system by preventing voltage collapse events and system outages by injecting needed amount of real and reactive power whenever the system has a deficit. While DERs can greatly assist in maintaining the power system reliability by providing backup power promptly whenever and wherever needed, some of the DER technologies like Combined Heat and Power (CHP) employed most commonly in simple cycle gas turbine can utilize the excess heat which would have been wasted otherwise and can increase the efficiency

[1]International Council of Large Electric Systems
[2] Institute of Electrical and Electronic Engineers
[3] International Energy Agency

of the system by up to 70-80% [6]. Due to the fact that DERs, especially, renewable energy based ones use cleaner energy sources like wind and solar power, they are capable of producing emission-free power and hence, have greater incentive to be considered due to the low carbon footprint. Similarly, as all the DERs are modular and have capability of providing local power to the consumers, these small generators help in cutting off the transmission losses which indirectly reduces the cost and emission associated with generating equal amount of power from the central generation. And, with efficient technologies like CHP, the amount of energy consumed from the grid is greatly reduced and hence, the resulting emissions [3, 6]. Despite all the mentioned benefits from the DERs, several technical and economic challenges imposed with the increased integration of the DERs to the grid and even when used in the micro-grid mode cannot be denied [1]-[7].

1.2 DIFFERENT DER TECHNOLOGIES

This section summarizes various types of DER technologies which are commonly used in the grid connected and islanded micro-grids [8-11]. DERs can be broadly categorized as: Non-Renewable energy-based and Renewable energy based. Combustion engine generator sets, Gas turbines and micro-turbines are few examples of non-renewable based DERs and wind power, solar generation, fuel cells, etc. are few examples of renewable energy based DERs.

Non-Renewable energy-Based DERs

Combustion Engine Generator Sets:

Combustion Engine Generator Sets are the units consisting of an internal combustion piston-driven engine, an electrical generator along with necessary controls to make it operate in a stand-alone or grid connected modes. This kind of sets can be of variable sizes and can be used with variety of fuel types like biogas, methane, natural gas, propane, gasoline, diesel and landfill gas. The needed mechanical power for the electrical generator is provided by the engine which also helps in maintaining the desired operating frequency in proportion to the rate of engine rotation. A truck type diesel engine running at 1800 rpm can help to generate a 60 Hz output voltage waveform from a four pole synchronous generator in the United States [10]. The electrical generator can be either induction or synchronous generator. However, since induction generator is not capable of controlling voltage or reactive power independently, it cannot be used in a stand-alone application. For this reason, synchronous generator is more popular.

Combustion/Gas Turbines:

Gas turbines comprises of a compressor, combustor and the turbine generator set which converts the rotational energy to electrical power. The energy is extracted from the flow of combustion gas. A simple cycle gas turbine is a mature technology which works on the Brayton or Joule thermodynamic cycle. The atmospheric air is compressed, and this compressed air is heated through fuel combustion. The heated air-fuel mixture is allowed to expand through a turbine which will drive the generator. The gas turbines have

relatively higher efficiency and slight increase in efficiency of one of the system components impacts the overall efficiency by a very high percentage. It has been observed that only small change in system components have increased the efficiency of gas turbines from 25% in the 1950s to 35-38% in the present models[8].

Micro-turbines:

Micro-turbines work on the same principle as combustion turbines and can be driven by all the fuel types mentioned for gas turbines. These are small, lightweight and single-staged gas turbines with the size ranging from 25 to 500 kW[10]. Micro-turbines work based on a Brayton cycle engine using air and fuel mixture to produce the shaft power. The electrical generator could be either a Permanent Magnet Synchronous Generator or a gear reducer with a synchronous generator. Micro-tubine comprises of several components: compressor; combustion chamber, turbine, generator, recuperator and power controller. Recuperator or heat exchanger is a vital component of a micro-turbine which helps in recovering waste heat from the turbine exhaust and using it to preheat the compressed air. With the use of 85% effective recuperator, the overall efficiency of a micro-turbine can be increased from 15-17% to as high as 33% [8]. The micro-turbine operates in a high frequency range of 49 kHz to 96 kHz under load and hence, the generator output frequency ranges from 1500-4000 Hz[10]. In order to connect the micro-turbine/generator output to the grid, AC-DC-AC conversion is required so that the generator output is 60 Hz AC.

Micro-turbines can be operated in grid-connected as well as stand-alone mode with the capability of parallel connection. In the grid connected mode, the generator is operated like motor by importing power from the grid, thus, helping in rotation of the micro-turbine shaft initially. The voltage and frequency control functions are disabled in this mode, however, in stand- alone operation mode, it is required to control voltage and frequency independently.

Renewable energy-Based DERs

Solar Photovoltaic (PhV[4]) systems:

Solar Photovoltaic (PhV) systems utilize freely available sunlight to produce electricity through the use of semiconductor based solar cells. A PhV cell acts as a photo diode such that as the light energy in the form of photon strikes the cell surface, an electron-hole pairs are generated in the p-n junction of the cell. This phenomenon generates electricity which is dependent on the cell surface area, ambient temperature and incident irradiation. As the voltage produced by the solar cell itself is only limited to the forward drop across the p-n junction, the voltage and current produced by a single cell are very small in magnitude. Hence, a large number of solar cells are connected in series and parallel to obtain panels and series and parallel connections of large number of panels produce

[4] Solar Photovoltaic Generator in this dissertation is abbreviated as (PhV) unlike the commonly used abbreviation (PV) in order to avoid confusion with active power and voltage (P-V) control that is proposed in the work.

arrays. Most PhV arrays are provided with the maximum power point tracking (MPPT) systems so that the arrays can always generate maximum power output with the changing irradiance conditions. Since the output of the solar array is DC power, a utility interactive power inverter that converts the generated DC voltage to AC voltage of desired frequency should be used in order to connect the arrays to the grid. Hence, proper control of inverters can allow solar PhV to inject both real and reactive power to the grid. This capability of solar PhV is investigated in this dissertation.

Solar PhV offers many advantages like minimum environmental impact; sustainability because of the solar energy as fuel; reduction in customers' electricity bill due to zero fuel cost; long lifetime spanning 20-25 years and silent operation. Despite this fact, higher installation cost and low energy efficiency still act as major challenges to this technology. Due to the intermittency of the solar energy supply, most of the solar PhV installations have energy storage in the form of batteries in order to store the excess power during the time of excessive irradiance and use this power whenever needed.

Wind Energy Conversion Systems (WECS):

Wind Energy Conversion Systems (WECS) converts the kinetic energy of the wind into the electrical energy output. The main component of WECS is the wind turbine. The gust of wind rotates the wind turbine fan and a shaft which drives the electrical generator. Induction generators are mainly used in WECS. The wind turbine is connected to the generator through a gear box which helps in transformation of slow rotational speed at

the turbine side to a high rotational speed at the generator side. The main components of the wind turbine are the tower, rotor and the nacelle which houses the generator and the transmission arrangements. Wind turbine configuration can be either vertical axis or horizontal axis. The wind turbine output depends on various factors like wind speed, shape and size of the turbine. There is a dynamic fluctuation of the torque output of wind turbine due to the variations in wind speed. This variation in torque can cause the dynamic variation in output power and flicker in the output voltage. The constant speed wind turbine is not capable of tackling these variations but the variable speed wind turbine have a capability of providing smoother power output with stable bus voltage.

Fuel Cells:

Fuel cells convert the chemical energy from the fuel to the electricity through the chemical processes. Unlike batteries, which store the chemical energy, fuel cells convert this energy to usable form of electricity. Hence, these do not require re-charging and are capable of producing continuous supply of electricity so far as fuel and oxidant are provided[8]. Fuel cells can be operated using various hydrogen rich fuels like natural gas, biogas, methanol, ethanol, Kerosene, propane, etc. Due to the property of high reactivity that minimizes the use of expensive catalysts, hydrogen is considered as the most suitable fuel for the cell and oxygen is considered the most suitable oxidant due to its abundance in the atmosphere.

Fuel cells comprise up of a positive electrode or anode and negative electrode or cathode and an electrolyte. Fuel is supplied at anode and an oxidant at the cathode terminal of the cell. The oxidation of the fuel at anode and reduction of the cathode results in the electrochemical reaction and hence, the flow of electrons from anode to cathode through the external circuit if the cell is connected to the load.

Fuel cells can be stacked in series and parallel combination to build the generation plants with increased power capacity. However, in order to connect it to the grid, a power converter is needed to convert DC to AC of desired frequency. Fuel cells are light weight, compact, quiet in operation and modular with the size varying from few hundreds watts to a few megawatts.

Biomass and biofuels:

Biomass is the material extracted from plants and animals and their residues and wastes. This organic, carbon based material reacts with oxygen during metabolic processes and combustion to produce heat. This heat, if exceeds $400^{o}C$, can be used to generate electricity with steam turbine and generator sets. Biomass can be transformed to biofuels like methane, liquid ethanol, methyl esters, etc. through the biochemical processes. Biomass and biofuels are considered to be renewable resources only if the growth of biomass can cope with the use.

Small Hydro-power:

The hydroelectricity is generated through the turbine rotated with the help of high pressure falling water that drives the generator. Hydro-power is the most established and popular renewable resource for electricity production. Hydro-turbines have a very quick response for power generation and hence, are capable of handling the load variations. These can be directly connected to the grid.

1.3 INTEGRATION OF DERs TO THE GRID

The high penetration of DERs in the modern electricity grid can provide many potential positive benefits through their integration but they can have many negative impacts on the network if power output and voltage at the Point of common coupling (PCC) is not properly regulated through controls. The challenge mainly lies in the integration of varying renewable sources like Solar PhV and Wind Energy Conversion systems. DERs can provide a technical relief to the grid in the form of reduced losses, reduced network flows and voltage drops, however, there are several negative impacts due to high penetration of these variable resources which include voltage swell, voltage fluctuations, reverse power flow, changes in power factor, injection of unwanted harmonics, frequency regulation issues, fault currents and grounding issues and unintentional islanding[12]. Integration of DERs to the grid should ensure that there are not any negative impacts in safety, reliability and quality of the supply after the interconnection is done.

Several components are involved in the integration of DER to the utility grid. The system components of the DER interconnection system comprise of the following:

- DERs, power conversion and conditioning system which includes inverters and transformers, control of DERs, and, power distribution networks which comprise of panel board containing switches, circuit breakers, fuses, overcurrent devices, etc;
- Local Electric Power System (EPS) consisting of facility wiring, panel boards and components at the point of common coupling (PCC);
- Local EPS protective relaying, transfer switch for transferring conductor connections from one power source to another;
- paralleling switchgear to synchronize the DER/s operation with the area EPS, the PCC which is a point of connection of the local EPS with the area EPS;
- Meter which measures the usage of electric energy;
- Area EPS which is the local utility's distribution system or a grid;
- Area EPS protective relaying; Dispatching and controlling equipment required to interface with DERs and manage them; and
- The device which monitors and meters various functions supplied by the DERs.

Figure 1 shows the schematic of the various components involved while interconnecting DERs to the grid [13].

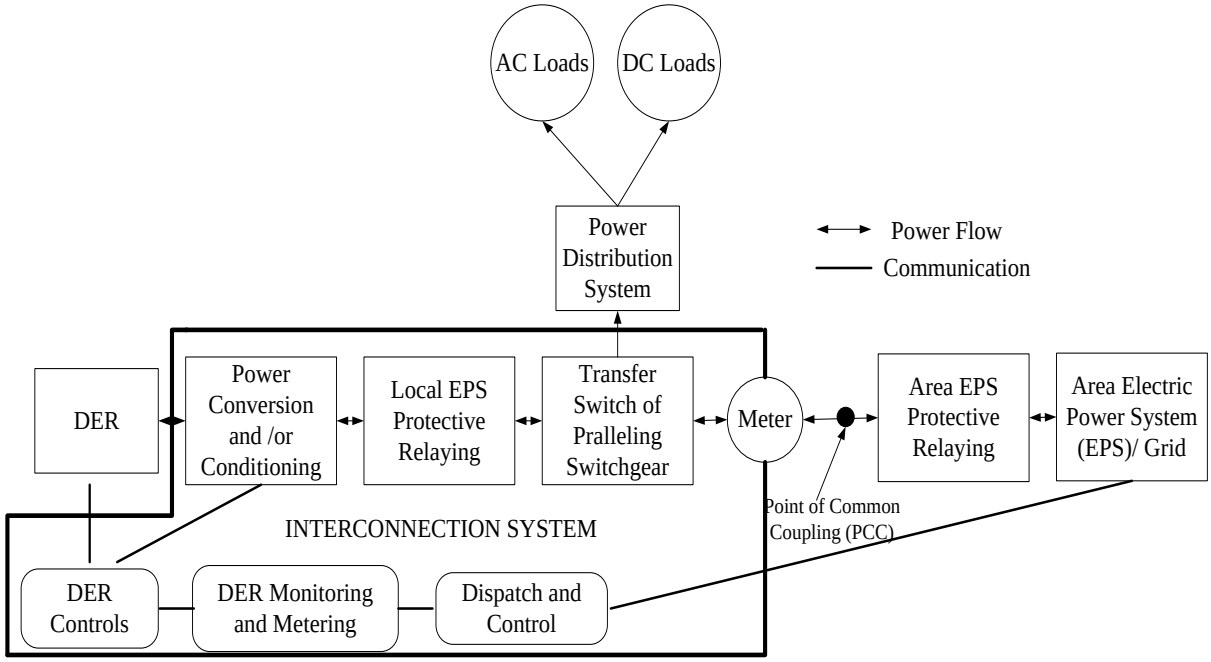

Figure 1. Interconnection System Schematic[13].

Depending on whether the DER being considered for interconnections is a reciprocating engine/combustion turbine, a micro-turbine, the PhV systems, a fuel cell or the wind generator, the electricity generated by DERs can be either directly connected to the area EPS through synchronous or induction generators or indirectly connected with the help of static power electronics (PE) interface. These interconnection interfaces are briefly described as follows [13, 14]:

Synchronous Generator:

The DERs like reciprocating engine/combustion turbine and micro-turbines can be connected directly to the area EPS with the help of synchronous machine interface. Synchronous generator is the most common type of electric generator used in power systems. These are the rotating machines which convert the mechanical power applied from the turbine shaft to the electrical power. The generator runs at a speed known as synchronous speed which is in synchronism with the frequency of the connected area EPS. The separately excited synchronous generators are even capable of supplying sustained fault current in all operating conditions. As compared to the induction generator, synchronous generator needs more complex controls so as to synchronize it to the area EPS as well as to control the field excitation. However, these generators provide a capability of controlling power factor through the adjustment of DC excitation current and can also provide power to the local EPS in the event of outage in area EPS.

Induction Generator:

Just like synchronous generator, induction generator is capable of converting mechanical power to the electrical power and have similar stator configuration, however, the rotor construction in induction generator is different than synchronous generator, in that, it does not require external dc field current for operation. Induction generator operates at a speed determined by prime mover which is slightly higher than synchronous speed and requires an external source to provide the magnetizing current required for the magnetic field between stator and rotor. Out of the two induction generator rotor configurations:

cage rotor and round rotor, cage rotor has special advantage over synchronous machine counterpart in having lower cost, however, induction generator draws reactive power from the area EPS and hence, there should be a provision of VARs either from capacitors or PE based VAR generators when induction generators are used. Induction generators are applicable with the DERs in which the prime-mover power is not stable such as wind and small hydro applications.

Power Electronics (PE) Interfaces:

There are many DER technologies which generate the electrical voltage not in synchronism to the area EPS or a grid. The DERs like solar PhV, fuel cell, storage batteries generate DC power while wind generators produce the AC power from an asynchronous generator and micro-turbines produce a non-synchronous AC. Hence, an intermediate power conversion stage is required in order to convert the power generated by the DERs to the power with voltage magnitude and frequency in synchronism to the area EPS. The power electronics (PE) interface performs this task of connecting any type of DER systems to the grid by providing either DC - AC or AC - DC - AC conversion stages.

PE interfaces comprise of semiconductor switches with the devices like thyristors, diodes, insulated gate Bipolar transistors (IGBTs) or MOSFETs with proper control of the duty cycle of these switches to fulfill the desired objectives. With the proper controls of switches, PE interfaces may be capable of regulating voltage at the point of

connection, and providing desired amount of real and reactive power to the system[15, 16]. Similarly, with the help of proper control of PE interfaces, DERs can be capable of providing various types of ancillary service required for the proper operation of the power systems. These include spinning and non-spinning reserves, harmonic compensation, load following, back-up supply, peak shaving and network stability[17, 18]. Another very important advantage of the PE devices is a very fast response, hence, they are capable of responding to the fault and power quality disturbances within the sub-cycle range [14]. Similarly, the PE devices are solid state static devices which have higher efficiency and reliability as compared to the rotating machine based converters[13]. Figure 2 gives an overall picture of all the interconnection interfaces described above.

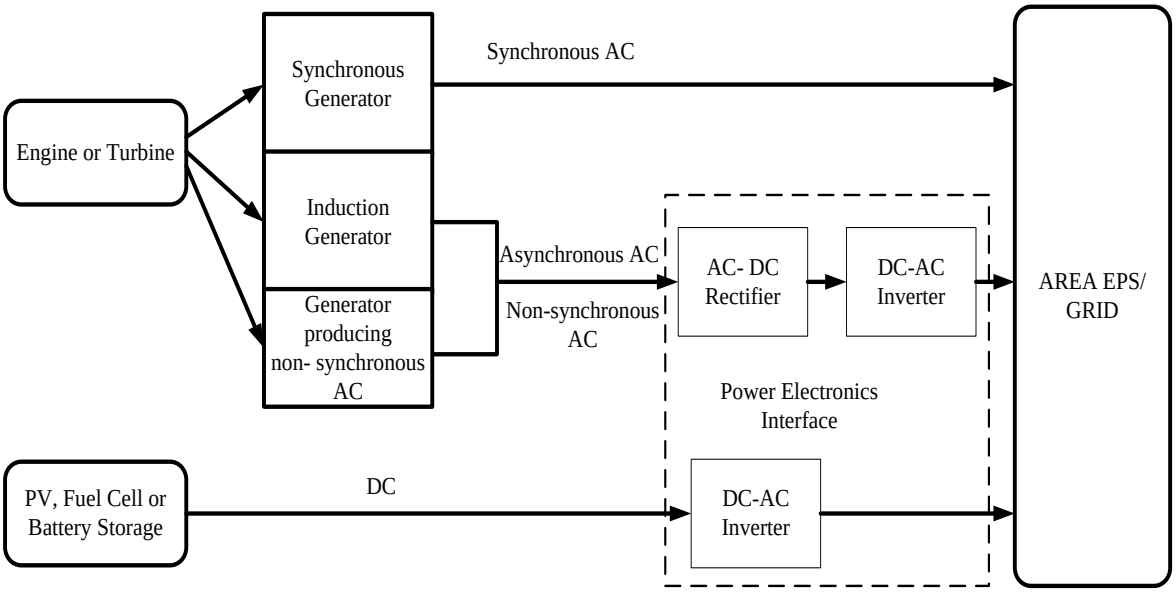

Figure 2. Interconnection interfaces of DERs to the grid.

The Institute of Electrical and Electronics Engineers (IEEE) has set a standard for the interconnection of DERs to the utility grid. The standard is termed as IEEE 1547, Standard for Interconnecting Distributed Resources with Electric Power Systems[10]. This standard has set uniform criteria for the interconnected DERs in terms of safety, operation, performance, testing and maintenance. The main focus of this standard is DERs connected to the radial distribution feeder. IEEE 1547 provides technical requirements for the safety and reliability of DER interconnection which includes voltage regulation, power monitoring, grounding, synchronization, connection to network distribution systems, back-feeds, coordinating equipment ratings, disconnecting means, abnormal operating conditions, power quality and islanding. Regarding the standards for voltage regulation, original version of IEEE 1547 does not allow

distributed generation (DG) to actively regulate the voltage at the PCC with the electric utility grid[10]. DG connection to the utility grid tends to affect the voltage profile. Also, the intermittent resources like wind and solar does not tend to coordinate with the utility efforts on voltage regulation. Similarly, large number of single phase DGs can cause voltage imbalances in a three phase systems. With these and several other issues of the interconnection of DG to the utility grid, this rule on voltage regulation has been imposed. However, with the new working group, 1547.8 formed by IEEE Standards Subcommittee 21, a recommended practice is under development which will identify the cases where local Volt/Var control is permitted especially in the case of high DER/PhV penetration.

1.4 MICROGRIDS

Microgrid is a collection of distributed generators or micro-resources, energy storage devices and loads which operate as a single and independent controllable system capable of providing both power and heat to the area of service [19]. The micro-resources that are incorporated in micro-grids comprise of small units, less than 100 kW provided with power electronics (PE) interface. Most common resources are Solar Photovoltaic (PhV), Fuel Cell (FC) or microturbines which are located close to the load centers and integrated together to produce power at the distribution voltage level. The PE interface and controls of the microresources ensure that desired power quality and energy output is maintained independently during operation. Hence, from the utility grid perspective, the microgrid is viewed as a single controllable unit capable of meeting local energy needs helping in reliability and security of the system.

Figure 3 shows a typical configuration of a microgrid[11]. Microgrid comprises mostly the resources which can produce both heat and power altogether such that overall efficiency of the system is maximized. The microsources and storage devices are connected to the feeders through the microsource controllers (MCs). Microgrid is connected to the medium voltage level utility grid at the point of common coupling (PCC) through the circuit breakers. The feeders are also supplied with several sectionalizing circuit breakers (SCBs) which help in isolating a part of the microgrid as needed. Microgrid can be operated in either grid connected or islanded modes. When connected to the grid, the operational control of voltage and frequency is done entirely by

the grid; however, microgrid still supplies the critical loads. In islanded condition, microgrid has to operate on its own independent of the grid. The operation and management in both the modes is controlled and coordinated with the help of microsource controllers (MCs) at the local level and central controller (CCs) at the global level. MC has a function of controlling the power flow and bus voltage profile of the microsource according to the load changes or any other disturbances. The CC, on the other hand, is responsible for the overall control of Microgrid operation and protection. It aids in maintaining specified bus voltages and frequency of the entire microgrid and also takes part in energy optimization for the microgrid.

The microgrid concept promotes the high penetration of modular DERs such that entire microgrid is supplied by different types of DERs by maintaining the specified operational criteria like voltage and frequency, specially, in the case of islanding. Hence, microgrid offers lots of advantages to the future grid in that it promotes the green and more efficient DERs and hence, less environmental impact and cost due to increased efficiency. Similarly, it helps in improving the power quality and reliability of the supply because of decentralization approach to match supply and demand.

Despite all the potential benefits the microgrid offers with its development, there are many challenges which need to be addressed for the successful operation of the micro grid. The most important one is the technical difficulty in managing large numbers of plug and play micro-resources and it requires a very robust communication infrastructure.

High costs of DERs and absence of operational standards also impose some challenges to its successful operation.

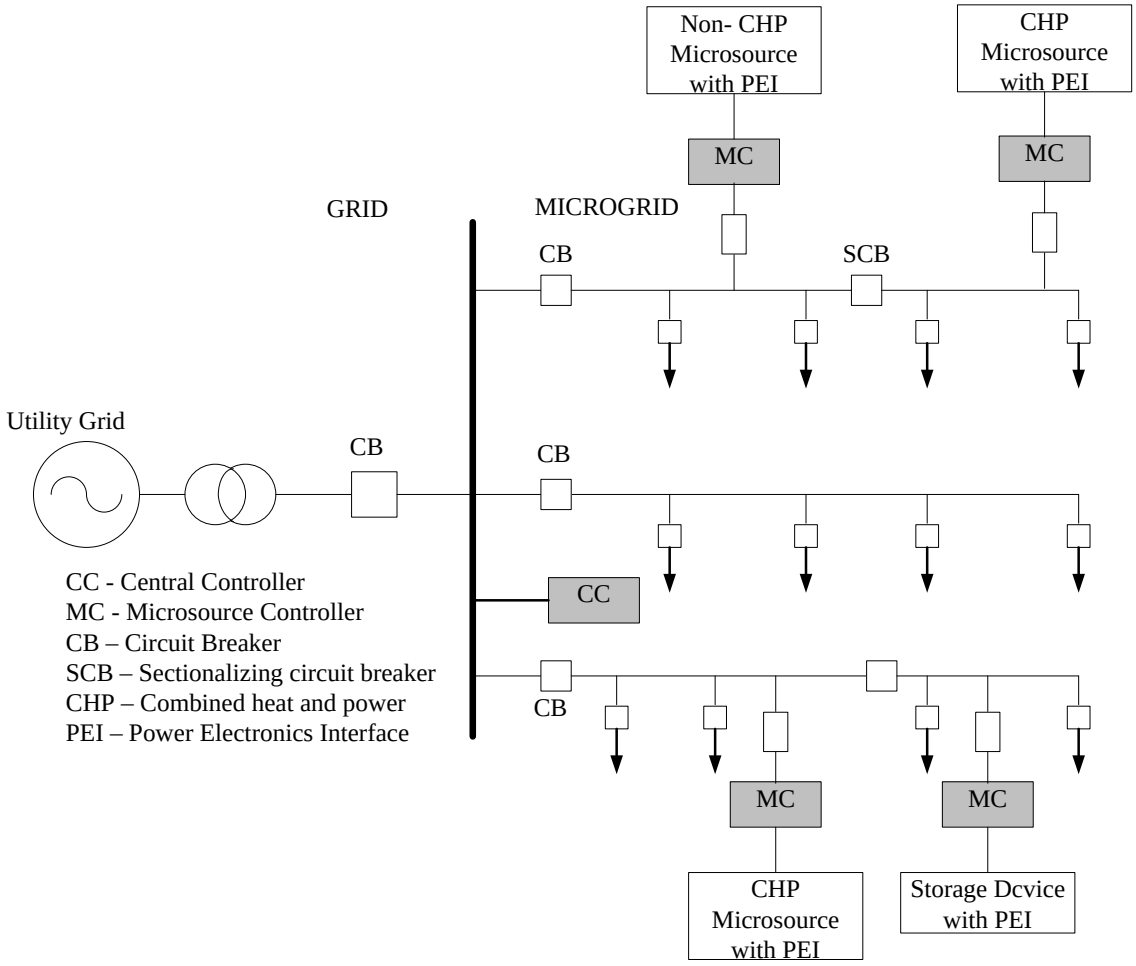

Figure 3. Typical Microgrid Configuration[11].

1.5 MOTIVATION

With the increasing environmental concerns, yet ever increasing electricity demand, the interest toward renewable based electricity generation, in present years, is the best

candidate to fulfill world's energy demand in the years to come. The world energy consumption is projected to be 30 TW by 2050 and to stabilize the atmospheric CO_2 by then, there should be a generation of 20 TW of non-CO_2 energy [20]. Hence, the renewable and sustainable resources like Solar PhV and others have to take up a major share in electricity generation in order to achieve this target. This provides a greater incentive to perform a research on integration and incorporation of Solar PhV into the modern power system. Due to the lack of transmission line capacity to cope with the increasing demand, more interest is growing towards distributed generators. DGs, in general, offer several other advantages over centralized counterpart in terms of peak shaving, high reliability, emergency backup, increased efficiency and several others. The renewable energy based DGs provide additional important advantage in terms of environmental friendliness.

According to the US Energy Information Administration (EIA), 7103 commercial and industrial DG units with a total capacity of 12.7 GW-electric was installed in 2007[6]. There is a lack of statistical data for residential sector, which might be negligible, yet with a growing trend. The DG capacity of the United States was 1.27% of the 995 GW electric capacity in 2007 which was an increase from 0.5% in 2000[6]. Figure 4 shows the present and projected future trend of electricity generation share from renewable energy based DGs. The generations from all the renewable DGs including solar PhV show the growing trend.

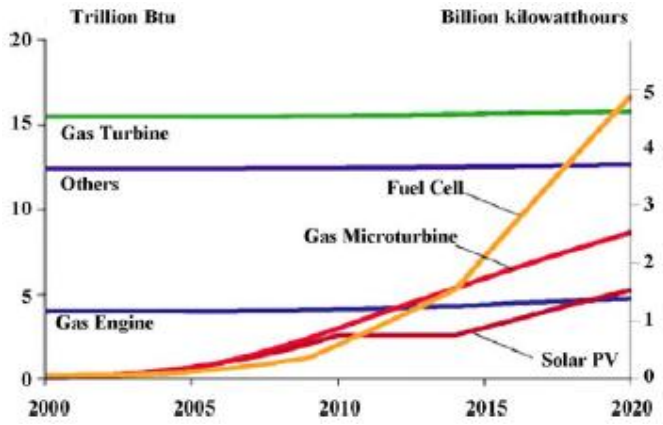

Figure 4. Projected electricity generation by selected DG sources[21].

On the other hand, voltage and frequency are two very important parameters for stable, secure and reliable operation of any power system. Voltage instability and collapse is caused due to the lack of reactive power in the system and frequency problems arise due to the imbalance between system load and generation. Insufficient reactive power source and mismatch between generation and loads due to line trip or generation outages have been reported to be main triggers for major blackouts in various parts of world in the past[22, 23]. Reactive power is best utilized for voltage control if it can be produced locally, at the point where it is needed. DERs are capable of producing VARs locally and at a faster speed. Moreover, with the proper control of PE interfaces of the DERs producing DC power like Solar PhV, controlled amount of real and reactive power can be produced. Thus, these small generators can play an active role in maintaining the voltage at the PCC within desirable range and can even contribute in maintaining system frequency at 60 Hz while participating in a micro-grid mode. Hence, it provides enough

inspiration to explore these capabilities of Solar PhV including storage even more. Furthermore, not many research works have been reported on the Solar PhV with storage being actively involved in frequency control scheme.

With large penetration of the DERs in future power systems, operation of grid in coordination with these small generators is a big challenge and micro-grid concept seems to cope with this challenge. This conglomeration of small DERs called micro-grid is capable of operating independently as well as in connection to the central grid. Hence, the control of individual participating DERs to control voltage and frequency of the micro-grid is an interesting area of research. In most of the present works, diesel generators are used for micro-grid frequency control. Hence, the performance of Solar PhV with storage to properly control voltage as well as frequency of the micro grid needs investigation. The major aim of this dissertation is thus, to scrutinize on how to effectively control voltage and frequency using Solar PhV in grid-connected as well as micro grid mode.

1.6 DISSERTATION OUTLINE

The rest of the dissertation is organized as follows:

Chapter 2 reviews all the recent and relevant works done in this area. Chapter 3 presents the proposed maximum power point tracking (MPPT) algorithm with active power and voltage (P-V) control capability of the solar PhV generators. The application of previously proposed active and non-active (P-Q) control algorithm with solar PhV generator is also presented. Chapter 4 describes the proposed coordinated voltage and

frequency (V-f) control with MPPT control and battery storage system and the application of previously proposed P-Q control algorithm also with MPPT and battery. Chapter 5 depicts major contributions from the dissertation and outlines some of the possible future direction of the work and hence, concludes the dissertation.

CHAPTER 2
LITERATURE REVIEW

This chapter presents the review of the past and on-going research findings in the area of voltage and frequency control including reactive and active power control strategies with Distributed Energy resources (DERs), in general, as applied to the micro-grids. A review of few literatures related to various methods of measurement of power system frequency is also discussed. It also presents the discussions about the research on modeling and controls of Solar Photovoltaic (PhV) in particular.

2.1 POWER SYSTEM FREQUENCY MEASUREMENT METHODS AND PROGRESSES

Unlike the measurement of bus voltage magnitude in power grids, the system frequency measurement is a critical issue. In North American interconnections, the power system frequency should be maintained in a very narrow band around 60 Hz during normal operation [24]. Hence, the measurement of the grid frequency should be very accurate and fast. Various methods have been adopted to measure the power system frequency with various levels of accuracy, speed and simplicity.

A very simple method adopted by the solid state relays in measuring the grid frequency is to detect zero crossing of the voltage waveform. But, however this method has a serious drawback of giving inaccurate results while measuring frequency of the voltage signal with distortion and noise as in this case, there will be multiple zero crossings[25]. Several

other methods have been proposed in the past to overcome a drawback of the zero crossing detection technique. These include: Discrete Fourier transform and recursive phasor computation [26], Kalman filtering technique [27] and least error squares method of estimating frequency [28], [29]. In [25], a very fast and accurate method of frequency measurement is presented using a Digital Signal Processing (DSP) based technique. Here, the digitized values of the voltage samples taken at a specified sampling rate are considered for measurement. This method is claimed to provide a correct and noise-free estimate of near nominal, nominal and off-nominal frequencies within the time span of 25 milliseconds (ms). In [30], an iterative technique is proposed for estimating power system frequency in the resolution of 0.01-0.02 Hz in the time span of only 20 ms. This method uses proper design and adjustment of orthogonal filters used to block harmonic components of the measured voltage. In current context, Wide area measurement systems (WAMS) implements Phasor measurement units (PMUs) and Frequency monitoring network (FNET) which is capable of measuring the power system states e.g. voltage, current, phasor angle, and frequency across a very large area [31-34]. The synchronization of phase and frequency with respect to the controllable oscillator, and hence, the measurement of these parameters for the actual signal can be taken with the help of Phase Locked Loop (PLL) [35][36]. The basic PLL comprises of a phase detector, a loop filter and a voltage controlled oscillator (VCO). The phase detector compares the input signal with the output of voltage controlled oscillator; a loop filter helps in filtering out the output from phase detector and VCO is essentially, an oscillator in which the output frequency deviation is proportional to the input signal.

2.2 VOLTAGE AND FREQUENCY CONTROL WITH DISTRIBUTED ENERGY RESOURCES (DERs) IN MICROGRIDS

Following some small disturbances like load variation or severe disturbances like faults, generator trips, etc., the system voltage and frequency are very likely to go beyond the acceptable range. According to the guidelines, the distribution level voltage should be maintained in the range of $\pm 5\%$ of the nominal value which is known as "ANSI Service Range A" or simply "ANSI Range A" [7]. In the modern power systems, DERs can help in augmenting the voltage dips caused by the mentioned disturbances. Unlike the grid connected mode where the central generators maintain the system frequency at 60 Hz, participating DERs have complete responsibility of maintaining the system frequency in case of islanded micro grids. In order to maintain the voltages and frequency of the system at the desired level, inverters associated with DERs should have proper controls. Various research have been done to investigate the voltage control methods with DERs in grid-connected mode and both voltage and frequency control methods in islanded microgrids.

The frequency control of traditional synchronous generators is performed through governor droop control [37]. The micro-grid voltage and frequency control can also be performed using the same principles as traditional droop control methods [38][39][40]. The real and reactive power control based on the adaptive droop controller is proposed in [40]. This work uses the frequency locked loop based on second order generalized integrator (SOGI-FLL) in order to measure voltage and current phasors with greater

precision. In [41], other two DERs control paradigms besides microgrid e.g. Cell and Virtual Power Plant (VPP) are discussed. The Cell concept was first introduced in Denmark in 2004 and it comprises of radially operated distribution network below a 150/60 kV transformer. The operation of cell under contingencies leading to the cell islands is performed by a cell controller. VPP, on the other hand, is the aggregation of large number of low-power DERs into a big equivalent generator that can even participate in the energy markets and provide ancillary service to the system. Some other cooperation and control methods among the participating micro-resources in the micro-grid like inverter modes control, primary energy source control, reverse droop control, autonomous control and multi-agent based PQ control proposed by various authors have been pointed out and discussed in [42].

In contrast to the traditional concept about close coupling between real power (P) and power system frequency (f) and reactive power (Q) and bus voltage (V), research have found out that in low voltage microgrid with line resistance (R) highly greater than line reactance (X), there exists a very close coupling between voltage and real power as well as the coupling between frequency and reactive power [43-45]. In [44] a voltage power droop/frequency –reactive power boost (VPD/FQB) control scheme which is capable of controlling multiple Voltage source converters (VSCs) to operate in parallel is proposed. In this case, voltage control loop is designed with the help of transfer function which relates d-axis VSC current to the microgrid bus voltage and the frequency control loop

design is performed with the help of another transfer function relating q-axis VSC current to the microgrid bus frequency.

In order to operate the microgrid system stably in the islanded mode where the voltage and frequency references are hard to achieve, the necessity of having a reference signal in the microgrid inverter control is pointed out in [43]. In this work, the necessary voltage reference signal is obtained from the main grid and an inverter is allocated as a master unit which will provide this signal to the microgrid. All other inverters would be operated in a constant PQ mode. The implementation of tradition control techniques like root locus and frequency domain analysis in microgrid control is carried out in [45].

In [46] the mathematical model and the voltage/frequency control strategy for an islanded DER units connected to the grid through a power electronic interface is proposed. The method proposed here is based on dq-frame current control scheme. This work utilizes the built-in Phase Locked Loop (PLL) in the DER systems for synchronization to the grid voltage. A feed-forward signal is utilized to eliminate the coupling between d-axis and q-axis control loops.

In order to cope with high penetration of DERs in the low voltage grid, there should be a proper communication between the participating DERs. The implementation of Autonomous Electricity Networks (AEN) for the control and interaction of a group of DERs is proposed in [47]. The work uses a communication overlay toolbox called

Agora+. Both technical and economic objectives have been considered to develop the control methods. The primary droop control ensures the control of voltage and frequency under contingencies, the gossip based secondary control optimizes the power quality, and the gossip based tertiary control is applied for economic dispatch. All together these three controls take care of both technical and economic aspects.

With the inverter integrated system, the power quality and unbalances in the voltage waveform are also very important issues to be taken care of while performing the voltage and frequency control. The control algorithms which take care of power quality and unbalance compensation issues are proposed in [48, 49]. If the control of the output current of the inverter is done in an explicit current control loop, it makes the inverter to act as a high impedance path that blocks the harmonic currents caused by the grid voltage distortion [48]. In order to correct the harmonic distortion in the voltage waveform, it proposes a control method which filters the voltage waveform to identify the harmonic distortion and uses this feedback to generate a current reference that is added to the active and reactive current references. The controller based on Dumped Load (DL) which helps in active power balance of the system and hence, in turn, aid in frequency control is proposed in [49]. In this work, the same DL is used as a compensator of the unbalanced currents among the phases. Here, synchronous machine and induction machine based DERs are considered for study.

Other control schemes based on robust controller and optimization methods applied to hierarchical control are also implemented in voltage and frequency control problems of the islanded micro-grid [50-52]. A hierarchical control scheme to coordinate the micro-resources in the islanded micro-grid to contribute in restoring the system frequency is proposed in [50]. The three hierarchical structures for the micro-grid control comprises of Distribution Management System (DMS) in the first level, Central Autonomous Management Controller (CAMC) in the second level and MicroGrid Central Controller (MGCC) in the third level. The control scheme uses optimization based on standard linear optimization technique to obtain the information about the required change in real power in the system and its distribution among the participating DERs. The objective is to minimize the cost of micro-resources. The robust controller for micro-grid control operation based on L_1 robust control theory is presented in [51] and the one based on H_∞ theory is proposed in [52]. In [51], Particle Swarm Optimization (PSO) to is applied to solve the optimization problems. In [52], the master DER is designed to control voltage of the micro-grid based on H_∞ robust control and the remaining DERs control the real and reactive power based on the conventional dq-current control strategy.

The penetration of renewable energy based DERs as compared to fossil fuel based DERs are increasing in the recent years. Hence, the research and challenges on integrating renewable-based DERs like Solar Photovoltaic (PhV) and wind in grid connected and islanded micro-grids are growing. Very few researches have been done regarding voltage and frequency control using solar PhV and storage [53-57]. The application of solar PhV

in voltage and frequency regulation in an islanded micro-grid consisting of a synchronous generator, a solar panel with a single phase inverter and a varying resistive load is discussed in [53]. In this work, Phase Locked Loop (PLL) is used to measure the frequency and phase of the generated signal. The active current injection to the system in order to maintain micro-grid frequency is calculated with the help of Predictive Current Control algorithm. The maximum power point tracking (MPPT) of the solar array is done by using a hill climbing algorithm which changes the duty ratio of the booster and monitors the output power. A detailed mathematical model of solar PhV array based on the diode model is described in [54]. A three level inverter topology with neutral point clamp (NPC) is used instead of a conventional two-level six-pulse inverter structure that provides additional degree of freedom so that more accurate sinusoidal waveform can be attained. However, NPC inverters have a drawback in that capacitor banks must be used to maintain the constant voltage of half the magnitude of the DC side voltage. Three levels of control namely external, middle and internal level controls are defined for a grid connected PhV system. The external level control is responsible for controlling active and reactive power exchange from the PhV and the grid, the middle level control helps in dynamically tracking the reference value set by the external level and the internal level control generates the switching signal for the three- level voltage source inverter (VSI). The power modulation process of PhV generators for frequency regulation purpose is discussed in [55]. The rapid fluctuation of PhV generator output is stabilized with the help of a double layer capacitor which also helps in changing output of the generator at a limited ramp rate. The voltage control and the frequency control are decoupled with each

other by adding a term considering the effect of real power change on system voltage in a voltage control algorithm and incorporating a term related to the change in system voltage in the frequency control algorithm. Several methods of load frequency control in a micro-grid comprising wind power, Solar PhV and diesel generators are examined in [56]. The load demand estimation and proportional control methods are discussed for the wind generation and the frequency control of the PhV generator is carried out by using variation of active power. The importance of shunt connected voltage source inverter (VSI) with PhV generator in order to compensate for the voltage sags in the grid connected mode is discussed in [57]. This work proposes a controller for the PhV system based on the droop control method for voltage and frequency control by controlling reactive and active power respectively. The control method used comprises of: the outer loop provides the voltage reference based on the voltage-reactive power droop, while the active power reference is obtained from the MPPT of solar array; the inner loop comprises of a repetitive controller that is capable of compensating for third and fifth order harmonics and a PI controller that improves the stability of the system through the low-pass filtering function.

The improvement on the traditional droop based voltage and frequency control by decoupling the active and reactive power control, a new method of a virtual frequency-voltage frame control is proposed in [58]. The original voltage and frequency is transformed to a new virtual frame using some transformation matrix so as to achieve completely decoupled control of active and reactive power in the low voltage micro-

grids. It is pointed out that, in this method, if the transformation angles are chosen different for different DERs, then, the microgrid voltage and frequency will be converted to different values in different virtual frames and proper power sharing among the DERs using the voltage and frequency signals cannot be undertaken. Hence, this method requires that the transformation angle for all the DERs in the microgrid should be the same.

2.3 POWER ELECTRONICS (PE) INTERFACE FOR INTEGRATION OF DISTRIBUTED ENERGY RESOURCES IN POWER SYSTEM

Most of the Distributed Energy Resources (DERs), either renewable or non-renewable based, are capable of producing either Direct Current (DC) or asynchronous alternating current (AC) output voltage. In order to integrate them into the grid, it is required that the DC supply is converted to AC supply with desired voltage magnitude and frequency synchronous to the grid. This is where the power electronics interface comes into picture. The power electronics converters can convert the DC voltage to a desired value of AC voltage or from asynchronous AC to DC and then DC to synchronous AC of 60 Hz. With proper controls of - inverter switching, the DERs can be controlled to inject desired amount of real and reactive power to the grid as required.

Advancements in PE interface technologies for the integration of DERs into the grid or in islanded case as in micro-grid have increased the capability of such interface in providing

lots of benefits to the system through its components and control strategies [14, 59-64]. The benefits offered by the PE interfaces is discussed in [14] such as providing improved power quality, reactive power and voltage support, improved DER fault current coordination, interoperability with other DERs, fast switching capability in the case of micro-grids and PE modularity and standardization. The further enhancement in performance of PE interfaces can be achieved through proper communication between various DERs as pointed out in [59]. The topology of the Voltage Source Inverters (VSIs) and the material used for the construction of switches of VSI have a greater impact on the performance characteristics of the PE interfaces [60, 61]. In [60], a novel DC/AC converter topology is proposed where a fly back type auxiliary circuit is integrated with an isolated C′uk-derived VSI in order to obtain higher voltage gain. With this topology, the capacitors of the C′uk and flyback circuits are connected in parallel while charging and in series while discharging such that lower voltage rating devices can be used and the conversion efficiency would be enhanced as well. Since PE converters comprise of many switching components, the efficiency can be increased if the switching losses are minimized. As compared to Silicon based MOSFET switches, Silicon carbide (SiC) based switches offer very less switching as well as conduction losses and have an ability of operating at higher temperature [61]. With these and several other advantages over silicon, silicon carbide has a very promising future to be used in manufacture of switches used in the PE interfaces for integration of DERs.

In addition to helping DERs in providing ancillary services to the grid or isolated power systems, PE interfaces have a capability of compensating for the system harmonics which is a very important power quality issue [62, 64]. The harmonic component of the DER output voltage is obtained using a second order generalized integrator (SOGI) based band pass filter in [62] whereas shunt active power filter (APF) is used to compensate for the harmonics and reactive currents caused due to the non-linear loads in [41]. In [63] proposes a droop control based method is proposed which uses reactive volt-ampere consumption of harmonics of each converter. With this approach, the harmonic filtering workload can be evenly distributed among the participating converters even without communications. The removal of the harmonic distortion of the grid voltage can also be achieved by the combination of using the resonant harmonic filter and injecting the local voltage signal with the same amount of distortion [64]. This method helps in removal of harmonic distortion even at low quality factor (Q). Since, the difference in amplitude of the grid voltage and the voltage at Point of common coupling (PCC) is small due to injection of the voltage signal with same distortion, the grid harmonic current is reduced.

Based on the control mechanism being adopted, VSIs can also be classified as voltage controlled VSI (VCVSI) and current controlled VSI (CCVSI) [65, 66]. VCVSI uses the amplitude and phase of the output voltage to control the power flow. The voltage across the coupling inductor is controlled to get the desired current flow in VCVSIs. Hence, they can provide voltage support to the load as they act as a constant voltage source. CCVSI, however, uses the switching instants to obtain the desired current. CCVSIs provide

current support because they act as a constant current source. The control method used for VCVSIs are usually Pulse Width Modulation (PWM) technique whereas generally, hysteresis current control technique is used for CCVSIs [66]. CCVSIs have faster response characteristics than VCVSIs as reported in [65, 66].

2.4 REACTIVE POWER MARKET WITH DERS

With the increasing penetration of small DERs in modern power systems, there is an increased complexity and challenges to integrate these generators in the deregulated electricity market framework. Moreover, with the integration of more stochastic generations like Solar and Wind, the need of ancillary services in the form of voltage and frequency support has become the area of special attention. As mentioned in the previous sections, with the proper control of power inverters, DERs are capable of producing reactive power in addition to active power. The economic potential of DERs to provide reactive power in microgrid is discussed in [67, 68]. The DERs should have a proper incentive to produce reactive power in the microgrid and this can be provided only with the price signals in the deregulated market environment. In [67], four different market models for reactive power dispatch from DERs in the microgrid environment are proposed which are described briefly as follows:

- No compensation framework in which the generator producing active power are required to produce power so as to maintain particular value of power factor.
- Installed capacity based framework in which the generator is paid for its capability of producing reactive power based on the installed capacity, however,

in this framework, there is no real time payment according to the kVARs produced.

- Cost based compensation framework in which various cost components like additional investment cost, additional variable cost and the opportunity cost of reactive power supply is considered for providing compensation to the producers.
- Auction based framework in which the system operator selects the supplier of kVArh based on the market clearing price and need of reactive power compensation.

In different market structure, there are various market incentives for the reactive power producers for the provision of ancillary services [67]. For example: the New York Independent System Operator (NYISO) provides capability as well as lost opportunity cost compensations. Similarly, California Independent System Operator (CAISO) mandates the generators to operate with a power factor in the range of 0.90 lagging and 0.95 leading and it pays the generators the opportunity cost if it forces them to dispatch reactive power outside of this range.

The mathematical formulation of ancillary service market framework for medium voltage microgrid for voltage support is presented in [69]. The formulation is an optimization problem of minimizing the reactive power bids from all the generators with the technical active and reactive power balance constraints, the total reactive power generation constraints, and voltage and apparent power limits of the system. Similarly, in [70], a

multi-objective optimization problem for dispatch of both active and reactive power considering the volatility of wind generation is proposed. The system operational objectives like maximizing expected system's voltage stability margin and minimizing transmission congestion probability are considered in the optimization problem. This problem is solved for transmission system level.

The review of effective ancillary service market designs is done in [71]. Ancillary service market can either be dynamic with hourly or faster prices or it can be cost based in which the prices are set in advance. The ancillary service markets which affect the real time operations like voltage and frequency support will have dynamic markets whereas other services like black start capability are cost based. Out of all the ISOs and Regional Transmission Organizations (RTOs) of the North American Power System, only Southwest Power Pool does not have ancillary service market at present. Ancillary services prices could be calculated as given by the shadow price of the ancillary service inequality constraint [71] which is the cost of marginal resource providing ancillary service. Another consideration for ancillary service market could be locational based requirement. The increased ramping rate requirement due to the high penetration of variable renewable energy resources is pointed out in this paper.

CHAPTER 3
P-Q AND P-V CONTROL OF SOLAR PHV GENERATORS

This chapter describes the modeling and control approach adopted for solar PhV generation in the present work. The modeling of solar PhV based on one diode model is described in detail and the PhV system configurations are explained. Active and nonactive power control algorithm used with PhV is described next. It is followed by a discussion on the proposed solar PhV MPPT control algorithm which has been integrated to the voltage control algorithm to fulfill the active power and voltage (P-V) control objective applicable to grid connected microgrids. The chapter also presents convincing simulation results to validate the applied and proposed control techniques.

3.1 MODELLING OF SOLAR PHV AND SYSTEM CONFIGURATION

Modeling of Solar PhV

The fundamental building block of Solar PhV array is a solar cell which is a photodiode that is capable of converting solar irradiance into dc current through the photovoltaic effect [72, 73]. The commonly accepted solar cell model is a one diode model [54, 74-76]. The current work uses the single diode model of the solar cell to model the Kyocera KC200GT solar array, which is shown in Figure 5. The reason to choose this specific solar module is for easy validation of the simulated *I-V* curve with the experimentally available curve from the datasheet. The modeling is performed analytically based on the underlying equations of the solar cells which can be extended to solar panels and then to solar array through series and parallel combinations of solar cells and solar panels, respectively.

The practical PhV array is composed of a certain number of solar cells in series. The I-V characteristics of a solar array, as shown in Figure 6, are represented by the following mathematical equation (1)

$$\boldsymbol{I = I_{PV} - I_o\left[\exp\left(\frac{V+R_sI}{V_{therm}a}\right) - 1\right] - \frac{V+R_sI}{R_{sh}}} \quad (1)$$

where I_{PV} and I_o are the photo current and the diode saturation currents, respectively. $V_{therm} = N_s kT/q$ is the thermal voltage of the array, N_s being the cells connected in series for greater output voltage, k is the Boltzmann constant ($1.3806503 \times 10^{-23} J/K$), T (Kelvin) is the temperature of the p-n junction of the diode, and q ($1.60217646 \times 10^{-19} C$) is the electron charge. Also, R_s and R_{sh} are the equivalent series and shunt resistances of the array, respectively, and a is the ideality factor usually chosen in the range $1 \leq a \leq 1.5$. Here a is taken as 1.

Equation (1) gives the *I-V* characteristic of the solar array as shown in Figure 6 in which the significant operating points such as short circuit (0, I_{sc}), Maximum Power Point (MPP) (V_{mpp}, I_{mpp}), and open circuit (V_{oc}, 0) are marked clearly. The photocurrent of the PhV array depends linearly on the solar irradiation and the cell temperature, as shown by (2) [74].

Here, $I_{PV,n}$ is the photocurrent at the standard test condition (STC, 25℃ and 1000 W/m^2), K_I is the short circuit current/temperature coefficient, ΔT is the difference between the

actual and nominal temperature in Kelvin, G is the irradiation on the device surface, and G_n is the nominal radiation, both in W/m^2.

$$\boldsymbol{I_{PV} = (I_{PV,n} + K_I \Delta T) \frac{G}{G_n}}. \quad (2)$$

$I_{PV,n}$ can be calculated based on (3).

$$\boldsymbol{I_{PV,n} = \frac{R_{sh} + R_s}{R_{sh}} I_{sc}}. \quad (3)$$

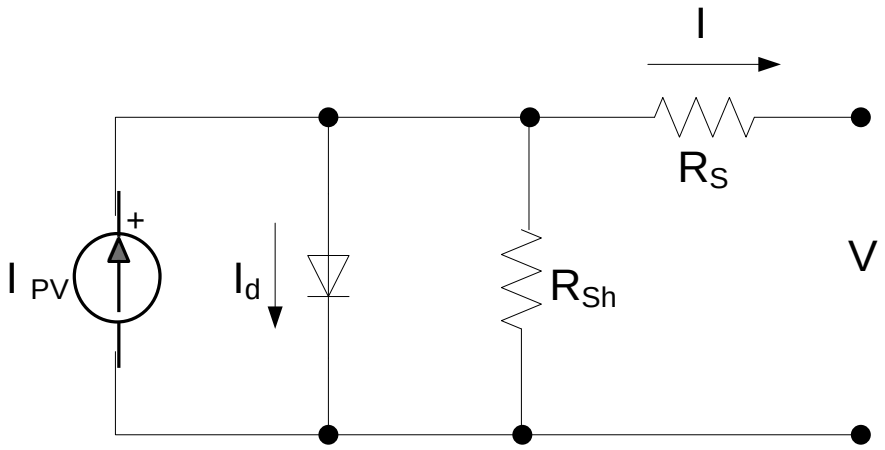

Figure 5. One diode equivalent circuit of Solar PhV.

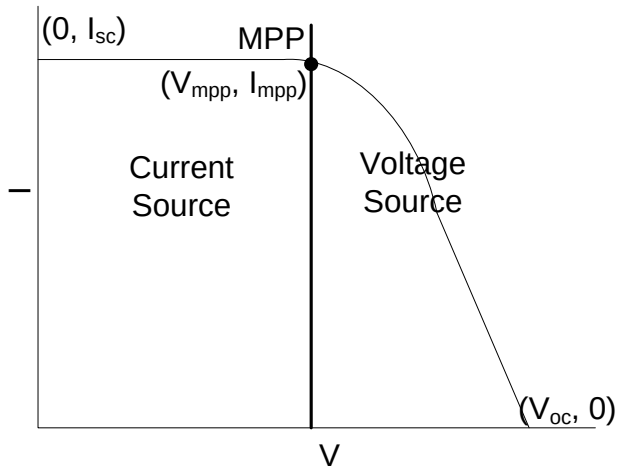

Figure 6. I-V characteristics of a practical PhV array.

Using these fundamental equations and parameters from the data sheet, the PhV model is developed analytically and verified with the panel datasheet. The I-V characteristics of KC200GT for different irradiation levels at the cell temperature of 25°C as obtained from the simulation and the datasheet are shown in Figure 7 a) and b), respectively.

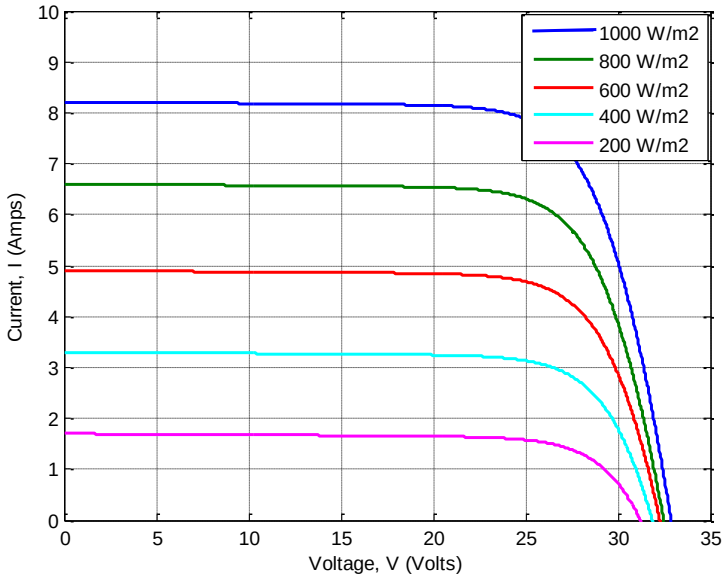

a) Simulation

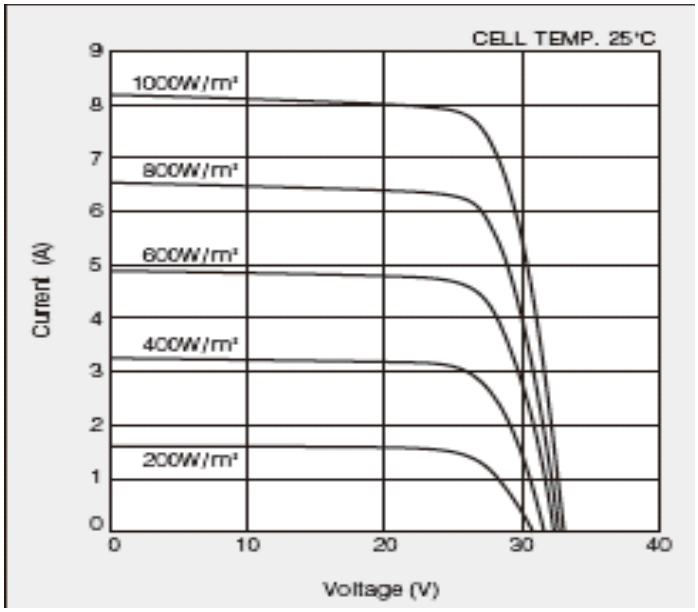

b) Datasheet

Figure 7. The I-V characteristics of Kyocera KC200GT at a cell temperature of 25^{o}C obtained from a) simulation and, b) datasheet.

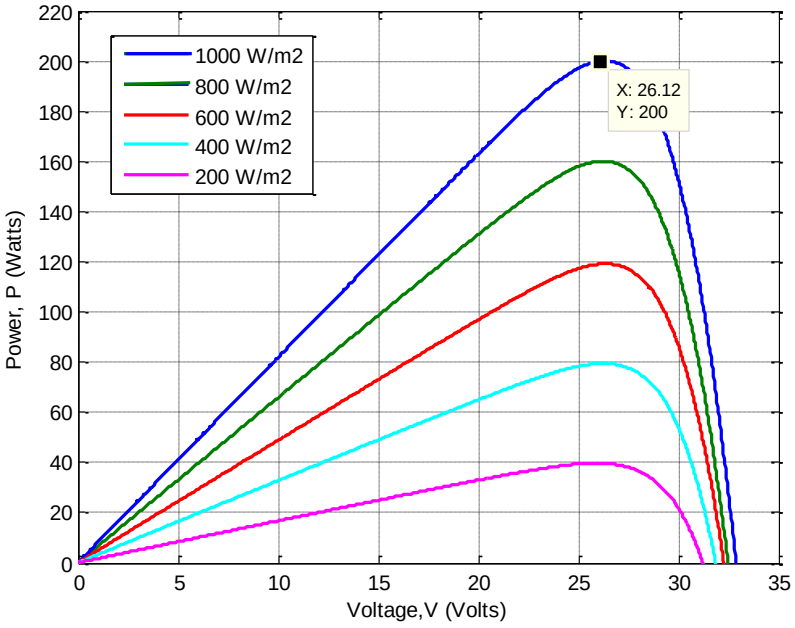

Figure 8. The *P-V* characteristics of Kyocera KC200GT at a cell temperature of 25°C for different irradiation levels.

Figure 8 shows the P-V curve of the KC200GT panel. The maximum power point obtained for the irradiation level of 1000 W/m^2 from the simulation is 200 Watts as shown in the figure, which is the same as the one obtained from the datasheet. The parameters for PhV panel KC200GT is shown in Table 1.

Table 1 PhV Panel Parameters at 1000 W/m^2 and 25^{o}C

Model	Kyocera KC200GT
P_{MPP}	200W
V_{MPP}	26.3V
I_{MPP}	7.61A
V_{OC}	32.9V
I_{SC}	8.21A

PhV System Configuration

A system configuration of PhV considered in this chapter is shown in Figure 9 (a and b). Figure 9a shows the PhV configuration for P-Q control only and Figure 9b shows the configuration for PhV for P-V control. A single stage configuration is considered here for P-Q control and a double stage configuration is considered for P-V control in order to handle different objectives. An instantaneous active power and nonactive power theory [16, 17, 77] was implemented to develop the control algorithm.

The PhV system is connected in parallel with the grid through a coupling inductor L_c. The coupling inductor can alleviate the ripples in the PhV output current. The connection point is referred to as the point of common coupling (PCC) as mentioned in chapter 1, and the PCC voltage is denoted as $\boldsymbol{v_t}$.

The equivalent local load is also connected at the PCC. The rest of the system is simplified as an infinite voltage source with a system impedance of $R+j\omega L_s$. The PhV

source is connected to the inverter with a DC link capacitor. The PhV energy source is the active power source, and the capacitor is the nonactive power source of the DER system. The inverter current $\boldsymbol{i_c}$ is controlled so that the desired amount of active power and nonactive power is provided from the PhV system. The instantaneous values of the PCC voltage and the inverter current are measured and provided to the controller.

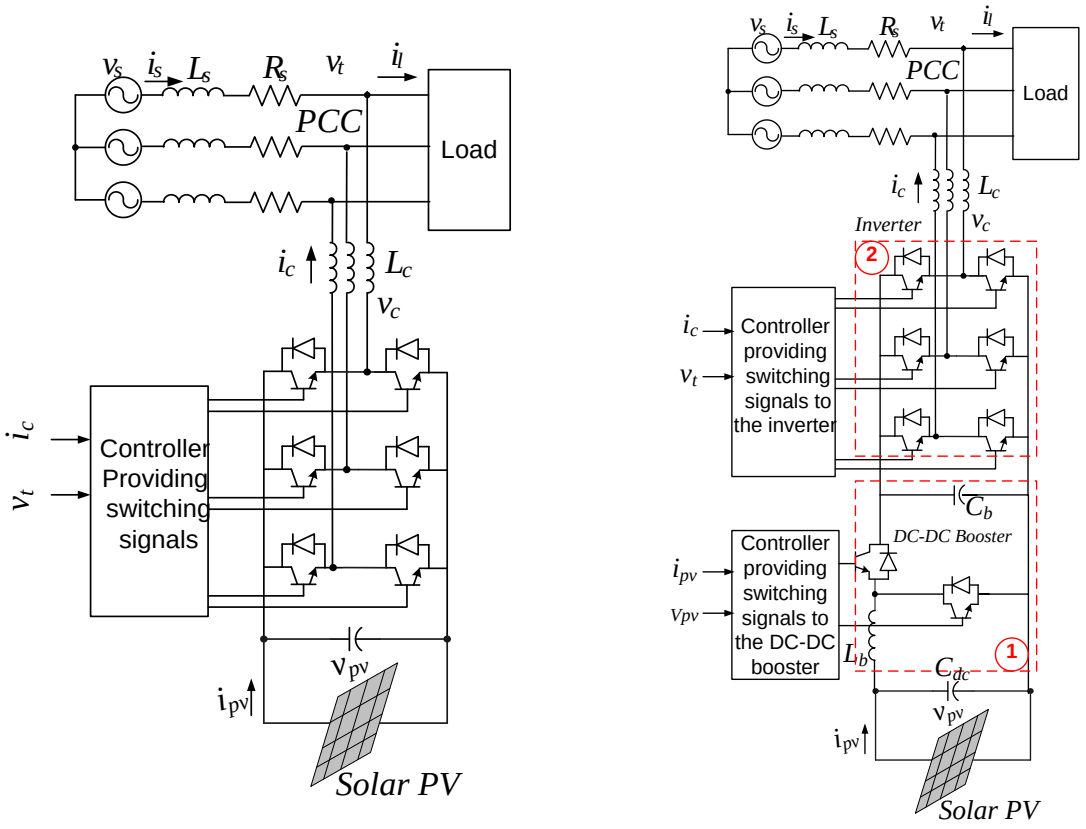

a) b)

Figure 9. Integrated PhV system configuration: a) P-Q Control; b) P-V Control.

Table 2 shows the parameters considered for DC/DC booster and inverter in the model.

Table 2 Parameters used for DC/DC booster/inverter

L_c	3.5mH
f_s (booster/inverter)	20kHz
L_b	0.9mH
C_b	0.4982F
C_{dc}	0.2mF

3.2 ACTIVE AND NON-ACTIVE (P-Q) CONTROL METHOD

The theory behind active and non-active (P-Q) control method is instantaneous non-active power theory proposed in [77]. The instantaneous power definitions are extensions of the standard steady-state power definitions. They are instantaneous active current, instantaneous nonactive current, instantaneous active power, and instantaneous nonactive power. Similarly, the rms values of voltages and currents are also defined as instantaneous values.

The power system in this study is considered to be a three-phase balanced system; hence, the instantaneous power theory can be simplified, as shown in the following derivations. The PhV system shown in Figure 9 can also be simplified as the single-phase equivalent circuit in Figure 10, assuming that the three-phase system is balanced. Let $v_t(t)$ and $v_c(t)$ denote the instantaneous PCC voltage and the inverter output voltage (harmonics are

neglected), respectively, where α is the phase angle of $v_c(t)$ relative to the PCC voltage. These are given by (4) and (5) below.

$$\boldsymbol{v_t(t) = \sqrt{2} V_t \cos(\omega t)} \quad (4)$$

$$\boldsymbol{v_c(t) = \sqrt{2} V_c \cos(\omega t + \alpha)}. \quad (5)$$

The rms values of $v_t(t)$ and $v_c(t)$ are given in (6) and (7), respectively.

$$\boldsymbol{V_t(t) = \sqrt{\frac{2}{T}\int_{t-\frac{T}{2}}^{t} v_t^2(\tau) d\tau}} \quad (6)$$

$$\boldsymbol{V_c(t) = \sqrt{\frac{2}{T}\int_{t-\frac{T}{2}}^{t} v_c^2(\tau) d\tau}} \ , \quad (7)$$

where $T/2$ is one-half of the period of the voltage and is the average interval used here. V_t(t) and $V_c(t)$ are instantaneous variables as a function of time *t*. All other rms and power definitions are also functions of time; therefore, they are valid in both steady state and transients.

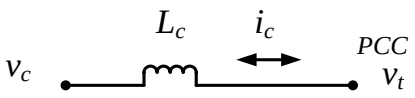

Figure 10. Simplified circuit diagram of a parallel connected PhV.

The current from the inverter to the utility is denoted as $i_c(t)$ given by (8).

$$\boldsymbol{i_c(t) = \frac{\sqrt{2}}{\omega L_c}[V_c \sin(\omega t + \alpha) - V_t \sin(\omega t)]}\,, \tag{8}$$

where α is the phase angle between the PCC voltage $v_t(t)$ and the inverter current $i_c(t)$. The average power at the inverter side is denoted as $P(t)$ and is given by (9).

$$\boldsymbol{P(t) = \frac{2}{T}\int_{t-\frac{T}{2}}^{t} v_t(\tau) i_c(\tau) d\tau = \frac{V_t V_c}{\omega L_c} \sin \alpha}\,. \tag{9}$$

The instantaneous active current component of the inverter current $i_c(t)$ is defined as

$$\boldsymbol{i_{ca}(t) = \frac{P(t)}{V_t^2(t)} v_t(t)}. \tag{10}$$

The instantaneous nonactive part of the inverter current is defined as

$$\boldsymbol{i_{cn}(t) = i_c(t) - i_{ca}(t)}. \tag{11}$$

The $i_{ca}(t)$ and $i_{cn}(t)$ are the active component and the nonactive component of the inverter current $i_c(t)$, respectively. By controlling these two current components, the active power and the nonactive power from the PhV can be controlled independently.

The rms values of $i_{ca}(t)$ and $i_{cn}(t)$ are defined as $I_{ca}(t)$ and $I_{cn}(t)$ as in (12) and (13), respectively.

$$\boldsymbol{I_{ca}(t) = \sqrt{\frac{2}{T}\int_{t-\frac{T}{2}}^{t} i_{ca}^2(\tau) d\tau}} \tag{12}$$

$$\boldsymbol{I_{cn}(t) = \sqrt{\frac{2}{T}\int_{t-\frac{T}{2}}^{t} i_{cn}^2(\tau) d\tau}}\,. \tag{13}$$

The apparent power $S(t)$ and the average nonactive power $Q(t)$ of the PhV are given by (14) and (15).

$$\boldsymbol{S(t) = V_t(t) I_c(t) = \frac{V_t}{\omega L_c} \sqrt{V_t^2 + V_c^2 - 2 V_t V_c \cos \alpha}} \quad (14)$$

$$\boldsymbol{Q(t) = V_t(t) I_{cn}(t) = \sqrt{S^2(t) - P^2(t)} = \frac{V_t}{\omega L_c} (V_c \cos \alpha - V_t),} \quad (15)$$

where $Q(t)$ is defined as positive if the inverter injects nonactive power to the utility, and negative if the inverter absorbs nonactive power from the utility. $P(t)$ and $Q(t)$ in (9) and (15) can be approximated by the first terms of the Taylor series if the angle α is small, as shown in (16) and (17):

$$\boldsymbol{P(t) \approx \frac{V_t V_c}{\omega L_c} \alpha} \quad (16)$$

$$\boldsymbol{Q(t) \approx \frac{V_t}{\omega L_c} (V_t - V_c).} \quad (17)$$

In (16) and (17), with the assumption that the variation of V_t can be neglected, that is, V_t is constant, then the average nonactive power $Q(t)$ is proportional to the magnitude of the inverter output voltage $v_c(t)$. However, the average active power $P(t)$ is dependent on both the amplitude V_c and the phase angle α of $v_c(t)$.

A P-Q control scheme is developed accordingly with two feedback control loops as shown in Figure 11. The inner loop controls the nonactive power $Q(t)$ by controlling the amplitude of $v_c(t)$ while the outer loop controls the active power $P(t)$ by controlling the phase angle α of $v_c(t)$. The instantaneous inverter output voltage $v_c(t)$ is controlled to be in

phase with the PCC voltage $v_t(t)$. A PI controller PI_1 is used to control the magnitude of the inverter output voltage, $v_c(t)$ using (18)

$$v_{c1}^{*} = \left[1 + K_{P1}(Q^{*} - Q_{act}) + K_{I1}\int_0^t (Q^{*} - Q_{act})dt\right] v_t(t) \qquad (18)$$

Here, Q^{*} is the reference and Q_{act} is the actual value and K_{p1} and K_{i1} are the proportional and integral gains of the PI_1. The result of this control loop is $v^{*}_{c1}(t)$ which is in phase with the PCC voltage $v_t(t)$.

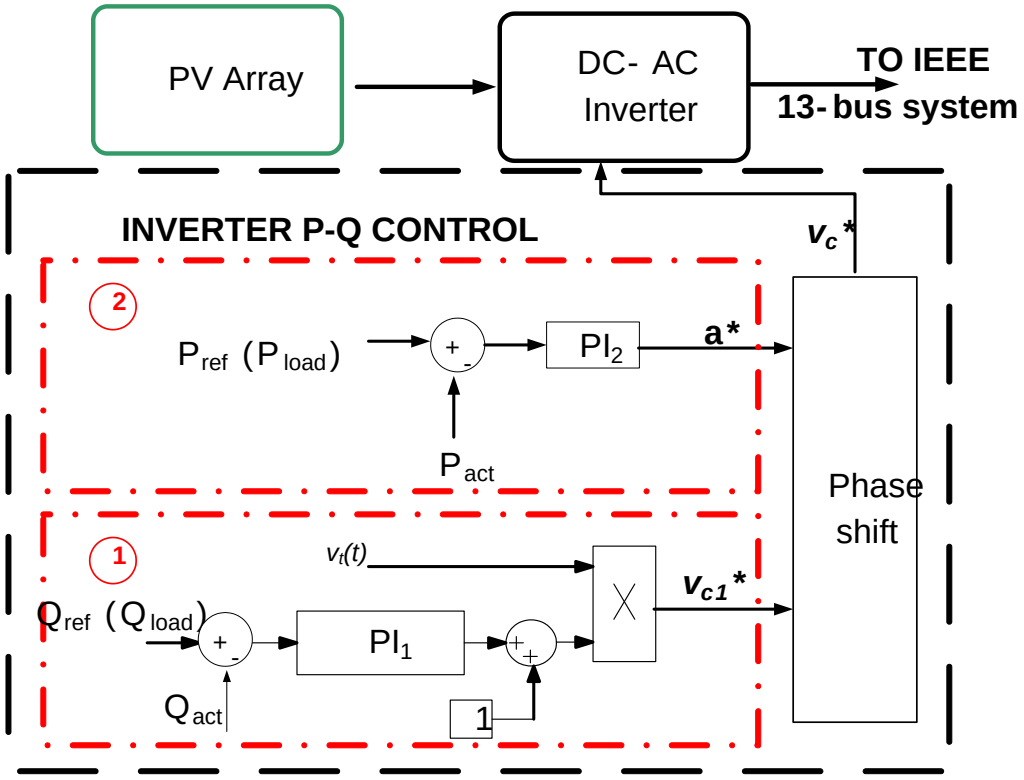

Figure 11. Active and nonactive power control diagram.

The outer loop is for the control of active power *P(t)* by controlling the phase angle α of $v_c(t)$. The output of this loop is α^* decided by the PI controller PI_2 by which the phase angle of $v^*_{c1}(t)$ is shifted to achieve the desired value of *P(t).* This can be represented by (19).

$$\boldsymbol{\alpha^* = K_{P2}(P^* - P_{act}) + K_{I2}\int_0^t (P^* - P_{act})dt} \quad (19)$$

Here, K_{p2} and K_{I2} are proportional and integral gains of PI_2 and P^* and P are reference and actual value of active power respectively.

3.3 MPPT (P) AND VOLTAGE (V) CONTROL METHOD

Due to the high cost and low efficiency of the solar PhV generators, it is desirable that the PhV array always operates at the maximum possible power available at a particular irradiation level and temperature. This control is termed as Maximum Power Point Tracking (MPPT). There are several ways of finding the maximum power of the PhV panel [73]. One way of obtaining Maximum Power Point (MPP) is to plot a set of hyperbolas defined as IV = constant, and noting the point where the hyperbola is tangent to the panel I-V curve. Another method is by differentiating the cell power equation and setting the result equal to zero. The voltage obtained to satisfy this condition could be verified to be a representative of the maximum and hence, the MPP can be identified. The next method to find out MPP is to plot the power versus voltage (P-V) curves and noting down the maximum point. This work uses the last method to find out the MPP. The P-V curves for different level of irradiation is obtained separately and the maximum power

point of each curve is noted down. The data of MPP versus irradiance is loaded into a look up table. A linear approximation method is adopted to find out the MPP corresponding to the intermediate irradiance data that is not entered into the lookup table. The most common methods found in literatures for finding MPP are Perturb and Observe (P&O) method and incremental conductance (IC) method [78-81]. In P&O method, the panel voltage is increased or decreased at subsequent steps and the PhV power output is compared to the one in the previous cycle. If the perturbation leads to an increase/decrease in the panel power then the next perturbation is performed in the same or opposite direction. In the incremental conductance method, solar array voltage is adjusted to the MPP voltage through the measurement of incremental and instantaneous array conductance as dV/dI and V/I. The method used in this work is simpler than P&O method as there is no need of perturbing the voltage and observing the PhV power but the maximum PhV power can be directly extracted from the lookup table.

This section describes the MPPT and voltage (P-V) control algorithm which is shown in Figure 12. A DC-DC booster circuit is added in front of the inverter as shown in Figure 9b making it is as a two stage configuration. This MPP operation of PhV can be the case when these PhV generators are connected to the utility grid and try to support the grid by supplying the clean power and at the same time avoiding the installation of the expensive storage system. Since it is connected to a utility system, out of the available PhV generators, only a small portion of the total energy suppliers, is assumed to be dispatched at its maximum power point for economic consideration. With this configuration, the

loads equal to the MPP of the installed PhV generator would be supplied by these generators and only the remaining portion of the loads would be supplied by utility.

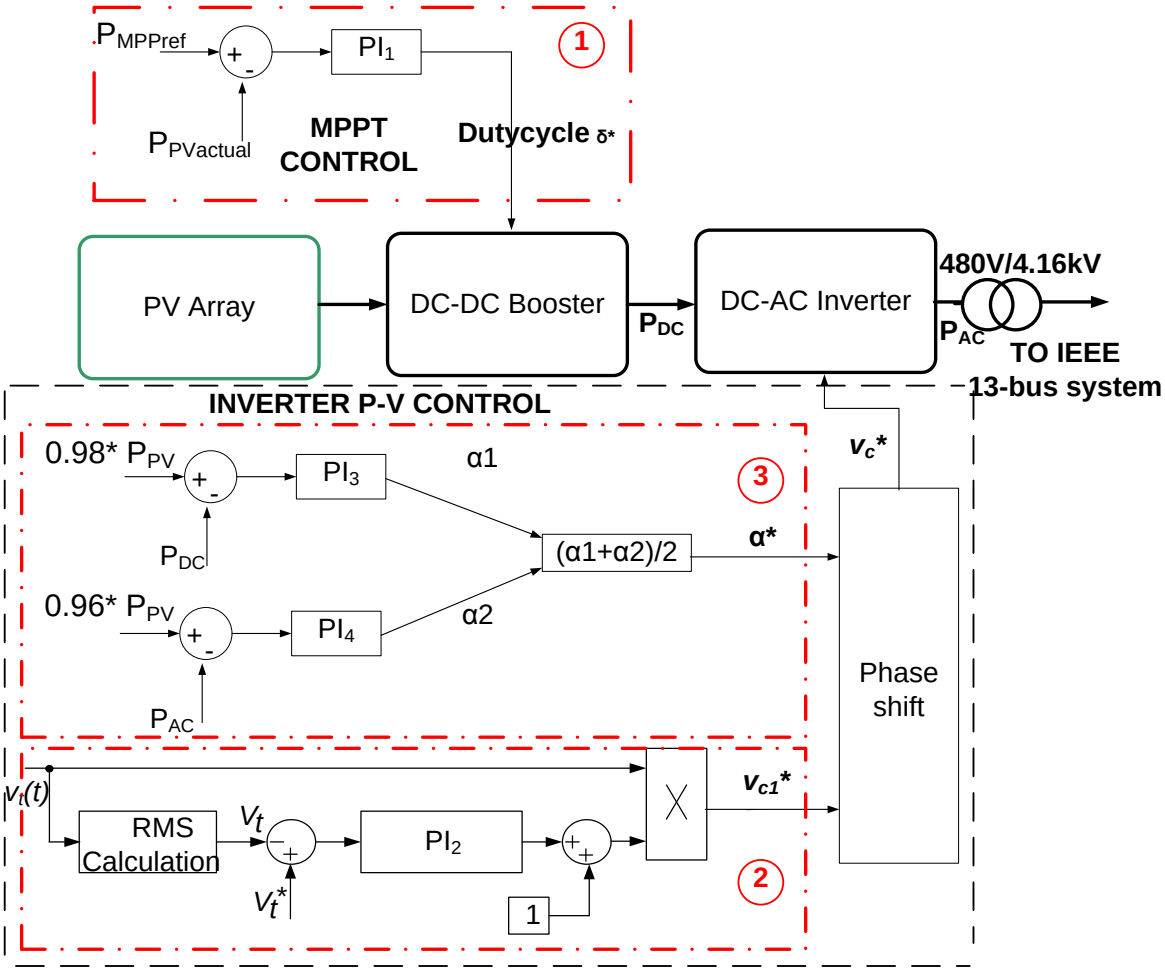

Figure 12. MPPT and Voltage (P-V) control diagram of solar array.

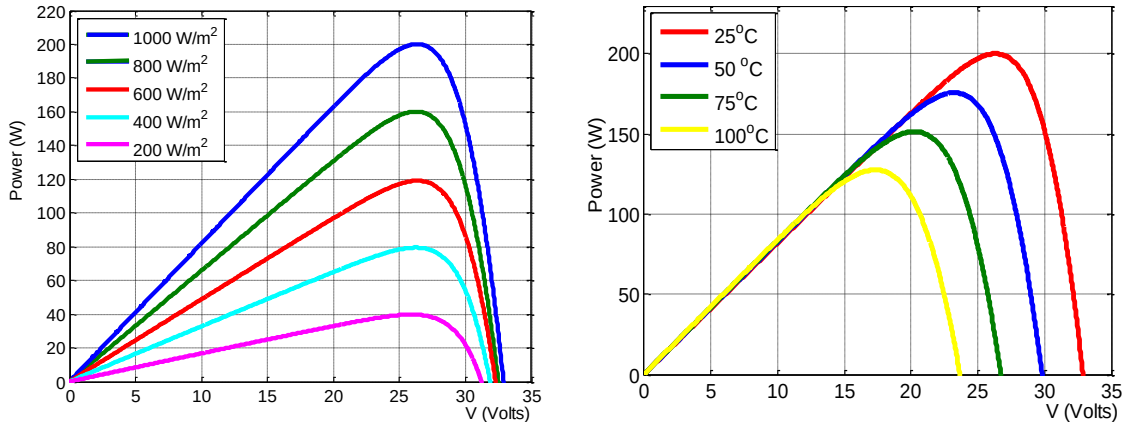

a) b)

Figure 13. PV Curves of KC200GT panel: a) with varying irradiance; b) with varying cell temperature

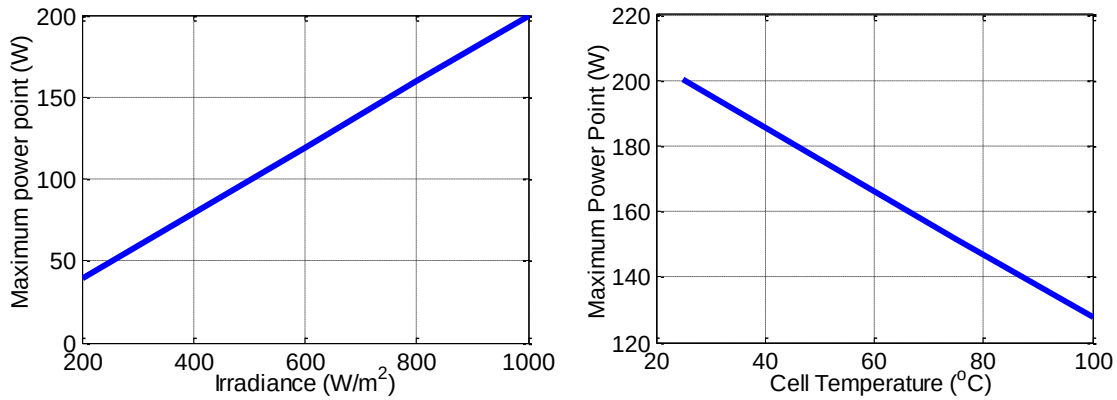

a) b)

Figure 14. Relationship of KC200GT panel Maximum Power Point (MPP) with a) irradiance; b) Cell Temperature.

The PV curves of KC200GT solar panel for varying irradiance and varying temperature are shown in Figure 13a and 13b, respectively. Also, Figure 14a and 14b show the relationship between maximum power point (MPP) of the solar panel with irradiance and

cell temperature respectively. MPP seems to be directly proportional to the irradiance level and inversely proportional to the panel cell temperature, however, both the relationships are linear. Hence, a look up table with a linear approximation to find the missing data is a reasonable assumption to make. In this work, the MPP is obtained from the look up table for the corresponding irradiance level and cell temperature at first. Then, three different control loops are used for the MPPT and voltage control as shown in Figure 12. The loop 1 is a MPPT control at the PhV array side which uses the reference MPP, P_{MPPref} from the look up table, compares the actual PhV power output (P_{PV}) with this reference, and feeds this error to a PI controller, PI_1 which outputs the duty cycle δ^* for the DC-DC booster such that the array always operates at the referenced point by changing this duty cycle. The equation for this control loop is given by (20). Here, $K_{p1}$and K_{i1} are the controller's proportional and integral gains, respectively, for this particular control loop.

$$\delta^* = K_{p1} * \left(P_{MPPref} - P_{PV}\right) + K_{i1} * \int_0^t (P_{MPPref} - P_{PV})\ dt \qquad (20)$$

At the inverter side, there are three PI control loops in order to transfer this maximum active power to the output of the inverter. The control loops comprise of the inner loop 2 for voltage control at the AC side [15] and the outer loop 3 comprising of other two PI controllers for the control of active power output of the inverter and indirect control of DC side voltage. These control methods are developed for the inverter connected to the IEEE 13 bus distribution feeder.

For voltage control at the AC side, feedback PI controller, PI_2 is used. As shown in the control diagram in Figure 12 (loop 2), the PCC voltage is measured and the rms value of $v_t(t)$ is calculated. Then, the rms value $V_t(t)$ is compared to a voltage reference $V_t^*(t)$ (which could be a voltage specified by the utility) and the error is fed to a PI controller. The inverter output voltage $v_c(t)^*$ is the reference to generate pulse width modulation (PWM) signals to drive the inverter. The output voltage of the inverter is controlled so that it is in phase with the PCC voltage, and the magnitude of the inverter output voltage is controlled so that the PCC voltage is regulated at a given level $V_t^*(t)$. The control scheme can be specifically expressed as (21).

$$v_c^*(t) = v_t(t)\left[1 + K_{P2}\left(V_t^*(t) - V_t(t)\right) + K_{I2}\int_0^t \left(\left(V_t^*(t) - V_t(t)\right)dt\right)\right] \quad (21)$$

where K_{P2}, K_{I2} are the gains of the PI controller.

The loop 3 is the outermost loop to control the active power output at the inverter side. The basic control methodology is the same as previously described in section 3.2. However, it comprises of two different control loops to control the active power at the AC and DC sides, respectively. The control of the active power at the DC side is denoted by (22). Here, the reference signal is obtained from the output power of the PhV array, P_{PV} multiplied by efficiency of the DC-DC booster which is taken here as 98% in order to account for the losses in the converter circuit. This reference is, then, compared with the measured DC power output of the booster, P_{DC} shown in Figure 12 and the error is fed to the PI controller, PI_3. The output of this loop is a phase shift contribution α_1^* from the DC side of the inverter. Similarly, another PI controller loop, PI_4 is used to obtain the phase

shift contribution, α_2^* required to control the active power at the output of the inverter to be equal to 96% of the $P_{PV.}$ This value of efficiency is considered so as to account for the combined losses of the DC-DC booster and inverter circuits. The equation for this control loop is given by (23). The phase shift contributions from DC and AC sides, α_1^* and α_2^* are then averaged as given by (24) to obtain the final phase shift, α^* of the voltage waveform , v_{c1*} which will then generate the voltage reference signal v_{c*} for the inverter PWM.

$$\alpha_1^* = K_{P3}(0.98 * P_{PV} - P_{DC}) + K_{I3}\int_0^t (0.98 * P_{PV} - P_{DC})dt \quad (22)$$

$$\alpha_2^* = K_{P4}(0.96 * P_{PV} - P_{AC}) + K_{I4}\int_0^t (0.96 * P_{PV} - P_{AC})dt \quad (23)$$

$$\alpha^* = (\alpha_1^* + \alpha_2^*)/2 \quad (24)$$

Here, the reason behind considering phase shift contributions from both DC and AC side active power is to control the DC side voltage to the desired value. By making α_1^* and α_2^* in a close range through the controller gains, it can be assured that the active power at the DC and AC sides is balanced. This coupled with the voltage control loop assures that the DC side voltage is maintained at the value desired by the AC side voltage. This is a very unique characteristic of the proposed control algorithm in that the DC side voltage is controlled indirectly through other control loops. A simple explanation follows next.

Since the inverter is considered to be 98% efficient, we have:

$$\boldsymbol{P_{AC} = 0.98 * P_{DC}} \quad (25)$$

which means ,

$$\boldsymbol{P_{DC} = 1.0204 * P_{AC}} \quad (26)$$

Substituting the value of P_{AC} ,

$$\boldsymbol{P_{DC}} = \mathbf{1.0204} * \frac{\boldsymbol{V_t V_c}}{\boldsymbol{\omega L_c}} \boldsymbol{\alpha} \quad (27)$$

That is,

$$V_{DC} = \frac{\left(1.0204 * \frac{V_t V_c}{\omega L_c} \alpha\right)}{I_{DC}} \quad (28)$$

From (27), P_{DC} is also dependent on all the parameters at the AC side of the inverter. Hence, it is clear that the DC side active power is also directly related to the phase shift of the AC side voltage waveform for the given V_t (*t*) and V_c*(t).*

Since the voltage magnitude at the AC side, V_t (*t*) is being controlled, the active power control loop at the AC side determines the current drawn from the DC side. Also, the active power control loop at the DC side assures that the required amount of current, I_{DC} is being drawn from the PhV array. But, since the DC side voltage is dependent on all other quantities being controlled as given by (28), V_{DC} will be indirectly controlled to a value required to maintain the voltage at the AC side at the referenced utility voltage which will be verified from the results presented in the following section. Note, the controller gain values for the DC active power control loop should follow the pattern of the AC side active power loop so that the phase shifts, α_1^* and α_2^* can be reasonably averaged to obtain α^*.

3.4 SYSTEM CONFIGURATION

The system diagram of the IEEE 13 bus distribution test system is shown in Figure 15. It also shows the location of PhV generator considered in this chapter. It consists of a substation, 13 buses or nodes, 11 lines, and 8 loads. The loads comprise of a combination

of constant impedance, constant current and constant power (ZIP) loads as shown in the figure. The substation is connected to the 115 kV transmission system and the voltage is stepped down to 4.16 kV (RMS, line-to-line) by a distribution transformer (T1). There is one more transformer (T2) which steps down 4.16 kV to 480V to supply a particular load.

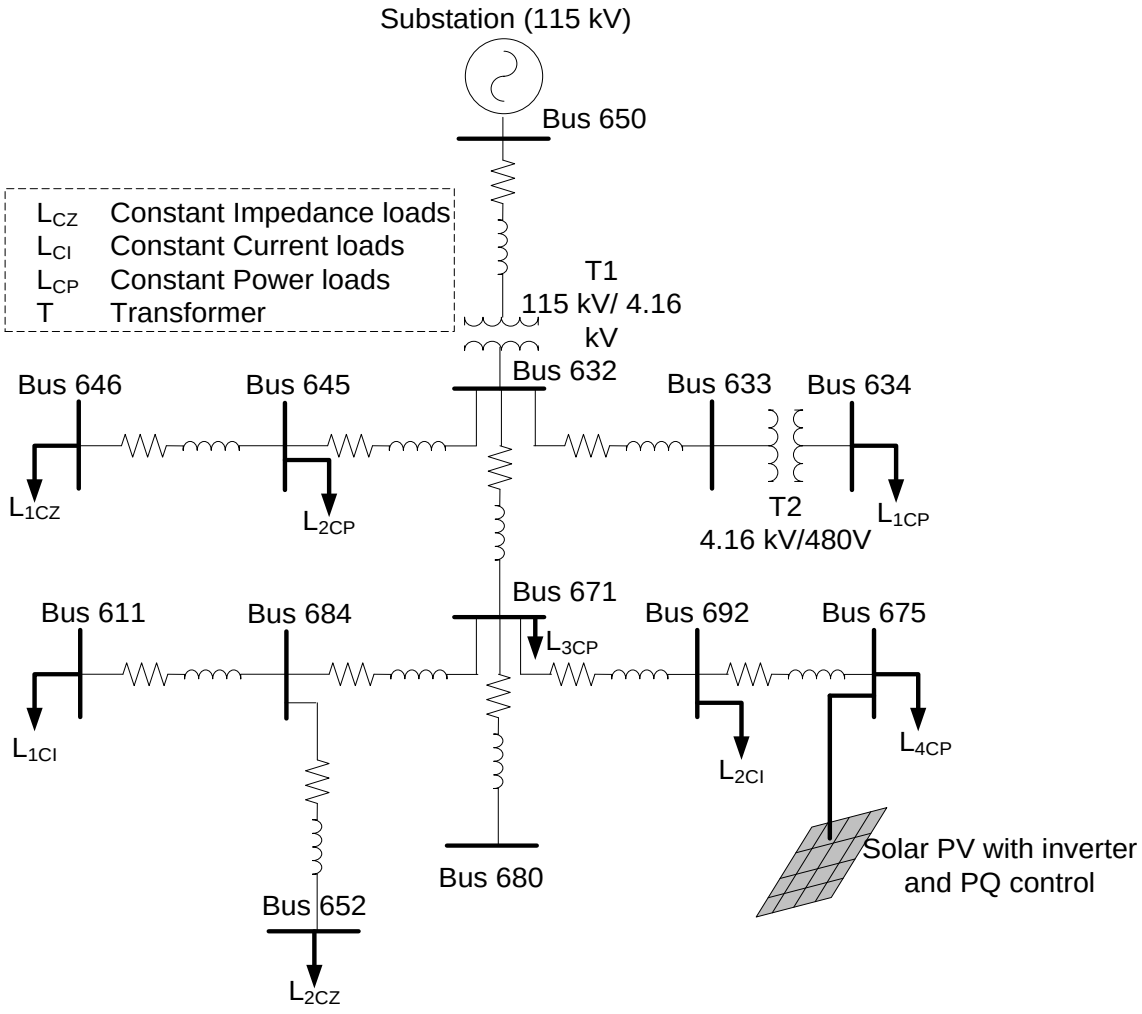

Figure 15. Diagram of IEEE-13 bus distribution feeder.

3.5 SIMULATION RESULTS AND DISCUSSIONS

Active and reactive power (P-Q) Control

In order to demonstrate the P-Q control algorithm in the IEEE 13-bus distribution feeder, Bus 675 is chosen for study. The P and Q references of the inverter-based PhV generators are taken from the active power load, P_{load}, and the reactive power load, Q_{load}, of Bus 675. The base case load of Bus 675 is 29 kW and 25 kVar. Two cases are considered for this study.

- Case1: P_{load} is increased to a peak value of 43.5 kW at t = 6 s and Q_{load} is increased to a peak value of 34.5 kVar at t = 9 s.
- Case 2: both P_{load} and Q_{load} are increased to the above mentioned values at t = 6 s.

Figure 16 (a and b) shows the active and reactive power profiles of the PhV generator as compared to the local load profile of Bus 675 for Case 1. As shown in the figures, both active and reactive load profiles at both loading levels are closely tracked by the PhV generators installed at that bus. The ripples seen in Figure 16 (a) at t = 9s is an effect of reactive load change at that instant. Similarly, Figure 17 (a and b) shows similar profiles with both loads increasing at the same time instant. It is observed that the active and reactive power injection from inverter-based PhV systems closely tracked the load profiles before and after the load increase. Thus, with the proper inverter control proposed in section 3.2, the PhV systems can supply the local load through their dynamic behavior.

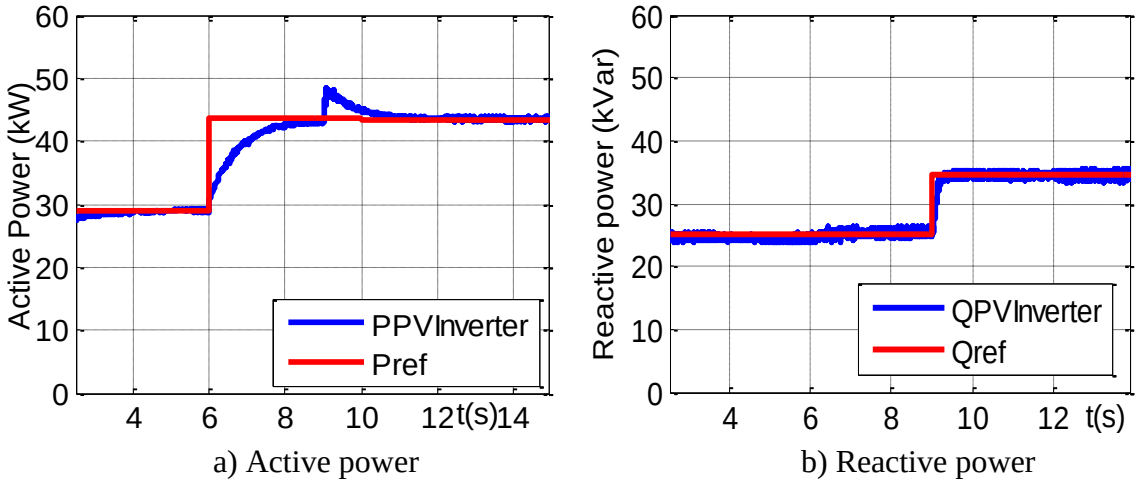

a) Active power b) Reactive power

Figure 16. Case 1: Active power and reactive power at Bus 675.

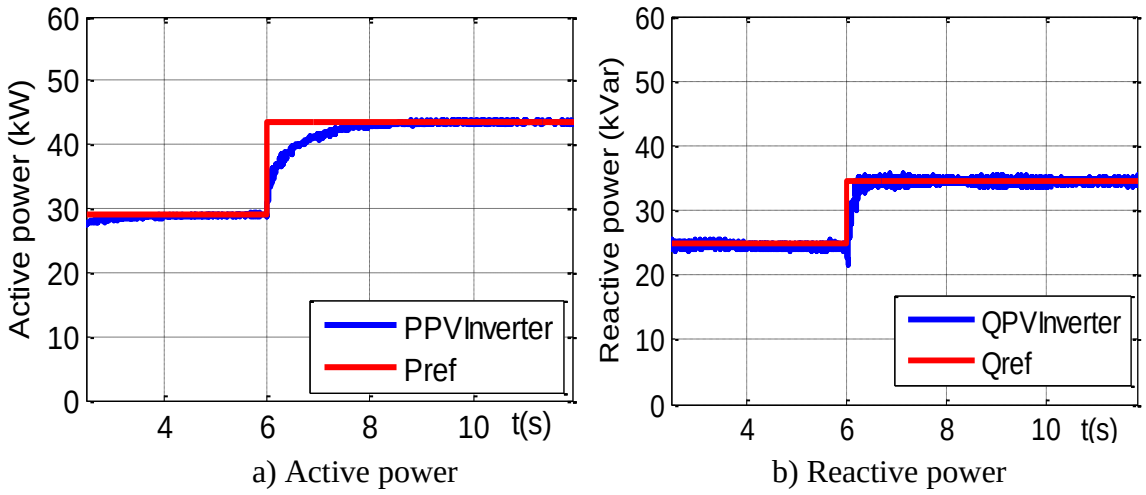

a) Active power b) Reactive power

Figure 17. Case 2: Active power and reactive power at Bus 675.

The controller gain parameters chosen for P-Q control study are shown in Table 3.

Table 3 Controller gain parameters for P-Q Control

Q Control Loop	K_{p1}	4.5×10^{-8}
	K_{i1}	5×10^{-7}
P Control Loop	K_{p2}	2.5×10^{-10}
	K_{i2}	3×10^{-9}

MPPT and Voltage (P-V) Control

The proposed MPPT and voltage (P-V) control is also tested for a PhV generator connected to the same bus 675 of the IEEE 13-bus feeder. With the topology as shown in Figure 9b, the PhV generator with the booster and inverter is connected to the system. Since, the IEEE 13-bus distribution feeder at Bus 675 is at 4.16kV (RMS, line-to-line), this voltage is stepped down to 480V (RMS, line-to-line) while connecting the PhV array/converters assembly in order to avoid a large DC voltage requirement.

Two scenarios are considered for simulation to prove the effectiveness of the proposed control method.

- Case 1: Change in solar irradiance level
- Case 2: Change in PhV cell temperature

Both of the above cases directly impact the power output of the PhV array and hence, affect the MPP.

The PhV array under study for the proposed PV control has 125 strings with each string having 4 panels in series. The MPP for a single panel of KC200GT at 1000W/m^2 and 25^{o}C (STC) is 200 W. Hence, the MPP reference power for the entire array at STC is 125×4×200 = 100 kW. The value of MPP reference point for all the values of considered irradiance are obtained from the lookup table approach as described in Section 3.3.

Figure 18 (a through e) shows the simulation results for the case when there is an increase in solar irradiance from 800 W/m^2 to 1000 W/m^2 at time t = 15s. Figure 18a shows the PhV array active power output. The MPP reference for the irradiance of 800 W/m^2 is 79.25 kW. With the controller loop 1 in Figure 12, the duty cycle, δ^* for the operation of DC-DC booster is obtained because of which the PhV array is capable of operating at the referenced MPP point as evident from the plot. It is clear that the actual PhV array power output follows the reference very closely. Figure 18b shows the inverter active power output which clearly reveals the effectiveness of the active power control strategy in tracking the referenced waveform which is about 96% of the output of the PhV array as explained in Section 3.3. Hence, this value is around 4% less than the one shown in Figure 18a.

From Figure 18c, it is clear that the AC side RMS voltage is maintained at 273V (0.98pu) before and after the change in irradiance. Figure 18d shows the plot of DC side voltage or inverter input voltage. It can be seen that it is stably maintained in the range of 700V to 800V before and after the irradiance level is increased. This is in the range of a value

which is theoretically desired in order to achieve 480 V_{RMSLL} at the AC side of the inverter. From theory, $V_{DC} \cong 1.634 * V_{RMSLL}$ which would be: $\cong 1.634 * 480 \cong 785\, V$ in the present system. Hence, the indirect control of DC side voltage considering the power balance between the AC and DC side of the inverter is clearly demonstrated in this case. Figure 18e shows the average active power at the DC and AC sides of the inverter. It can be seen that the active power is properly balanced while considering the inverter losses. Hence, the DC side active power is slightly greater than the AC side power.

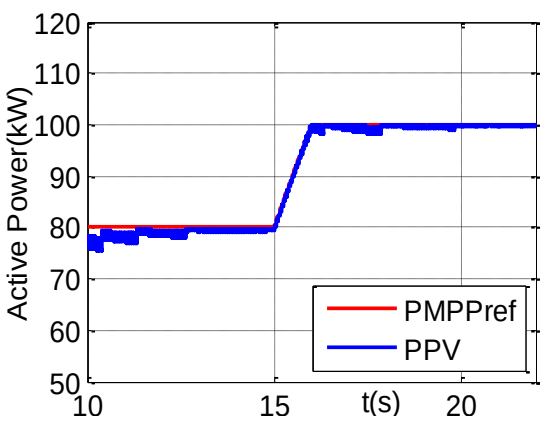

a) PhV array active power output

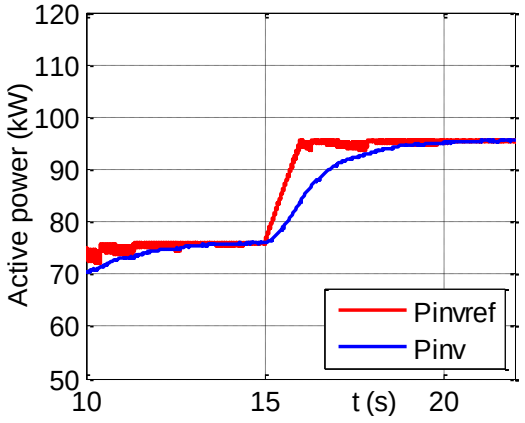

b) Inverter active power output

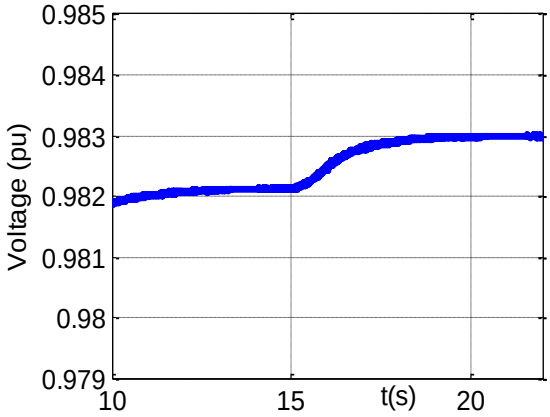

c) Voltage at PCC (RMS)

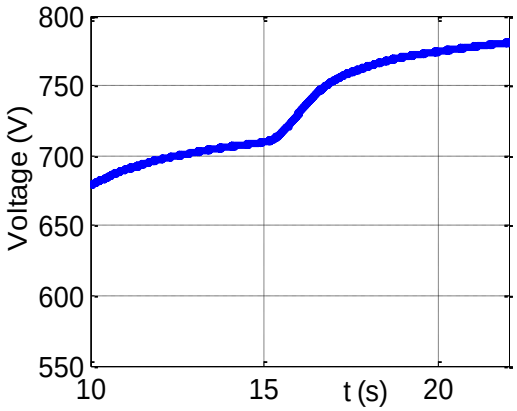

d) DC-DC booster output voltage

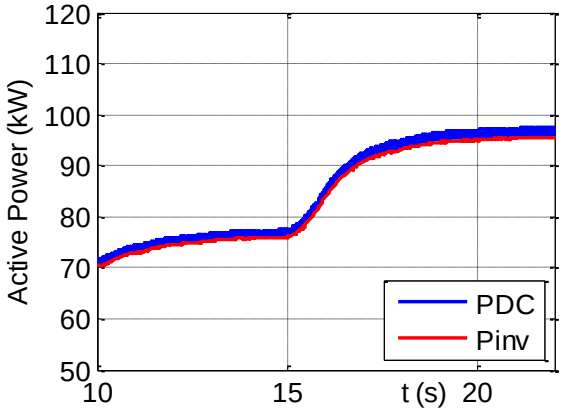

e) Active power at DC and AC sides

Figure 18. MPPT and Voltage (P-V) control results with varying irradiance.

Figure 19 (a through e) shows the results for Case 2 when the cell temperature of the PhV array increases from 25^{o}C to 75^{o}C at time t = 13s at the irradiance level of 1000 W/m^{2}. There is an inverse relationship between the cell temperature and MPP. Hence, with the temperature increase, the MPP reference decreases from 100 kW to 75.7 kW. Figure 19a shows the plot of active power output of the PhV array. It is clearly visible that the controls act effectively in tracking the referenced MPP very closely even for the decrease in MPP as in this case. The inverter active power output also closely tracks the reference which is 96% of the PhV power as shown in Figure 19b. It can be observed from Figure 19c that the AC side RMS voltage is maintained at 273 V (0.98 pu) throughout the simulation period. Most importantly, Figure 19d shows the effectiveness of indirect DC side voltage control with the proposed method in this scenario as well. The voltage is maintained at around 700V which is a reasonable value according to the discussions in Case 1 above. Figure 19e shows the active power at the DC and AC sides of the inverter. It clearly proves the effectiveness of the proposed control strategy in maintaining the power balance considering the inverter losses.

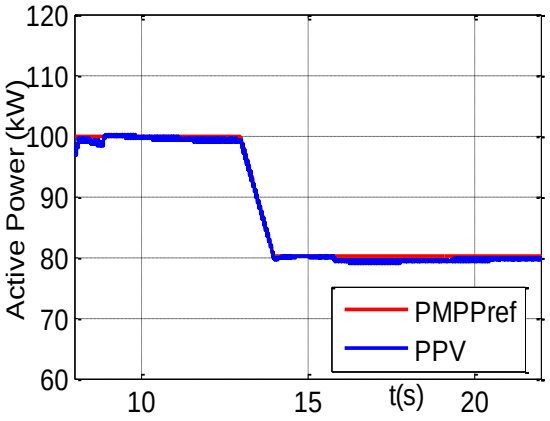

a) PhV array active power output

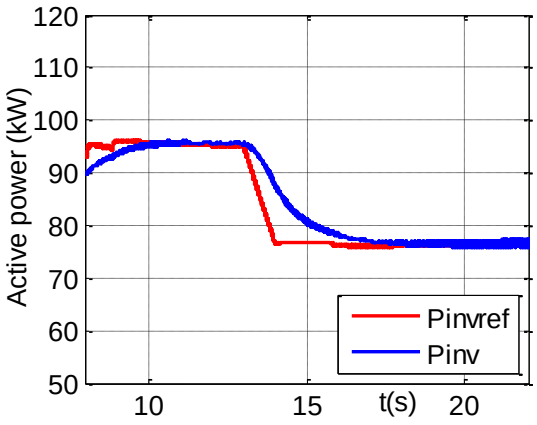

b) Inverter active power output

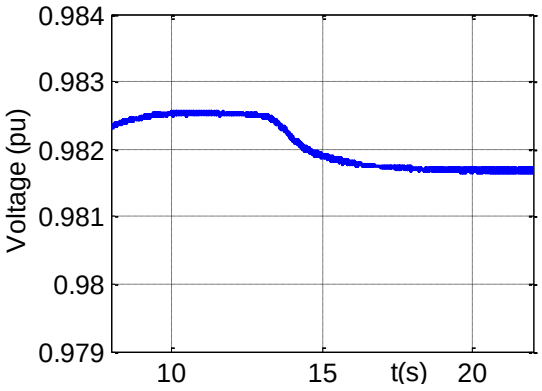

c) Voltage at PCC

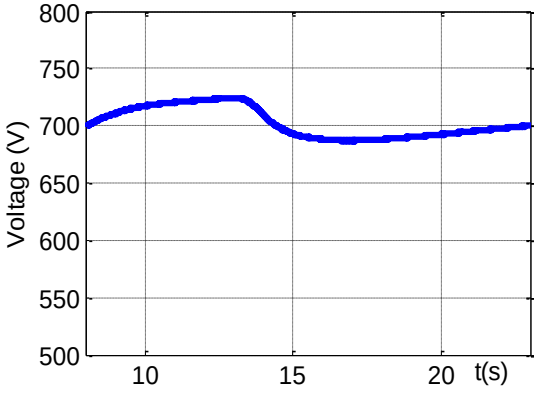

d) DC-DC booster output voltage

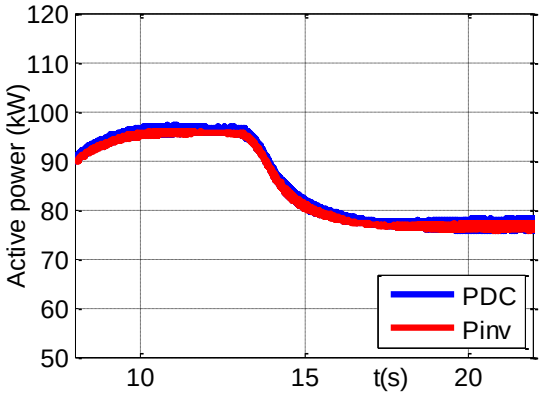

e) Active power at DC and AC sides

Figure 19. MPPT and Voltage (PV) control results with varying cell temperature.

The controller parameters chosen for P-V control is shown in Table 4.

Table 4 Controller gain parameters for P-V Control

MPPT Control Loop	K_{p1}	0.16×10^{-8}
	K_{i1}	0.16×10^{-5}
Voltage Control Loop	K_{p2}	0.001
	K_{i2}	0.02
P_{DC} Control Loop	K_{p3}	1.5×10^{-9}
	K_{i3}	1.5×10^{-8}
P_{AC} Control Loop	K_{p4}	1.5×10^{-9}
	K_{i4}	1.5×10^{-8}

3.6 CHAPTER CONCLUSION

In this Chapter, P-Q and P-V controls for solar arrays are discussed. The contribution of this Chapter can be summarized as follows:

- The capability of active and reactive power control is investigated in IEEE 13-bus distribution test feeder. The dynamic behavior of solar PhV generators following the local load pattern is presented. It is effective in power flow control and in maintaining the voltage stability in future power systems.
- Next, a unique algorithm for MPPT and voltage control for PhV generators is proposed in a two stage configuration. The reference value of MPP is procured by plotting series of PV curves for different irradiance levels and cell temperatures. Then, feeding this data into a look up table to linearly approximate the value of corresponding MPP with respect to the change of these parameters. The DC side

voltage is controlled indirectly through the power balance of the DC and AC stages which is a unique characteristic of the proposed method.

- These controls ensure that the demands are properly served and the voltages at the AC and DC side are properly maintained at the desired values as required by the utility. Moreover, the MPPT control ensures that the installed solar PhV generators are optimally utilized for the given irradiance level. The simplicity of the proposed control algorithms and popularity of PI controllers support a wide acceptance of the control methods presented.

Note, the proposed control methods, which are based on instantaneous non-active power theory, can be implemented in the grid integrated solar PhV generators for efficient P-Q and P-V controls. The significance of both the proposed control methods is that these are entirely developed in abc reference frame considering the measurement based approach. Hence, it leads to a simple control approach that avoids the conversions between the reference frames like from abc to dq0 and vice versa. Furthermore, the approach is not sensitive to measurement noise as it is dependent on the measurements of the past cycles rather than at a particular time instant.

CHAPTER 4
COORDINATED V-F AND P-Q CONTROL OF PHV GENERATORS WITH MPPT AND BATTERY STORAGE IN MICROGRIDS

The microgrid concept allows small distributed energy resources (DERs) to act in a coordinated manner to provide the necessary amount of active power and ancillary service when required. The greater incentive to the deployment of renewable energy based DERs like solar Photovoltaic (PhV) generators in microgrid is due to environmental concerns and fast depletion of fossil fuels. In this Chapter, an approach for coordinated and integrated control of solar PhV generators is proposed with the maximum power point tracking (MPPT) control and battery storage control such that voltage and frequency (V-f) support is provided for an islanded microgrid. Also, active and nonactive/reactive power (P-Q) control with solar PhV, MPPT and battery storage is proposed. The control strategies show effective coordination between inverter V-f (or P-Q) control, MPPT control, and energy storage charging and discharging control. The simulation studies are carried out with the IEEE 13-bus feeder test system in grid connected and islanded microgrid modes. The results clearly verify the effectiveness of proposed control methods.

4.1 SOLAR PHV MODELING AND PHV SYSTEM CONFIGURATION

The modeling and validation of solar PhV generators is the same as described in Section 3.1 of Chapter 3. Therefore, it will not be repeated here. PhV system configuration, however, is entirely different and would be described here in detail.

Figure 20 shows the solar PhV system configuration for V-f and P-Q control with PhV operating at MPPT including the battery storage backup. It is a two-stage configuration where a DC-DC boost converter is used for MPPT control. The system also considers a battery back-up in case of emergencies while maintaining the voltage and frequency of the microgrid or while trying to supply the critical loads.

A battery is connected in parallel to the PhV generator to inject or absorb active power through a bidirectional DC-DC converter which can act either as a boost or buck converter with the help of controller signals provided to the converter switches. When the battery is absorbing power, the converter acts as a buck converter and when battery is injecting power to the grid, it acts as a boost converter.

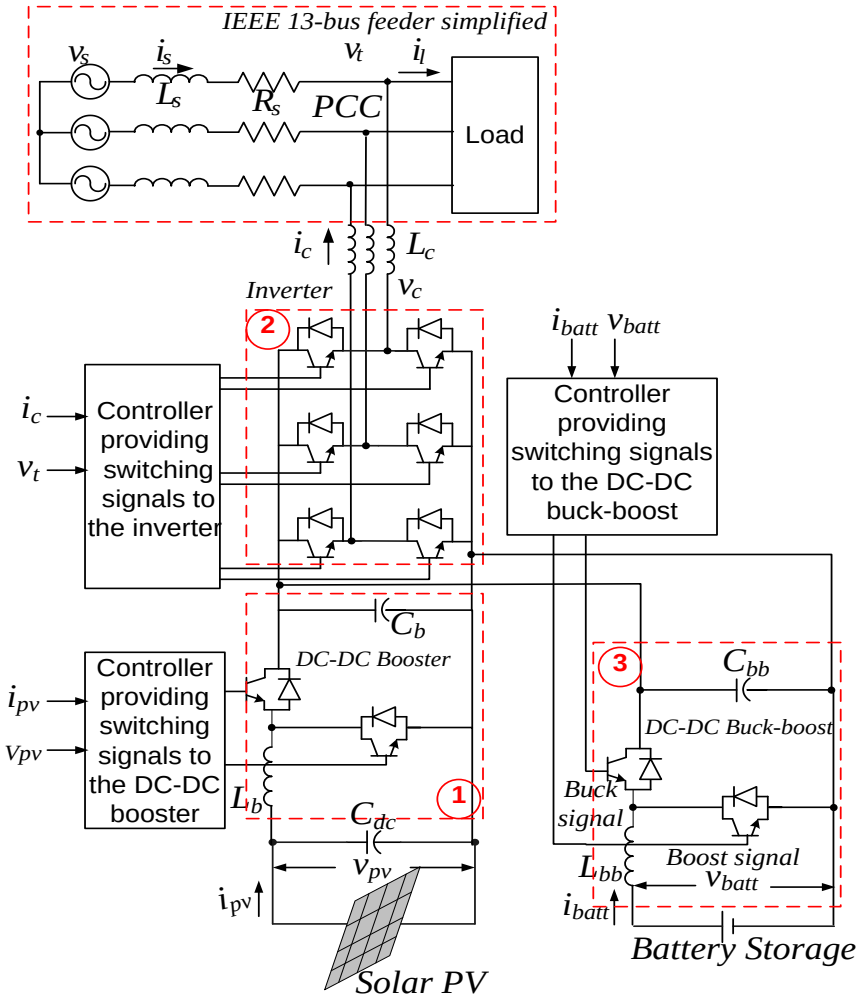

Figure 20. System configuration of V-f control with solar PhV generator operating at MPPT with a battery storage system.

The PhV system is connected to the grid through a coupling inductor L_c. The coupling inductor filters out the ripples in the PhV output current. The connection point is referred to as the point of common coupling (PCC), and the PCC voltage is denoted as v_t. The rest of the system in Figure 20 denotes the IEEE 13-bus distribution feeder which is simplified as a substation with the feeder equivalent impedance, $R + j\omega Ls$. The detail of the IEEE-13 bus system has been already described in Chapter 3. The PhV source is

connected to the DC link of the inverter with a capacitor C_{dc}. The parameters considered for bidirectional DC/DC converter is shown in Table 5. The parameters of DC/DC booster remain the same as mentioned in Section 3.1 of Chapter 3.

Table 5 Parameters considered for bidirectional DC/DC converter

f_s	20kHz
L_{bb}	0.9mH
C_{bb}	0.4982F

The control algorithms developed are based on the instantaneous non-active power theory as described in Chapter 3 with the active and reactive/nonactive power given by (29) and (30) as explained before.

$$\boldsymbol{P(t)} \approx \frac{\boldsymbol{V_t V_c}}{\boldsymbol{\omega L_c}} \boldsymbol{\alpha} \tag{29}$$

$$\boldsymbol{Q(t)} \approx \frac{\boldsymbol{V_t}}{\boldsymbol{\omega L_c}} (\boldsymbol{V_t - V_c}) \tag{30}$$

where, α is the phase angle of $v_c(t)$ relative to the PCC voltage.

Battery Modeling and Sizing

In this work, the battery model is taken from the MATLAB *SimPowerSystems* library with appropriate parameters which will be used for the proposed V-f and P-Q controls. The detailed description about the battery model is given in [82]. Due to the intermittent and uncertain nature of solar power output and also the highly fluctuating load demands,

deep cycle lead acid batteries are the most common type of battery storage in microgrid applications such that the maximum capacity of the battery can be utilized. Hence, in this paper, a battery is modeled as a lead acid battery with appropriate choice of parameters for deep cycle application. It is assumed that the lead acid battery can be discharged up to SOC of 20% for both proposed control methods, and it is assumed that it is able to charge up to SOC of 80%.

The battery model in [82] is an analytical model with two equations representing the battery discharge and charge models. The battery discharge and charge model for a lead acid battery is given by (31) and (32), respectively.

$$\boldsymbol{V_{Batt} = V_o - R.i - K\frac{Q}{Q-it}(it + i^*) + Exp(t)} \quad (31)$$

$$\boldsymbol{V_{Batt} = V_o - R.i - \left[K\frac{Q}{it-0.1Q}\right]i^* - \left[K\frac{Q}{Q-it}\right].it + Exp(t)} \quad (32)$$

where V_{batt} is the battery voltage(V), V_o is the battery constant voltage (V), K is polarisation constant (V/Ah) or polarisation resistance (Ω), Q is the battery capacity (Ah), $it = \int idt$ = actual battery charge (Ah), A is exponential zone amplitude (V), B is exponential zone time constant inverse (Ah^{-1}), R is the internal resistance(Ω), i is the battery current (A), and i^* is the filtered current(A).

In this model, the term for polarization voltage and polarization resistance is considered to model the Open Circuit Voltage (OCV) of the battery more accurately. The term inside

the first square bracket in Eq. (32) represents the polarization resistance and the second square bracket represents the polarization voltage.

The size of the battery is selected to provide a maximum backup power to compensate for the solar PhV generation in case of very little or no irradiance level. In the present case, the MPP of PhV generator is 100 kW at STC. Hence, the battery is chosen to provide this amount of power for maximum of 1 hour in the case of the critical case such as no irradiance. Since, the battery backup considered in this work is for short timeframe applications like frequency control and supplying power to critical loads in the event of emergency situations, 1 hour of battery backup is considered to be enough for other backup generators to take over the controls of providing frequency or active power balance to the microgrid.

The battery chosen for this work is MK power battery, model no: ES20-12C. This particular model of the battery is chosen based on the maximum discharge current capability of 300A for 5secs and maximum charging current of 6A to provide backup power for 1 hour in extreme condition of zero irradiance. The calculation of ES20-12C model battery design for the purpose of V-f and P-Q control is as follows:

Maximum discharge current in 5 secs = 300 A

Total battery voltage considered = 500 V.

Voltage of individual battery pack = 12V

Total number of batteries in series = 500/12 = 41.6 ≈ 42.

Nominal capacity of a battery = 20 Ah = 20 A for 1 hour

Considering maximum discharge current of 300 A, total number of strings in parallel = 300/20 = 15 strings in parallel

Hence, total maximum energy = 20 Ah × 42 × 12V × 15=151200Wh = 151.2kWh (for 1 hour)

Figure 21 show the discharge characteristics of the battery considered for study. Figure 21a shows a plot for the value of nominal current of 100 A which shows distinct nominal and exponential zones of the curve. Figure 21b shows the discharge curves for different values of discharge currents. It is clear that the discharge time drastically decreases with the increase in discharge current. With the nominal current of 100A, the battery can provide power for a little more than 3 hours. However, at the maximum current of 300 A, it can provide power only for around an hour before it fully gets discharged.

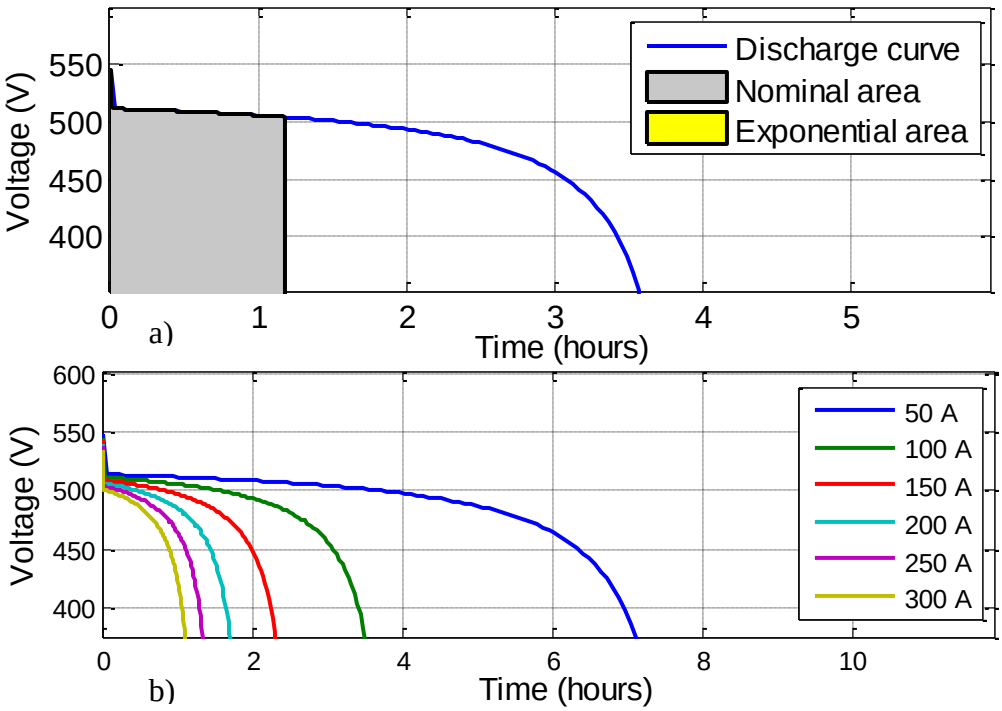

Figure 21. Battery discharge characteristics a) Nominal discharge current (100A); b) Varying discharge currents.

IEEE 13 bus distribution test feeder

The IEEE-13 bus distribution feeder configuration is the same as described in Chapter 3.

The location of Solar PhV generator for V-f and P-Q control is as shown in Figure 22

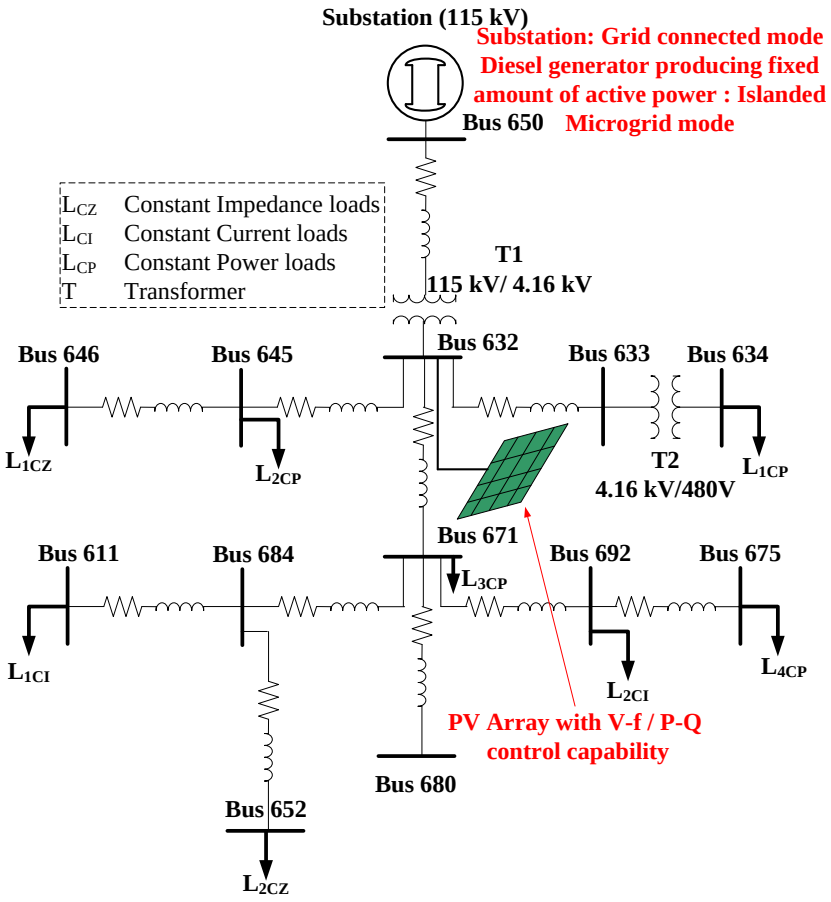

Figure 22. IEEE-13 bus distribution feeder showing solar PhV generator for V-f and P-Q control.

In the grid connected mode, the substation at 115 kV is considered as a source; however in an islanded microgrid case, the substation is replaced by a diesel generator producing a fixed amount of active power as referenced by the central controller (CC) of the microgrid.

4.2 VOLTAGE AND FREQUENCY (V-f) CONTROL WITH MPPT AND BATTERY

The MPPT and battery integrated V-f control diagrams are shown in Figure 23 and Figure 24, respectively. The control comprises of one loop for MPPT control, two different loops for V-f control at the inverter side, and another loop for battery power management.

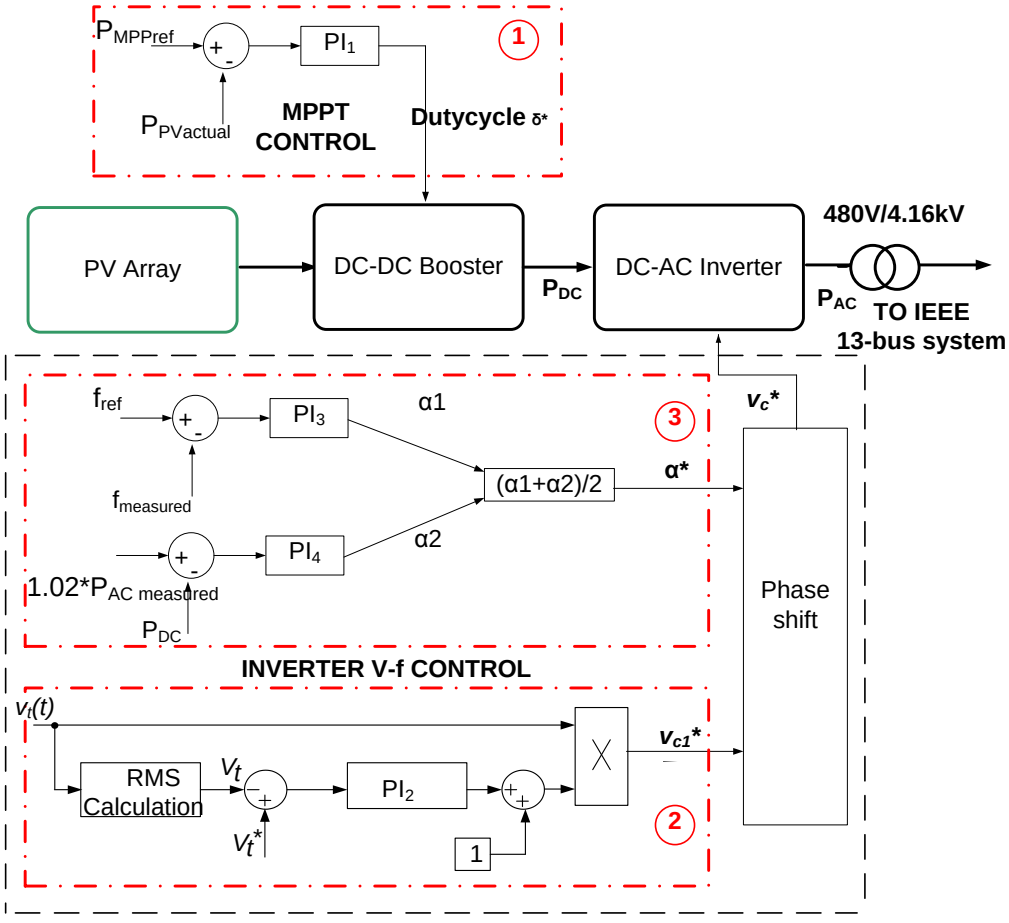

Figure 23. Integrated Solar PhV MPPT and V-f control diagram.

The loop 1 in Figure 23 is a MPPT control which is the same as described in Chapter 3. The actual PhV power output, P_{PV} is compared with the MPP reference, P_{MPPref} from the look up table of irradiance versus MPP and this error is fed to a PI controller, PI_1 which outputs the duty cycle δ^* for the DC-DC booster so that the array always operates at the referenced point by changing this duty cycle. The equation for this control loop is revisited as given by (33). Here, K_{p1} and K_{i1} are the controller proportional and integral gains respectively for this control loop.

$$\delta^* = K_{p1} * \left(P_{MPPref} - P_{PV}\right) + K_{i1} * \int_0^t (P_{MPPref} - P_{PV})\ dt \tag{33}$$

For voltage control at the AC side, another feedback PI controller, PI_2 is used. The control logic is exactly the same as described in Section 3.3. The control scheme can be specifically expressed as (34), which is exactly the same as (21). This equation is revisited here for convenience.

$$v_{c1}^*(t) = v_t(t)\left[1 + K_{P2}\left(V_t^*(t) - V_t(t)\right) + K_{I2}\int_0^t \left(\left(V_t^*(t) - V_t(t)\right)dt\right)\right] \tag{34}$$

where K_{P2}, K_{I2} are the gain parameters of the PI controller 2.

The frequency control is carried out by controlling the active power output at the inverter side as shown in the outermost loop 3. The referenced microgrid frequency of 60 Hz is compared with the measured value, and this error is fed to the PI controller PI_3 that provides the phase shift contribution α_1^* so as to shift the voltage waveform in timescale.

Thus, the active power injected will be enough to maintain the frequency at the nominal value 60 Hz. The equation for this control is given by (35).

$$\alpha_1^* = K_{P3}\left(f_{ref} - f_{measured}\right) + K_{I3}\int_0^t \left(f_{ref} - f_{measured}\right)dt \quad (35)$$

There is another controller PI_4 used in the same loop 3. This controller maintains the active power balance between the AC and DC side of the inverter. The reference signal for PI_4 is obtained from the dynamically changing active power injection from the inverter at the AC side as determined by the output of PI_3. Then, this measured AC side active power, $P_{ACmeasured}$ is multiplied by a factor of 1.02 considering the efficiency of inverter as 98% such that the DC side active power is 102% of the AC side active power. The DC side active power is compared with this value of AC side power and the error is fed to PI_4 to obtain the phase shift contribution from this loop as α_2^*. The equation for this control is given by (36).

$$\alpha_2^* = K_{P4}(1.02 * P_{AC} - P_{DC}) + K_{I4}\int_0^t (1.02 * P_{AC} - P_{DC})dt \quad (36)$$

The phase shift contributions from DC and AC sides, α_1^* and α_2^* are then averaged as given by (37) to obtain the final phase shift, α^* of the voltage waveform , v_{c1*} which will then generate the voltage reference signal v_{c*} for the inverter PWM.

$$\alpha^* = (\alpha_1^* + \alpha_2^*)/2 \quad (37)$$

Here, the reason behind considering phase shift contributions from both DC and AC side active power is to control the DC side voltage to achieve the desired value. By making α_1^* and α_2^* in a close range through the controller gains, it can be assured that the active power at the DC and AC sides is balanced. This, coupled with the voltage control loop, assures that the DC side voltage is maintained at the value desired by the AC side voltage.

The controls shown in the diagram of Figure 23 and described above are also integrated with the battery power control shown in the diagram in Figure 24. The battery is incorporated into the PhV system configuration in order to supply or absorb active power to support the frequency control objective with the PhV generator. If there is abundant solar power and the active power required for frequency control is less than PhV MPP, then the battery will be charged; otherwise, if there is not enough solar power available or if the active power required for frequency control is more than maximum available power from PhV, then the battery will supply the deficit power in order to follow the load and maintain the microgrid frequency at 60 Hz. Hence, the control method for the battery charge/discharge depending on this requirement is developed as shown in Figure 24.

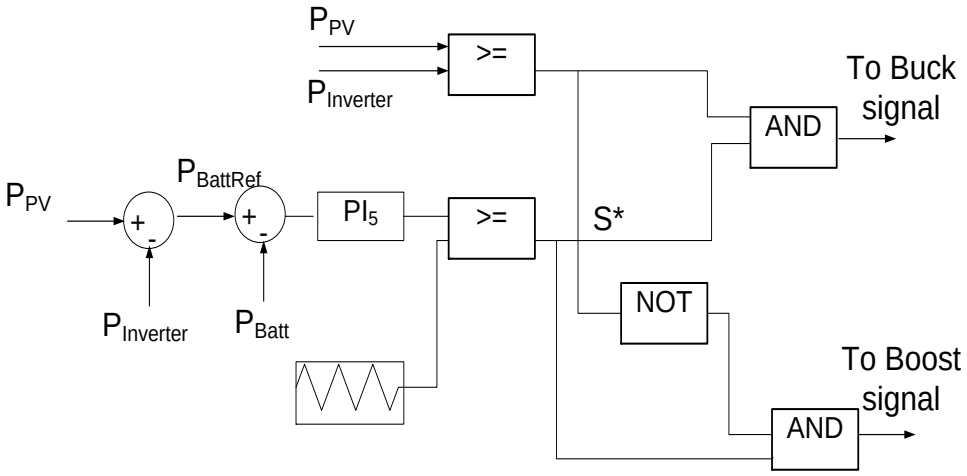

Figure 24. Battery power control diagram.

In Figure 24, the reference power to the battery, $P_{Battref}$ is generated dynamically by subtracting the inverter active power injection, $P_{inverter}$ from the power generated by PhV, $P_{PV.}$ The controller comprises of a PI controller, PI_5 which receives the error signal obtained after subtracting the actual battery power, P_{batt} from the battery reference, $P_{Battref}$. The signal obtained from PI_5 is then compared with a triangular waveform of unity magnitude to generate the signal, S^*. This is similar to common Pulse Width Modulation (PWM) in inverter controls. K_{p5} and K_{I5} are the proportional and integral gains, respectively. The equation for this control is given by (38).

$$S^* = K_{P5}\left(P_{Battref} - P_{Batt}\right) + K_{I5}\int_0^t \left(P_{Battref} - P_{Batt}\right)dt \quad (38)$$

One more step is considered to differentiate the charging and discharging mode of the battery. This is undertaken by comparing P_{PV} with $P_{inverter}$. If $P_{PV} >= P_{inverter}$, the battery is in charging mode, hence, the signal obtained from the PWM, S^* and the result of this comparison is passed through a logical AND to generate a switching signal to activate the Buck mode of the DC-DC converter. If $P_{PV} >= P_{inverter}$ is false, (i.e., $P_{PV} < P_{inverter}$), the opposite of this signal and S^* is passed through a logical AND to generate a switching signal to activate the boost mode of the DC-DC converter. Hence, with this control logic, the converter is capable of operating in both directions, therefore, effectively charging and discharging the battery whenever required. This will be verified through the results presented in Section 4.4 of this dissertation.

Modification of V-f control to consider Battery State of Charge (SOC) constraint

When there is abundant solar irradiance available and the active power required for the microgrid frequency control is less than active power produced by solar PhV generator at MPP i.e. $P_{fcontrol} < P_{PVMPP}$ and at the same time the battery SOC is 80%, then, the battery cannot be charged beyond this upper limit of SOC. In such case, decreasing the output power of solar PhV generator would lead to underutilization of the solar resource. Hence, a global control mechanism is required in a microgrid which can transition the PhV control from frequency control mode to constant power mode with power to be generated at P_{PVMPP}. Meanwhile, there should be a mechanism to allow any other generator of the microgrid to handle the frequency control problem. In the microgrid system under consideration, there is a diesel generator which can decrease its generation in order to match the PhV generation increase. Hence, the power balance of the system will be maintained to eventually control the microgrid frequency.

Similarly, when the irradiance is low such that the maximum power from PhV generator is not enough to maintain the microgrid frequency i.e. $P_{fcontrol} > P_{PVMPP}$ and at the same time, the battery SOC is 20%, then the battery will not be able to back up the PhV generator and hence, the frequency control function needs to be transferred to other available generator if possible, in this case, a diesel generator. Again, a global control mechanism becomes an absolute necessity to allow the transition of PhV generator control from frequency control mode to constant MPP mode and the transition of diesel generator control from constant active power mode to frequency control mode such that

the frequency stability of the microgrid can be maintained. Figure 25(a through d) shows the modifications of controls at different levels in the microgrid. Figure 25a shows the transition of the diesel generator control from constant active power control to frequency control. Instead of considering the error between the reference electrical power and the measured electrical power to generate the mechanical power reference, the frequency error is considered in the controls. Figure 25b shows the modification in V-f control loop of the PhV inverter which includes the transition to another loop to take care of the constant active power control at MPP. The transition timing can be obtained from a separate module which compares active power generated from the PhV generator with the inverter active power injection to maintain frequency and at the same time monitors the SOC of the battery and comes up with a time at which the controls should transition from one mode to the other. This logic, however, has not been implemented in the simulation. During the simulation process, the transition timing is heuristically selected as 8 seconds just to observe the smoothness and the effect of the transfer of controls.

The consideration of two different loops for the control transition as shown in Figure 25b may lead to a large surge during the transition process, because of the action of integral block which may sum up all the past errors and also due to the change in the scale of inputs. This type of hard transition can be avoided through an approach as shown in Figure 25c in which only the input gain parameters are changed during the simulation process but considers a common integral block for both the cases. The smoothness in the transition of controls can be observed later in the results presented.

Similarly, Figure 25d shows a slight modification in the battery control in order to take care of the battery SOC. When the SOC > 80% or SOC < 20%, then, both the charge and discharge mode are given the value of 0 such that this when logically ANDed to the other inputs as shown in the figure, the output is always zero for these two cases. The charge mode would take a value of 1 and the discharge mode would take a value of 0, and vice versa for discharge mode.

Through these slight modifications in the existing control structure, the IEEE 13-bus system acting as a microgrid can handle the problem of under frequency and voltage during islanding even without the battery acting as a buffer which can be observed from the results presented later.

Figure 25. Modifications in controls to consider Battery State of Charge (SOC) constraint; a) Modification of diesel generator active power control; b) Modification of PhV inverter V-f control; c) Consideration of smooth transition of controls; d) Modification of battery bidirectional DC-DC converter control

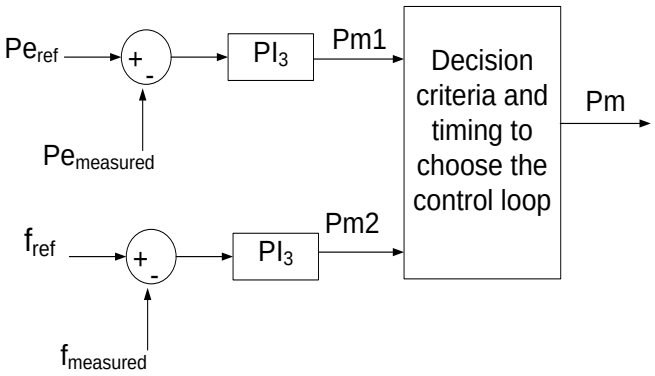
Pe_ref
+
-
PI3
Pm1
Pe_measured
Decision criteria and timing to choose the control loop
Pm
f_ref
+
-
PI3
Pm2
f_measured

a)

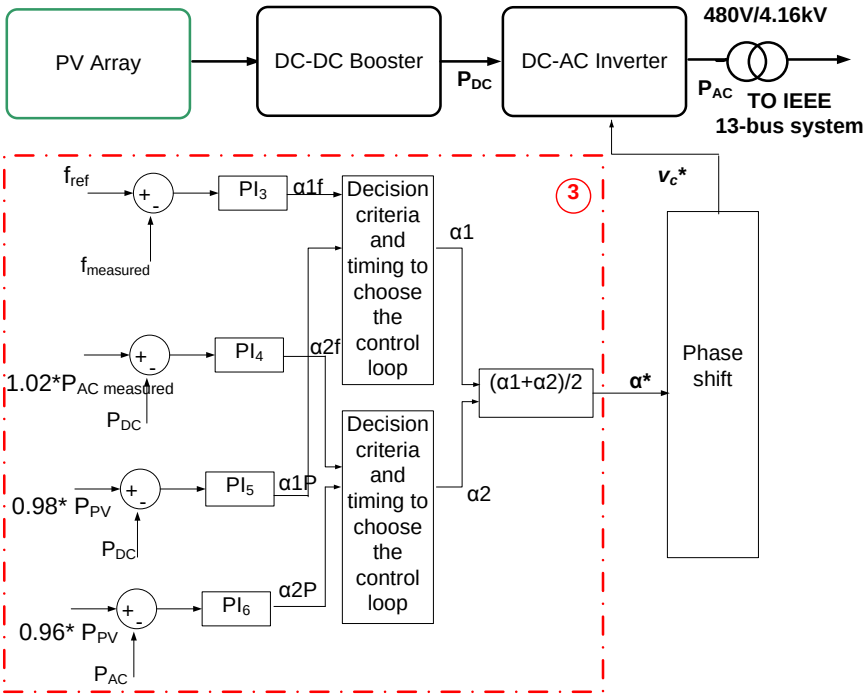
PV Array
DC-DC Booster
DC-AC Inverter
480V/4.16kV
P_DC
P_AC
TO IEEE 13-bus system
v_c*
3
f_ref
PI3
α1f
f_measured
Decision criteria and timing to choose the control loop
α1
PI4
α2f
1.02*P_AC measured
P_DC
(α1+α2)/2
α*
Phase shift
0.98* P_PV
PI5
α1P
P_DC
Decision criteria and timing to choose the control loop
α2
0.96* P_PV
PI6
α2P
P_AC

b)

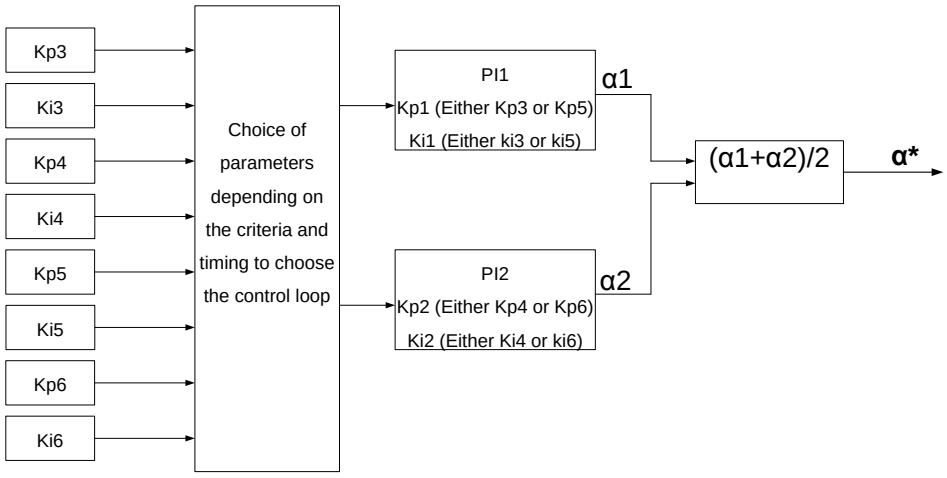

c)

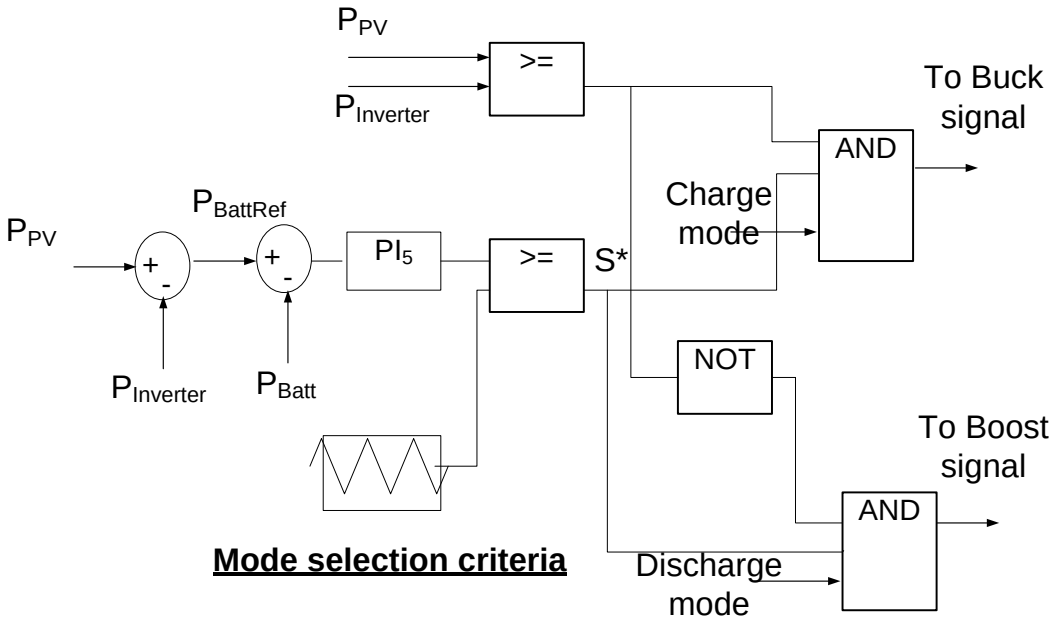

Mode selection criteria

If SOC <= 20% OR > = 80% , charge mode = 0; discharge mode = 0

d)

4.3 ACTIVE AND REACTIVE POWER (P-Q) CONTROL WITH MPPT AND BATTERY

This section presents the proposed coordinated active and nonactive/reactive (P-Q) power control with solar PhV integrated with PhV MPPT and battery controls. Either in grid connected or islanded mode, the microresources in microgrid may be required to supply the critical loads like hospitals, industries, etc. The proposed control strategy is applicable particularly to such cases. The MPPT control part to generate the duty cycle for a proper control of the DC-DC boost converter is the same as described in chapter 3 and section 4.2 above and hence, will not be repeated here. Figure 26 shows the P-Q control blocks only, leaving behind the MPPT control block which is actually also present in the entire integrated control system. The P-Q control initially proposed in [16] and implemented in a larger system in [83] is converted to a more robust control with the integration of MPPT control and battery storage control in the present work.

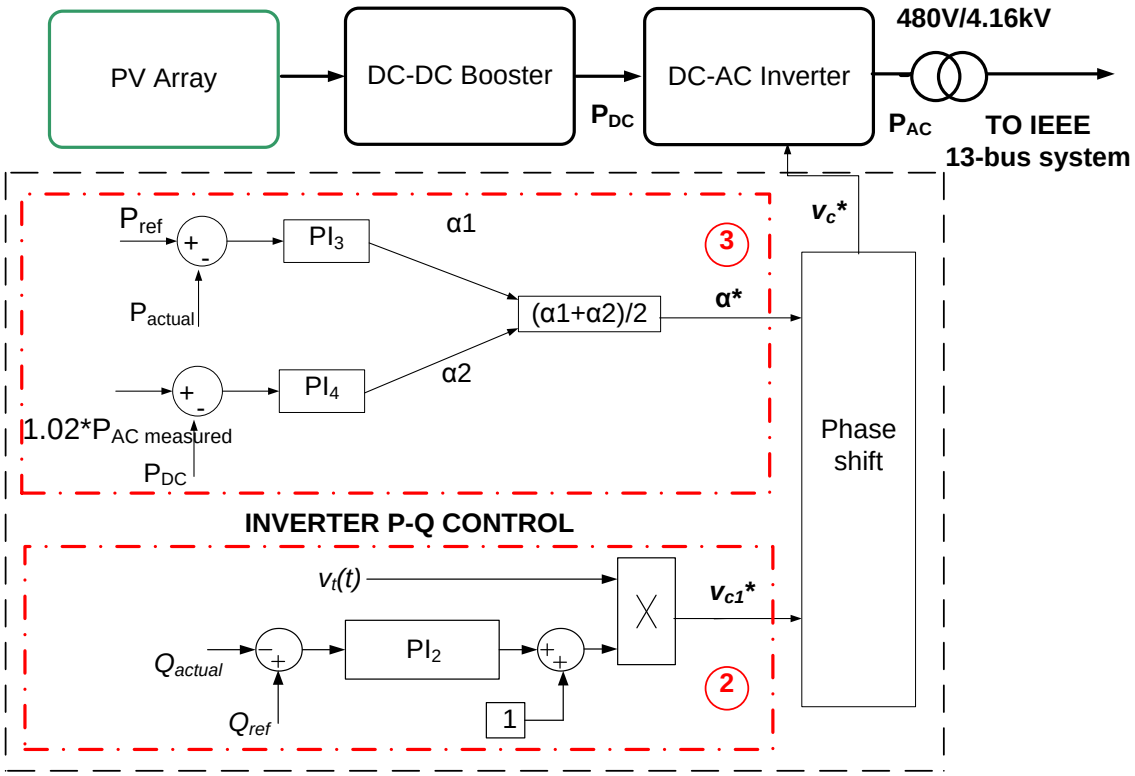

Figure 26. Integrated Solar PhV MPPT and P-Q control diagram.

The inverter side P-Q control is modified from the inverter V-f control. It is entirely based on the relationship of active and reactive power at PCC with inverter output phase and voltage magnitude as given by the equations (29) and (30), respectively. In this case, in loop 2 in Figure 26, the measured reactive power injection at PCC is compared with the referenced reactive load and this error signal is passed to the PI controller, PI_2. Then, the term obtained is multiplied by the terminal voltage v_t to obtain the reference voltage v_{c1}^* which is in phase with v_t. Loop 3 in Figure 26 handles active power control through the controller, PI_3 to generate the phase shift contribution α_1^* and at the same time to

ensure the active power balance between AC and DC sides through the controller, PI_4. This is already explained in detail in the previous section of V-f control. Thus, the equations for P-Q control are given by (39) through (42).

$$v_{c1}^{*} = \left(K_{P2}\left(Q_{ref} - Q_{actual}\right) + K_{I2}\int_0^t \left(Q_{ref} - Q_{actual}\right)dt + 1\right) v_t \quad (39)$$

$$\alpha_1^{*} = K_{P3}\left(P_{ref} - P_{actual}\right) + K_{I3}\int_0^t \left(P_{ref} - P_{actual}\right)dt \quad (40)$$

$$\alpha_2^{*} = K_{P4}(1.02 * P_{ACmeasured} - P_{DC}) + K_{I4}\int_0^t (1.02 * P_{ACmeasured} - P_{DC})dt \quad (41)$$

$$\alpha^{*} = (\alpha_1^{*} + \alpha_2^{*})/2 \quad (42)$$

Equation (39) represents the reactive power control loop, (40) represents the active power control loop, and (41) ensures the active power balance between the DC and AC sides of the inverter. Equation (42) averages the phase shift contribution obtained from the active power control at the AC and DC side such that the active power control at the AC side and the power balance objectives are taken into account.

The battery control integrated into the P-Q control is the same as the one described in the Section 4.2 above.

4.4 SIMULATION RESULTS AND DISCUSSIONS

This section presents the simulation results obtained with the application of the proposed control methods discussed in Section 4.2 and 4.3 to the IEEE 13-bus distribution feeder. First, the results obtained from coordinated V-f control are presented which is followed by the results from the coordinated P-Q control. In grid connected mode, the distribution

feeder is considered to be supplied by a central generator with a substation at Bus 650 and a diesel generator at 115 kV voltage level and a PhV generator connected at Bus 632 through a 480V/4.16kV transformer. In an islanded case, the distribution feeder is considered to be supplied by only by a diesel generator and a PhV connected at Buses 650 and 632, respectively.

Test of V-f control method

For the demonstration of the V-f control algorithm, two different irradiance cases are considered: Case 1 with Irradiance = 1000W/m^2 and Case 2 with Irradiance = 750W/m^2. While moving from the grid connected to microgrid mode, the diesel generator is controlled to generate fixed amount of active power according to the command from the central controller. The gain parameters of the controllers for V-f control with MPPT and battery for Case 1 is shown in Table 6. Slight changes in gain parameters are required when the irradiance changes to other values.

Table 6 Controller gain parameters for V-f Control (Case 1) with MPPT and battery

MPPT Control Loop	K_{p1}	6×10^{-8}
	K_{i1}	6×10^{-6}
Voltage Control Loop	K_{p2}	0.0004
	K_{i2}	0.005
Frequency Control Loop	K_{p3}	9.9×10^{-4}
	K_{i3}	5×10^{-3}
P_{DC} Control Loop	K_{p4}	0.8×10^{-9}
	K_{i4}	0.8×10^{-8}
Battery Control Loop	K_{p5}	1.5×10^{-8}
	K_{i5}	1.5×10^{-7}

The diesel generator produces a fixed amount of 1.25 MW for both cases throughout the simulation period as shown in Figure 27a. The same figure also shows the reactive power generated from the diesel generator for both cases. However, the active power generated by the diesel generator is not enough to fulfill the power demand of the microgrid.

Figure 27b shows the microgrid frequency which initially dips to 57.8 Hz due to the load-generation imbalance. The frequency control from the PhV generator starts at 2.2 sec which quickly regulates the frequency back to 60 Hz in 2 sec. Figure 27c shows the plot of the PCC voltage in p.u. It can be observed that the voltage is also quickly regulated at 1 p.u. after the control is started.

Figure 27d shows the active and reactive power injection from the PhV inverter to regulate the frequency and voltage of the microgrid. The active power injection from the inverter, which is required to maintain the frequency at 60 Hz in both cases, is around 80 kW. However, there is a difference in the share of the PhV generator and the battery energy storage while providing the required 80 kW to the microgrid. This is evident from Figure 27e which shows the active power from the PhV, the battery, and the inverter, respectively, for both cases. In Case 1, solar irradiance is abundant at 1000W/m^2 and hence, the PhV generates 100 kW which is more than required to maintain the microgrid frequency. The surplus 20 kW goes to charge the battery. Note, the negative sign in battery power means that it is a charging phase, i.e., the battery absorbs power. In Case 2, PhV generates only around 75 kW at MPP due to decreased irradiance. This is not sufficient to maintain the microgrid frequency at 60Hz. Hence, the deficit power around 5kW is supplied by the battery as shown by the green curve in Figure 27e. Here, the positive sign of battery power means that it injects active power to the microgrid.

Figure 27f shows the state of charge (SOC) of the lead acid battery considered for this study. The red curve representing the SOC for Case 1 shows that it gradually increases as the excess power is fed to charge the battery. The decreasing green curve for Case 2 in Figure 27f shows that the power is being extracted from the battery.

Figure 27. Results of coordinated V-f control with solar PhV including MPPT control and battery control; a) Diesel generator Active and reactive power; b) Microgrid frequency; c) Voltage at PCC; d) Inverter Active and reactive power; e) PhV Active power; f) Battery SOC; g) DC-DC booster output voltage; h) Active power at AC and DC sides

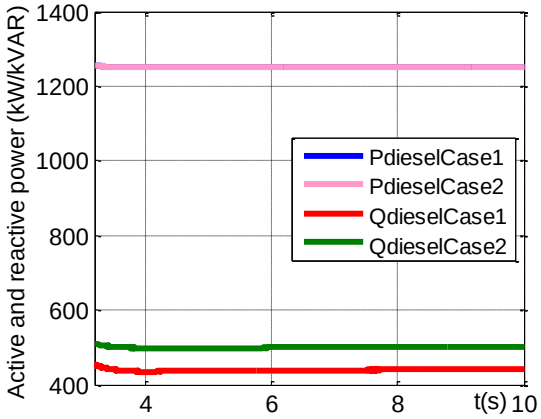
Active and reactive power (kW/kVAR)
1400
1200
1000
800
600
400
4
6
8
t(s)
10
PdieselCase1
PdieselCase2
QdieselCase1
QdieselCase2

a)

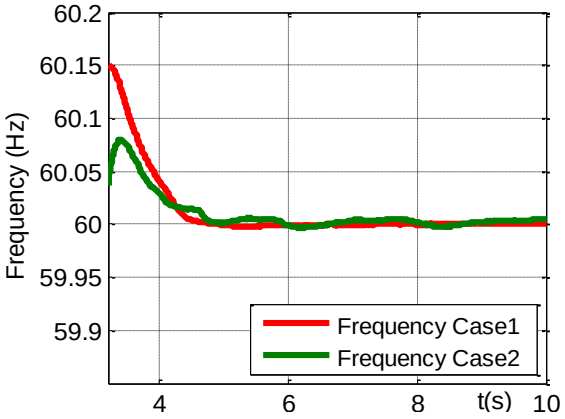
Frequency (Hz)
60.2
60.15
60.1
60.05
60
59.95
59.9
4
6
8
t(s)
10
Frequency Case1
Frequency Case2

b)

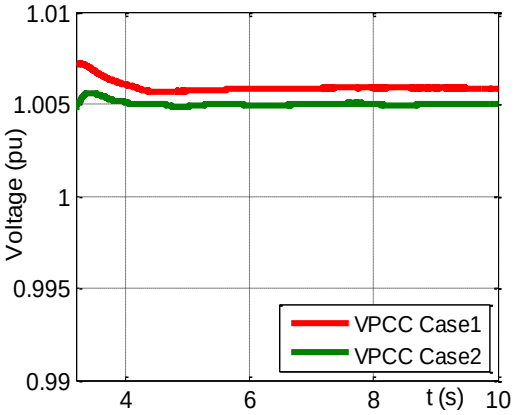
Voltage (pu)
1.01
1.005
1
0.995
0.99
4
6
8
t (s)
10
VPCC Case1
VPCC Case2

c)

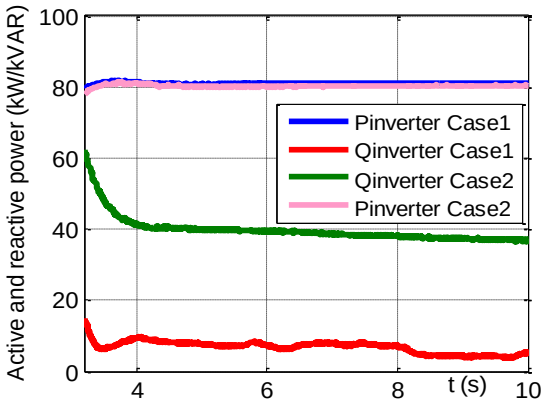
Active and reactive power (kW/kVAR)
100
80
60
40
20
0
4
6
8
t (s)
10
Pinverter Case1
Qinverter Case1
Qinverter Case2
Pinverter Case2

d)

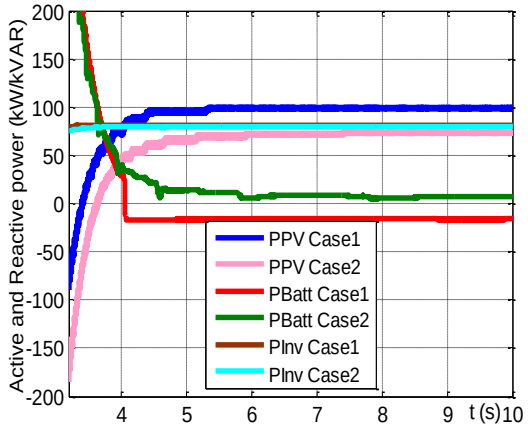
Active and Reactive power (kW/kVAR)
200
150
100
50
0
-50
-100
-150
-200
4
5
6
7
8
9
t (s)
10
PPV Case1
PPV Case2
PBatt Case1
PBatt Case2
Plnv Case1
Plnv Case2

e)

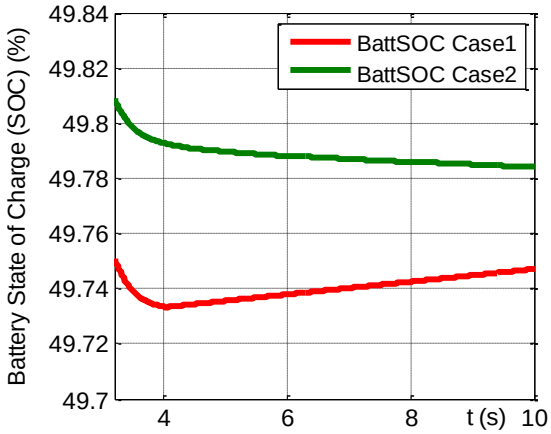
Battery State of Charge (SOC) (%)
49.84
49.82
49.8
49.78
49.76
49.74
49.72
49.7
4
6
8
t (s)
10
BattSOC Case1
BattSOC Case2

f)

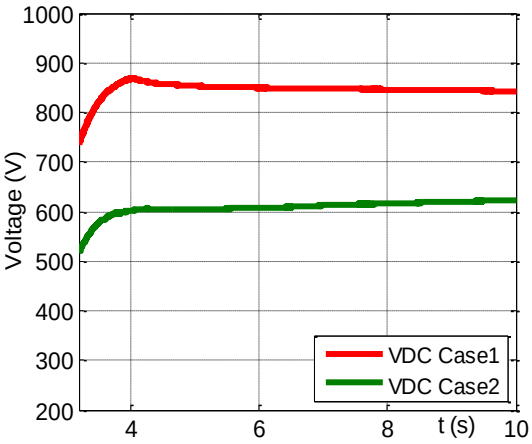
Voltage (V)
1000
900
800
700
600
500
400
300
200
4
6
8
t (s)
10
VDC Case1
VDC Case2

g)

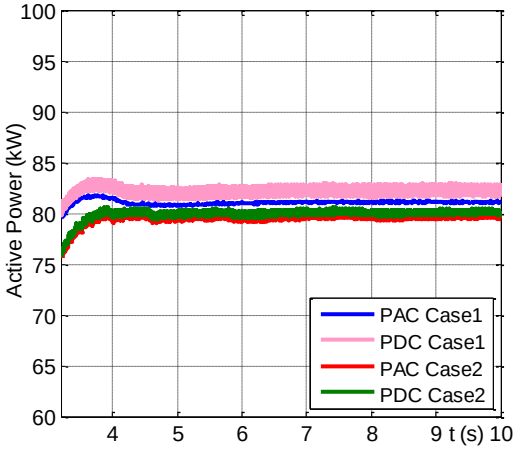
Active Power (kW)
100
95
90
85
80
75
70
65
60
4
5
6
7
8
9 t (s) 10
PAC Case1
PDC Case1
PAC Case2
PDC Case2

h)

Figure 27g shows the DC voltage for both cases. It can be seen that the voltages are stably maintained at around 850 V and 600 V for two cases, respectively. Figure 27h shows the active power at the DC and AC sides of the inverter for both cases. It is clearly shown that the DC active power is slightly higher than the AC side three phase average power in both cases. This accounts to some percentage (taken as 2% in the present work) of power losses between the DC and AC sides but the overall active power is balanced through controls. This power balance coupled with the AC side voltage control maintains the DC side voltage to a stable value which is again the uniqueness of the proposed coordinated MPPT and inverter control.

Detailed Test of V-f control with variable irradiance

In order to validate the model with changing values of irradiance, the control method is also tested for different values of irradiance. The irradiance level considered for study are 1000 W/m^2, 800 W/m^2, 600 W/m^2, 400 W/$m^2$and 200 W/m^2 respectively. Figure 28 (a through f) show the results obtained for coordinated V-f control with MPPT and battery with varying level of irradiance as mentioned above. Figure 28 (a and b) show the plot of microgrid frequency and per unit voltage at PCC for different values of irradiance. It is clear that the microgrid frequency is maintained at 60 Hz and the PCC voltage is maintained at around 1 p.u. for each of the cases. Figure 28c shows the active power injection from the PhV inverter. It is maintained at around 80 kW as demanded by the microgrid for frequency regulation irrespective of what PhV is generating. Figure 28d show that PhV generator is operating at the MPP corresponding to the level of irradiance for all the cases. It is clear from Figure 28e that battery storage is acting as a buffer in

providing less or more active power depending on the changes in irradiance or even sometimes charging the battery in the case of abundant irradiance. Table 7 summarizes these results showing the actual value of PhV generation, inverter injection and battery active power injection or absorption. This table shows that the inverter active power injection is almost equal to the addition of active power generated by PhV generator and the injection/absorption from the battery. There is a minor mismatch in active power balance which could be attributed to the losses in the circuit. Figure 28f shows the DC side voltage at the output of the booster circuit. These are maintained at the stable values required to maintain the voltage at AC side which ensures the power balance of the entire stages as described in above sections.

It is found out that as compared to the P-V control method where no battery storage is present in the system, in the case of V-f control with MPPT and battery, the DC side voltage is very sensitive to a slight change in the controller gains of battery control loop, PI_5 in coordination with the gains of DC side active power control loop, PI_4 and the frequency control loop, PI_3. Hence, the DC side voltage is seen to be varying in the range of 600V-900V depending on the choice of controller parameters. This sensitivity increases when the irradiance value is such that the PhV maximum power is almost enough to support the microgrid frequency and only a little contribution is required from the battery storage as in the situation when irradiance is 800 W/m^2. This opens up a future path of the current research in developing a smart adaptive PI controller gain tuning

algorithm that considers the sensitivity of gain parameters to the control of system variables.

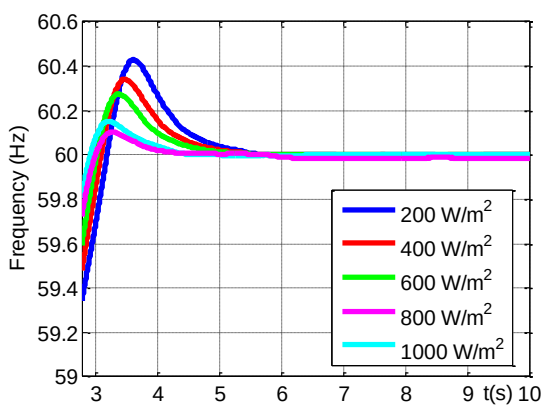

a) Microgrid frequency

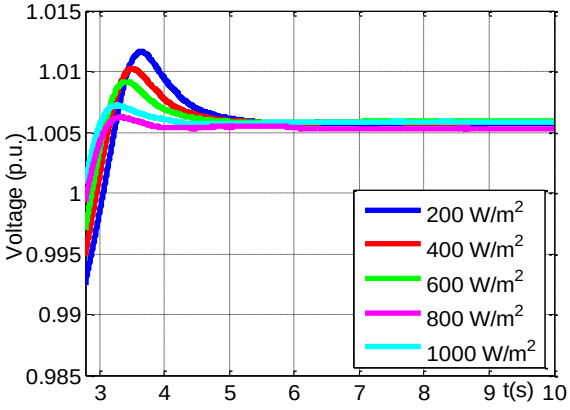

b) Voltage at PCC

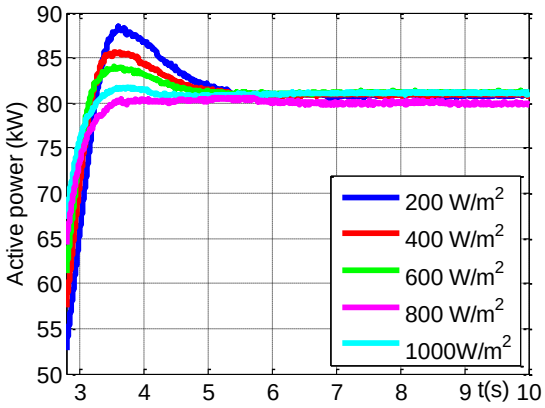

c) Inverter active power

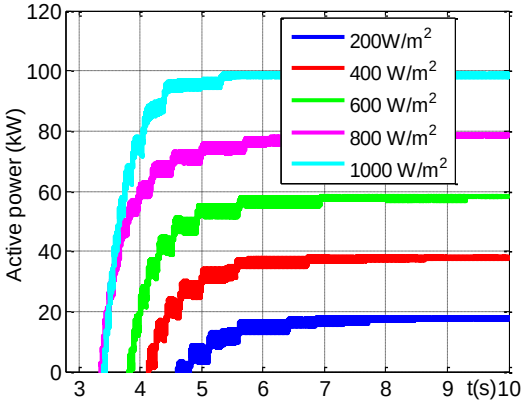

d) PhV Active power output

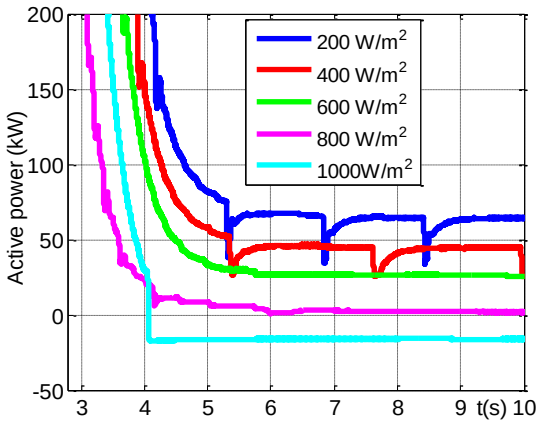

e) Battery active power output

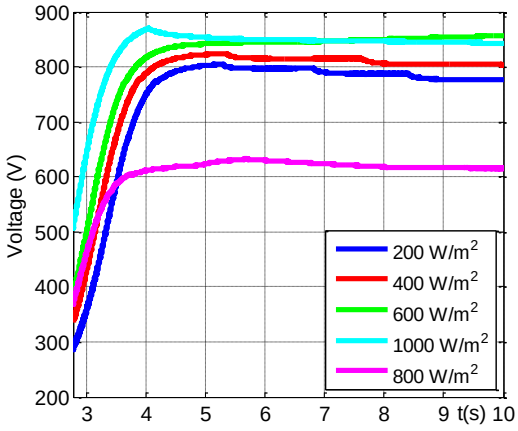

f) DC-DC booster output voltage

Figure 28. Results of V-f control with MPPT and battery considering variable irradiance cases.

Table 7 Summary table of V-f control with variable irradiance

Irradiance (W/m^2)	P_{PhVSS} (kW)	P_{battSS} (kW)	P_{invSS} (kW)	V_{PCCSS} (p.u.)	f_{SS} (Hz)
200	18.60	64.24	80.88	1.006	60
400	38.19	44.56	80.84	1.006	60
600	58.60	26.63	81.17	1.006	60
800	79.60	2.80	80.15	1.005	60
1000	99.20	-16.45	81.60	1.006	60

Test of V-f control method considering battery state of charge (SOC) constraints

In the present work, state of charge (SOC) of the lead acid battery used in the microgrid is considered in the range of 20%-80%. In the above discussions, the proposed V-f control algorithm is verified considering the case in which there is enough room to charge or discharge the battery in the microgrid. But, there could be a situation when the battery SOC is at the verge of these upper and lower boundaries.

Figure 29 (a through f) show the results obtained from this transition of controls at the PhV inverter and the diesel generator. Figure 29a and 29b show the active power from the diesel generator and the PhV inverter. It can be observed that the PhV generator performing frequency regulation of microgrid before t = 8 sec, quickly transitions to generate at MPP with the irradiance input of 1000 W/m^2, whereas the diesel generator active power control which was otherwise maintaining the active power output at 1250

kW, quickly transitions to frequency control mode. Hence, the diesel generator decreases its active power output to around 1237kW to cope with the increase in generation by solar PhV. Figure 29c and 29d show the microgrid frequency and voltage at PCC which are maintained at 60 Hz and around 1 p.u., respectively, as a result of the proposed controls. Figure 29e and 29f show the active power from the PhV generator and the battery, respectively. The PhV is generating at the maximum power around 100 kW and the battery power is almost zero showing that it is not absorbing any power, that is, it is not being charged even though the PhV generation is higher than what is required for frequency control as the SOC of the battery is at 80% for this case.

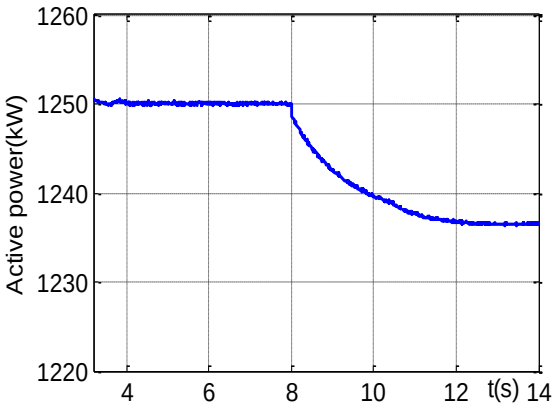

a) Diesel generator active power

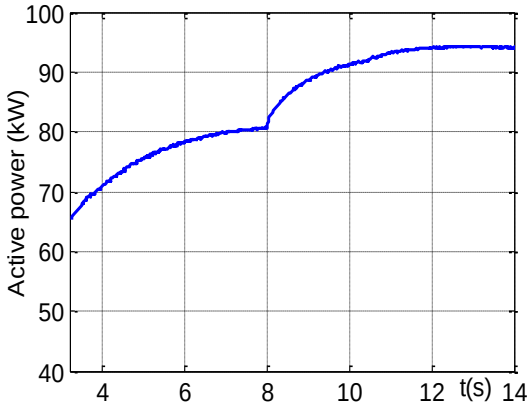

b) Inverter active power

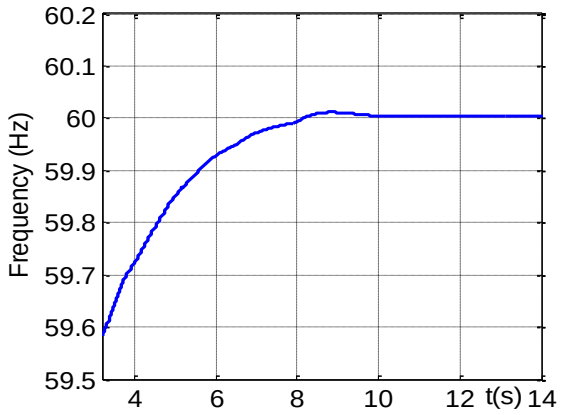

c) Microgrid frequency

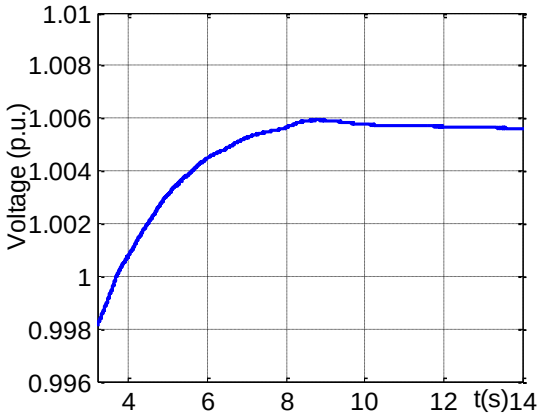

d) Voltage at PCC

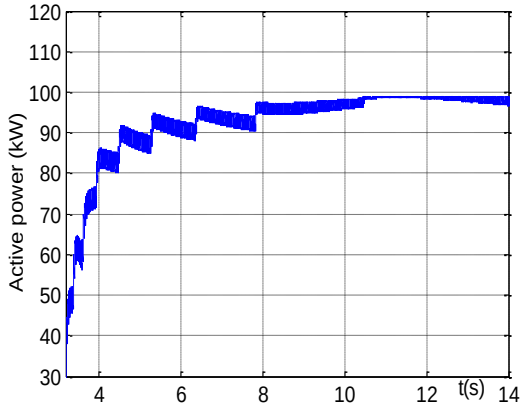

e) PhV active power output

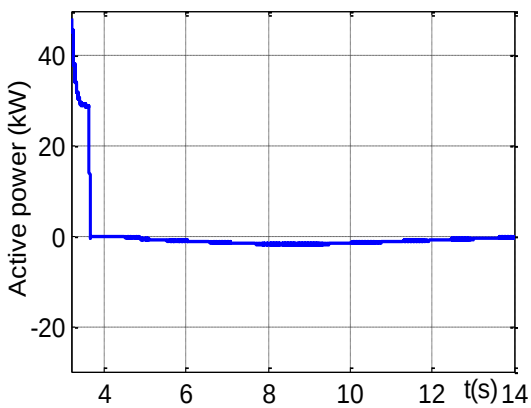

f) Battery active power output

Figure 29. Results of V-f control with MPPT and battery considering battery SOC upper constraint (80% charged: Case 1).

Similarly, an equally opposite scenario is possible. If the solar irradiance is low such that the maximum power generated by PhV generator is not enough to provide the frequency control, that is, $P_{fcontrol} > PhV_{MPP}$ and at the same time, the battery SOC is 20%, then the battery cannot provide extra active power required for frequency control. Again, similar situation as described for the above case will arise. Similar to the previous case, the PhV generator control should transition from frequency control to constant active power at MPP control, and the frequency control function should be taken over by the participating diesel unit which is otherwise producing constant active power of 1250 kW. P_{PVMPP} is approximately 75kW which is less than 80kW required for frequency control in the present case. The deficit active power should be provided by the diesel generator in order to maintain the system frequency at 60 Hz. The diesel generator is, otherwise, generating a constant active power of 1250 kW. Because of this transition of control from constant active power to frequency control, the generation from diesel generator increases to 1255 kW, therefore, fulfilling the requirement for frequency control. The PhV generation, on the other hand, is maintained at a constant power of around 72 kW equal to $0.96 \times P_{PVMPP}$. The plots of active power generation from the diesel generator and the injection from the PhV inverter are shown in Figure 30a and 30b, respectively.

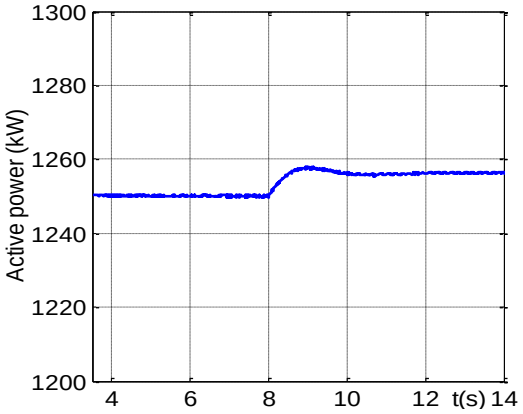

a) Diesel generator active power

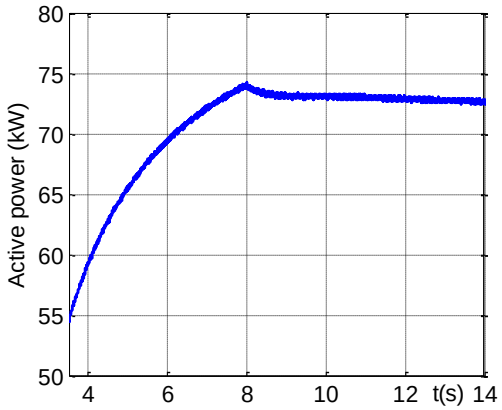

b) Inverter active power

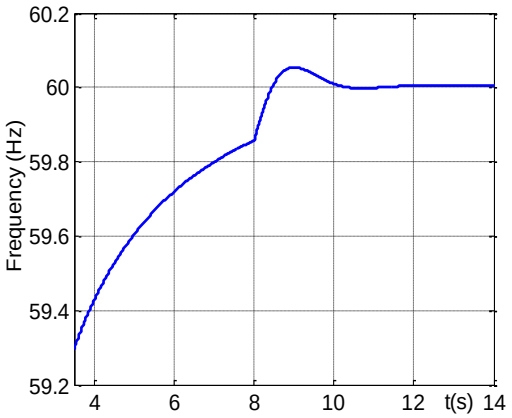

c) Microgrid frequency

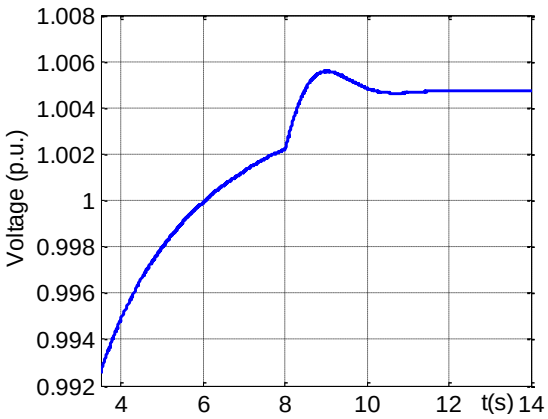

d) Voltage at PCC

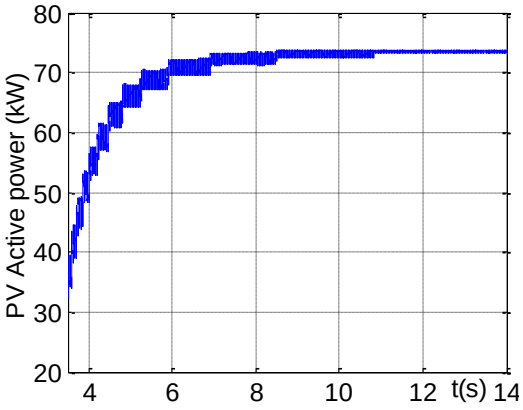

e) PhV active power output

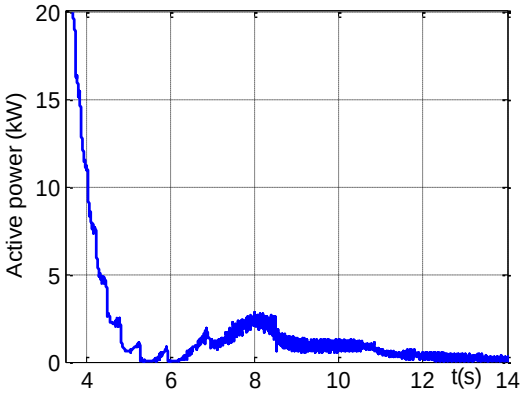

f) Battery active power

Figure 30. Results of V-f control with MPPT and battery considering battery SOC constraints (20% discharged: Case 2).

Figure 30c and 30d show the microgrid frequency and voltage at PCC, respectively. It is clearly shown that the PhV generator was initially trying to control the frequency but could reach only a value below 60 Hz due to low active power injection from the inverter. However, as the frequency control transfers from the PhV generator to the diesel generator at 8 sec, it quickly returns back to 60 Hz in around 2 sec. Similar nature of result can be observed for the voltage at PCC which is stably maintained at 1.005 p.u. after the transition of controls. Figure 30e and 30f show active power output of the PhV generator and the battery. The PhV is generating MPP power of 75kW and the battery power is close to zero showing that the battery is not able to inject any power in this case as SOC is at its minimum limit.

Test of P-Q control method

Next, the results of P-Q control with integrated MPPT and battery control is presented in Figure 31 (a through f). Like V-f control, two different cases, namely Case 3 and Case 4, are considered for simulation validation of this control as well. Cases 3 and 4 are similar to Cases 1 and 2 with slight differences as elaborated below.

Here, in Case 3, the critical active power load of a microgrid is less than the maximum available PhV power (i.e., $P_{ref} <= P_{PV}$), and in Case 4, we have $P_{ref} > P_{PV}$. Hence, the disturbance for this part is the load change which is very common in real operation. Moreover, since coordinated P-Q control method is to be validated, the load change is the most representative scenario to study the effectiveness of the proposed control. Hence,

the solar irradiance is considered constant at 1000 W/m^2 for both cases. The sample controller gain parameters used for Case 3 of P-Q control method is shown in Table 8. The gain parameters needed to be adjusted little bit for Case 4.

Table 8 Controller gain parameters for P-Q Control (Case 3) with MPPT and battery

MPPT Control Loop	K_{p1}	6×10^{-8}
	K_{i1}	6×10^{-6}
Voltage Control Loop	K_{p2}	5×10^{-8}
	K_{i2}	5×10^{-7}
P_{AC} Control Loop	K_{p3}	2.5×10^{-9}
	K_{i3}	2.5×10^{-8}
P_{DC} Control Loop	K_{p4}	2.5×10^{-9}
	K_{i4}	2.5×10^{-8}
Battery Control Loop	K_{p5}	0.02×10^{-8}
	K_{i5}	0.02×10^{-7}

Figure 31a shows the active and reactive power from the diesel generator. The diesel generator produces a constant active power of 1250 kW throughout the simulation period for both cases with a slight change in reactive power between the two cases. Figure 31b shows the reference and actual active and reactive power of the solar PhV inverter. The reference values of active power represent the critical loads of the microgrid as previously mentioned. The references of the active power for Cases 3 and 4 are 50 kW and 120 kW, respectively. Similarly, the references of the reactive power for Cases 3 and

4 are 20 kVAR and 70 kVAR, respectively. The references are chosen to demonstrate both charging and discharging processes of the backup battery energy storage. It can be observed from Figure 31b that the proposed coordinated controls are capable of serving the critical loads in as less as 2 seconds.

Figure 31c shows the plot of active power from the PhV generator, the inverter injection, and the active power to and from the battery. In both cases, the power from PhV is maintained constant at the MPP power of 100 kW through MPPT controls as shown by the overlapping blue and red curves. The active power injection from the inverter is maintained at the reference values of 50 kW and 120 kW in Cases 3 and 4, respectively. These reference values are demanded by the critical loads. The generation from PhV in Case 3 is more than the critical load by 50 kW. Thus, this surplus power is sent to charge the lead acid battery which is shown by a purple curve in Figure 31c.

Again, the negative sign of the battery power shows that it is being charged. For Case 4, the critical load is greater than the PhV generation at MPP and the deficit power of 20 kW is supplied by the battery as shown by the orange curve in Figure 31c. Here, the positive sign of battery power means that it is being discharged. Therefore, for Case 3, the power injection from the inverter comes only from the solar PhV generator, however, for Case 4, the injection comes from PhV and battery.

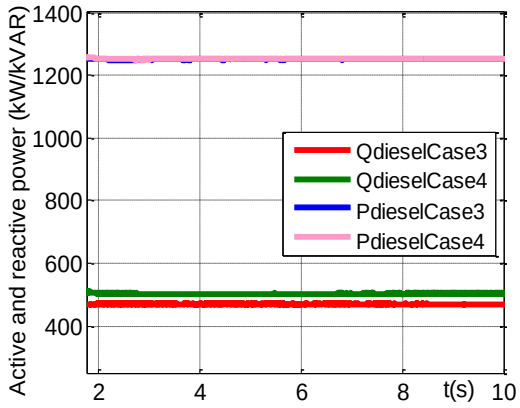

a) Diesel generator Active and reactive power

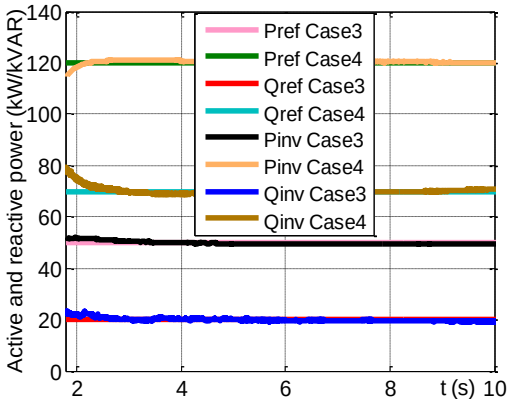

b) Inverter Active and reactive power

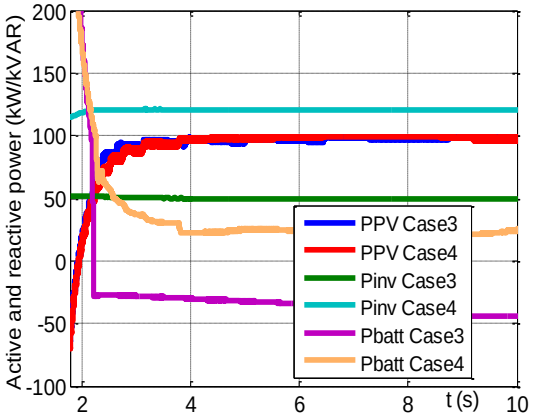

c) Battery active power

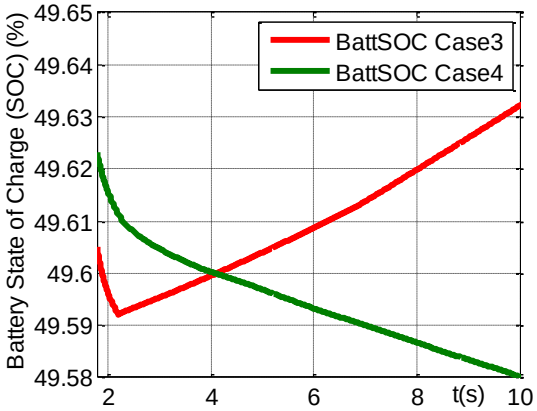

d) Battery SOC

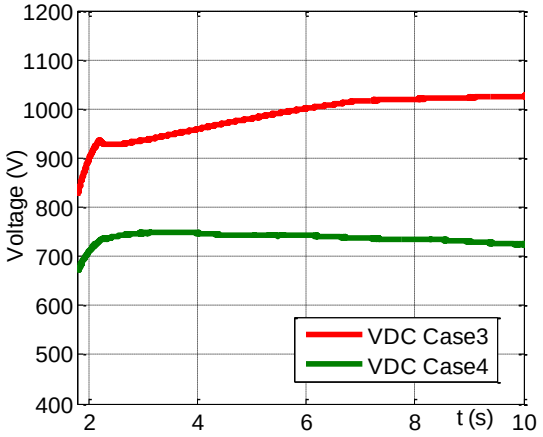

e) DC-DC booster output voltage

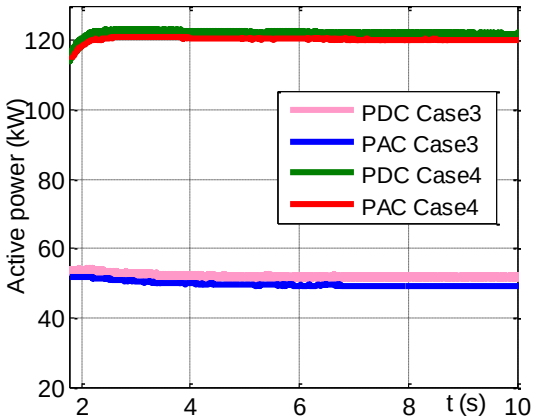

f) DC and AC side active power

Figure 31. Results of coordinated P-Q control with solar PhV including MPPT control and battery control.

Figure 31d shows the SOC of the battery. It is clear that the SOC increases in Case 3 and decreases in Case 4 as expected because of the respective charging and discharging scenarios. It validates the effectiveness of the battery control algorithm adopted in controlling the bidirectional power flow to and from the battery.

Figure 31e shows the DC side voltage at the inverter input. It is stably maintained at around 1012 V and 740 V for Cases 3 and 4, respectively. This also validates the indirect control of the DC side voltage through the power balance between AC and DC sides of the inverter. Similarly, Figure 31f shows the active power measured at the DC and AC sides of the inverter. Clearly, the DC side active power is slightly greater than the AC side power which means that the control algorithm also takes care of the efficiency of the inverter in the model. The effectiveness of the proposed coordinated P-Q control algorithm in microgrids is clearly demonstrated from the results presented.

4.5 CHAPTER CONCLUSION

The contributions of this chapter can be summarized as follows:

- The coordinated strategies of V-f control and P-Q control, respectively, for microgrids with solar PHV generator and battery storage are proposed and presented.
- In the control strategies, the solar PhV generator is operated at MPP, and the battery storage acts as a buffer in order to inject and absorb deficit or surplus power by using the charge/discharge cycle of the battery. Thus, the control strategies demonstrate

effective coordination between inverter V-f (or P-Q) control, MPPT control, and energy storage control.

- The proposed control methods are entirely developed in the abc reference frame, so it avoids the transformation to the dq0 reference frame and vice versa. Therefore, the proposed control is not sensitive to measurement noise as it is dependent on the measurements of the past cycle rather than at a particular time instant.
- The proposed V-f control method shows a very satisfactory performance in reviving highly reduced voltage and frequency back to the nominal values in a matter of few seconds only, which is much faster than conventional synchronous generator control. Hence, it has a potential to be applied in restoring the microgrid frequency and the voltage at PCC after disturbances.
- Similarly, the integrated and coordinated P-Q control algorithm can be effectively used in supplying some critical loads of a microgrid with solar PhV and battery.

CHAPTER 5
OVERALL CONCLUSIONS AND FUTURE WORK

5.1 CONCLUSIONS AND CONTRIBUTIONS

In this dissertation, first, the application of PhV-based DER systems for active and nonactive power control is investigated with a simulation study of the IEEE 13 bus distribution test system. The dynamic response of the PhV in following the local load pattern is presented. The ability of the DERs to provide nonactive (reactive) power in addition to active (real) power is very beneficial in maintaining the voltage stability and power flow control in future power systems. A method of MPPT control and PCC voltage control is developed. An indirect control of DC side voltage by maintaining the balance in power transfer at every stage from PhV to inverter output is proposed and investigated. Next, a voltage and frequency control algorithm for microgrid applications using solar PhV operating at MPPT along with BESS is proposed. The capability of PhV in controlling both voltage and frequency of microgrid can provide a greater incentive to the increased penetration and deployment of sustainable PhV generation in future microgrids. Again, the method of MPPT control and BESS control is also integrated with the proposed P-Q control algorithm so as to supply the critical loads of the microgrids in the event of emergency. The results presented clearly prove the effectiveness of this control technique. The specific contributions of this dissertation can be summarized as follows:

- Several control methods of solar PhV generators in grid connected and islanded microgrid scenarios are proposed, investigated and validated.

- The P-Q control algorithm without storage can be helpful in supplying the active and reactive power loads in grid connected microgrid case. The response time of the control is very short which means that the controls can quickly track the load variation.
- A new simplified, yet effective MPPT and voltage (P-V) control algorithm can be implemented for the maximal utilization of the solar resource in providing the total active power generation to the grid and at the same time providing local voltage support. The unique feature of this control algorithm lies in controlling the DC side voltage stably at the desired value without using the voltage and current control loops as in traditional control algorithms. It, therefore, provides greater insight of the controller parameters to be used in the system since the parameters for both active power control loops at the AC and the DC sides are close enough to be identified easily.
- The proposed coordinated V-f control with MPPT and battery control algorithm for microgrid takes only around 2 seconds to bring voltage and frequency back to nominal value once the islanding occurs in a microgrid. Hence, the algorithm has a great potential for V-f control in future microgrids.
- Similarly, the proposed coordinated and integrated P-Q control algorithm with MPPT and battery storage can be implemented in supplying the critical loads in the future microgrids.
- All the control methods developed are based on abc reference frame without conversion to the dq0 reference frame. Hence, it leads to a simple control

approach that avoids the conversions between the reference frames of abc and dq0. Furthermore, the approaches are not sensitive to measurement noise as these are dependent on the measurements of the past cycle rather than at a particular time instant.

5.2 FUTURE WORKS

The future works of the dissertation could be performed in one of the following directions:

Adaptive control for microgrid:

The controllers used for the V-f/P-Q control are the PI controller loops, for the voltage /reactive power control, frequency/active power control and to maintain the power balance between AC and DC sides. The tuning of each of the controller gains to obtain the desired voltage and frequency response or active and reactive power is a big challenge at present. Inappropriate choice of the controller settings may lead to under achievement or over achievement of the referenced signals or even lead to instability. Hence, the future direction of the current research could be to control these PI gains adaptively based on the system conditions. A sensitivity approach of adaptive control based on Taylor series expansion could be formulated and tested in the proposed coordinated V-f / P-Q control scheme.

Application of control algorithms to multiple PhV generators:

In the present work, the proposed control algorithms are applied to a case with a single PhV generator to demonstrate the effectiveness of the proposed methods. With the increasing penetration of Solar PhV generators in the future distribution systems, the control problem could be more complex which should address the share of various PhV generators to provide for example, voltage and frequency control. The proposed methods can be extended with some other additions to handle multiple solar PhV generators.

Consideration of variability of irradiance into the control methods:

In the present work, the control methods are separately tested for various level of irradiance, however, the dynamic variability of solar irradiance is not considered. In the case of high-penetration solar PhV generators in a microgrid, the consideration of stochastic nature of PhV generation could be essential. Hence, the future direction of this work could be to consider the variability of irradiance and hence, the active power outputs of the PhV generators and to observe the ability of the proposed control algorithms to handle this situation.

LIST OF REFERENCES

[1] F. A. Farret, Godoy Simoes, M. *Integration of Alternative Sources of Energy*.
[2] A. Keyhani, Marwali, M.N., Dai, M. (2010). *Integration of Green and Renewable Energy in Electric Power Systems*.
[3] G. Pepermans, J. Driesen, D. Haeseldonckx, R. Belmans, and W. D'haeseleer, "Distributed generation: definition, benefits and issues," *Energy Policy*, vol. 33, pp. 787-798, 2005.
[4] W. El-Khattam and M. M. A. Salama, "Distributed generation technologies, definitions and benefits," *Electric Power Systems Research*, vol. 71, pp. 119-128, 2004.
[5] J. A. P. Lopes, N. Hatziargyriou, J. Mutale, P. Djapic, and N. Jenkins, "Integrating distributed generation into electric power systems: A review of drivers, challenges and opportunities," *Electric Power Systems Research*, vol. 77, pp. 1189-1203, 2007.
[6] A. Thornton and C. R. Monroy, "Distributed power generation in the United States," *Renewable and Sustainable Energy Reviews*, vol. 15, pp. 4809-4817, 2011.
[7] T. Georgiadis. (2010). *Renewable Energy Grid Integration*.
[8] A. M. B. a. J.F.Kreider. (2001). *Distributed Generation (2001 ed.)*.
[9] J. T. a. T.Weir. (2006). *Renewable Energy Resources (Second ed.)*.
[10] P. G.W.Massey. (2010). *Essentials fo Distributed Generation Systems*.
[11] S. P. C. a. P. C. S.Chowdhury. (2009). *Microgrids and Active Distribution Networks (1 ed.)*.
[12] R. Passey, T. Spooner, I. MacGill, M. Watt, and K. Syngellakis, "The potential impacts of grid-connected distributed generation and how to address them: A review of technical and non-technical factors," *Energy Policy*, vol. 39, pp. 6280-6290, 2011.
[13] N. R. Friedman, "Distributed Energy Resources Interconnection Systems: Technology Review and Research Needs," National Renewable Energy Laboratory (NREL) Vienna, VirginiaSeptember 2002.
[14] B. Kroposki, C. Pink, R. DeBlasio, H. Thomas, M. Simoes, and P. K. Sen, "Benefits of power electronic interfaces for distributed energy systems," in *Power Engineering Society General Meeting, 2006. IEEE*, 2006, p. 8 pp.
[15] L. Huijuan, L. Fangxing, X. Yan, D. T. Rizy, and J. D. Kueck, "Adaptive Voltage Control With Distributed Energy Resources: Algorithm, Theoretical Analysis, Simulation, and Field Test Verification," *Power Systems, IEEE Transactions on*, vol. 25, pp. 1638-1647, 2010.
[16] X. Yan, L. Huijuan, D. T. Rizy, L. Fangxing, and J. D. Kueck, "Instantaneous active and nonactive power control of distributed energy resources with a current limiter," in *Energy Conversion Congress and Exposition (ECCE), 2010 IEEE*, 2010, pp. 3855-3861.
[17] X. Yan, L. M. Tolbert, D. T. Rizy, and J. D. Kueck, "Nonactive-Power-Related Ancillary Services Provided by Distributed Energy Resources," in *Power Engineering Society General Meeting, 2007. IEEE*, 2007, pp. 1-7.

[18] Y. Xiaoyan and L. M. Tolbert, "Ancillary services provided from DER with power electronics interface," in *Power Engineering Society General Meeting, 2006. IEEE*, 2006, p. 8 pp.
[19] R. H. Lasseter, "MicroGrids," in *Power Engineering Society Winter Meeting, 2002. IEEE*, 2002, pp. 305-308 vol.1.
[20] T. M. Razykov, C. S. Ferekides, D. Morel, E. Stefanakos, H. S. Ullal, and H. M. Upadhyaya, "Solar photovoltaic electricity: Current status and future prospects," *Solar Energy*, vol. 85, pp. 1580-1608, 2011.
[21] M. F. Akorede, H. Hizam, and E. Pouresmaeil, "Distributed energy resources and benefits to the environment," *Renewable and Sustainable Energy Reviews*, vol. 14, pp. 724-734, 2010.
[22] Y. V. Makarov, V. I. Reshetov, A. Stroev, and I. Voropai, "Blackout Prevention in the United States, Europe, and Russia," *Proceedings of the IEEE*, vol. 93, pp. 1942-1955, 2005.
[23] K. Yamashita, L. Juan, Z. Pei, and L. Chen-Ching, "Analysis and control of major blackout events," in *Power Systems Conference and Exposition, 2009. PSCE '09. IEEE/PES*, 2009, pp. 1-4.
[24] NERC, "Leading Indicators: Frequency Excursions," available at http://www.nerc.com/page.php?cid=4|37|257|270 (accessed December 12, 2011
[25] T. S. Sidhu, "Accurate measurement of power system frequency using a digital signal processing technique," *Instrumentation and Measurement, IEEE Transactions on*, vol. 48, pp. 75-81, 1999.
[26] A. G. Phadke, J. S. Thorp, and M. G. Adamiak, "A New Measurement Technique for Tracking Voltage Phasors, Local System Frequency, and Rate of Change of Frequency," *Power Engineering Review, IEEE*, vol. PER-3, pp. 23-23, 1983.
[27] A. A. Girgis and T. L. D. Hwang, "Optimal Estimation Of Voltage Phasors And Frequency Deviation Using Linear And Non-Linear Kalman Filtering: Theory And Limitations," *Power Apparatus and Systems, IEEE Transactions on*, vol. PAS-103, pp. 2943-2951, 1984.
[28] M. S. Sachdev and M. M. Giray, "A Least Error Squares Technique For Determining Power System Frequency," *Power Apparatus and Systems, IEEE Transactions on*, vol. PAS-104, pp. 437-444, 1985.
[29] M. M. Giray and M. S. Sachdev, "Off-nominal frequency measurements in electric power systems," *Power Delivery, IEEE Transactions on*, vol. 4, pp. 1573-1578, 1989.
[30] T. S. Sidhu and M. S. Sachdev, "An iterative technique for fast and accurate measurement of power system frequency," *Power Delivery, IEEE Transactions on*, vol. 13, pp. 109-115, 1998.
[31] R. K. Mai, Z. Y. He, L. Fu, W. He, and Z. Q. Bo, "Dynamic phasor and frequency estimator for phasor measurement units," *Generation, Transmission & Distribution, IET*, vol. 4, pp. 73-83, 2010.
[32] D. Tholomier, H. Kang, and B. Cvorovic, "Phasor measurement units: Functionality and applications," in *Power Systems Conference, 2009. PSC '09.*, 2009, pp. 1-12.

[33] S. S. Tsai, Z. Zhian, Z. Jian, and L. Yilu, "Analysis of wide-area frequency measurement of bulk power systems," in *Power Engineering Society General Meeting, 2006. IEEE*, 2006, p. 8 pp.
[34] V. Yari, S. Nourizadeh, and A. M. Ranjbar, "Wide-area frequency control during power system restoration," in *Electric Power and Energy Conference (EPEC), 2010 IEEE*, 2010, pp. 1-4.
[35] W. Tranter, R. Thamvichai and T. Bose, "Basic Simulation Models of Phase Tracking Devices using MATLAB", Synthesis Lectures on Communications, Morgan & Claypool Publishers Series 2010
[36] W. Tranter, R. Thamvichai and T. Bose, "Basic Simulation Models of Phase Tracking Devices using MATLAB", Synthesis Lectures on Communications, Morgan & Claypool Publishers Series 2010
[37] Hadi Saadat,"Power System Analysis", McGraw Hill 2002
[38] J. A. P. Lopes, C. L. Moreira, and A. G. Madureira, "Defining control strategies for MicroGrids islanded operation," *Power Systems, IEEE Transactions on*, vol. 21, pp. 916-924, 2006.
[39] B. Awad, J. Wu and N.Jenkins, "Control of Distributed Generation", Electrotechnik and Informationstechnik (2008), 125/12, pp. 409-414
[40] J. C. Vasquez, J. M. Guerrero, E. Gregorio, P. Rodriguez, R. Teodorescu, and F. Blaabjerg, "Adaptive droop control applied to distributed generation inverters connected to the grid," in *Industrial Electronics, 2008. ISIE 2008. IEEE International Symposium on*, 2008, pp. 2420-2425.
[41] B. Awad, J. Wu and N.Jenkins, "Control of Distributed Generation", Electrotechnik and Informationstechnik (2008), 125/12, pp. 409-414
[42] Pedrasa MA, Spooner T. A survey of techniques used to control microgrid generation and storage during island operation. Proc Australian Universities Power Engineering Conference; 2006. Available: http://www.itee.uq.edu.au/~aupec/aupec06/htdocs/content/pdf/30.pdf..
[43] H. Laaksonen, P. Saari, and R. Komulainen, "Voltage and frequency control of inverter based weak LV network microgrid," in *Future Power Systems, 2005 International Conference on*, 2005, pp. 6 pp.-6.
[44] C. K. Sao and P. W. Lehn, "Control and Power Management of Converter Fed Microgrids," *Power Systems, IEEE Transactions on*, vol. 23, pp. 1088-1098, 2008.
[45] N. L. Soultanis and N. D. Hatziargyriou, "Control issues of inverters in the formation of L. V. micro-grids," in *Power Engineering Society General Meeting, 2007. IEEE*, 2007, pp. 1-7.
[46] M. B. Delghavi and A. Yazdani, "A control strategy for islanded operation of a Distributed Resource (DR) unit," in *Power & Energy Society General Meeting, 2009. PES '09. IEEE*, 2009, pp. 1-8.
[47] K. De Brabandere, K. Vanthournout, J. Driesen, G. Deconinck, and R. Belmans, "Control of Microgrids," in *Power Engineering Society General Meeting, 2007. IEEE*, 2007, pp. 1-7.

[48] T. C. Green and M. Prodanović, "Control of inverter-based micro-grids," *Electric Power Systems Research*, vol. 77, pp. 1204-1213, 2007.

[49] I. Serban, C. P. Ion, C. Marinescu, and M. Georgescu, "Frequency Control and Unbalances Compensation in Autonomous Micro-Grids Supplied by RES," in *Electric Machines & Drives Conference, 2007. IEMDC '07. IEEE International*, 2007, pp. 459-464.

[50] N. J. Gil and J. A. P. Lopes, "Hierarchical Frequency Control Scheme for Islanded Multi-Microgrids Operation," in *Power Tech, 2007 IEEE Lausanne*, 2007, pp. 473-478.

[51] C. Il-Yop, L. Wenxin, L. Siyu, D. A. Cartes, and E. G. Collins, "Robust controller design for inverter-interfaced distributed generators considering islanded operation of a microgrid," in *Energy Conversion Congress and Exposition, 2009. ECCE 2009. IEEE*, 2009, pp. 554-561.

[52] M. Babazadeh and H. Karimi, "Robust decentralized control for islanded operation of a microgrid," in *Power and Energy Society General Meeting, 2011 IEEE*, 2011, pp. 1-8.

[53] L. D. Watson and J. W. Kimball, "Frequency regulation of a microgrid using solar power," in *Applied Power Electronics Conference and Exposition (APEC), 2011 Twenty-Sixth Annual IEEE*, 2011, pp. 321-326.

[54] M. G. Molina and P. E. Mercado, "Modeling and control of grid-connected photovoltaic energy conversion system used as a dispersed generator," in *Transmission and Distribution Conference and Exposition: Latin America, 2008 IEEE/PES*, 2008, pp. 1-8.

[55] N. Kakimoto, S. Takayama, H. Satoh, and K. Nakamura, "Power Modulation of Photovoltaic Generator for Frequency Control of Power System," *Energy Conversion, IEEE Transactions on*, vol. 24, pp. 943-949, 2009.

[56] T. Ota, K. Mizuno, K. Yukita, H. Nakano, Y. Goto, and K. Ichiyanagi, "Study of load frequency control for a microgrid," in *Power Engineering Conference, 2007. AUPEC 2007. Australasian Universities*, 2007, pp. 1-6.

[57] J. C. Vasquez, R. A. Mastromauro, J. M. Guerrero, and M. Liserre, "Voltage Support Provided by a Droop-Controlled Multifunctional Inverter," *Industrial Electronics, IEEE Transactions on*, vol. 56, pp. 4510-4519, 2009.

[58] L. Yan and L. Yun Wei, "Decoupled power control for an inverter based low voltage microgrid in autonomous operation," in *Power Electronics and Motion Control Conference, 2009. IPEMC '09. IEEE 6th International*, 2009, pp. 2490-2496.

[59] R. Majumder, G. Bag, and S. Chakrabarti, "Performance of power electronic interfaced DERs integrated with communication network," in *Power and Energy Society General Meeting, 2011 IEEE*, 2011, pp. 1-7.

[60] C. Pan, M. Cheng, and C. Lai, "A Novel Integrated DC/AC Converter with High Voltage Gain Capability for Distributed Energy Resource Systems," *Power Electronics, IEEE Transactions on*, vol. PP, pp. 1-1, 2011.

[61] J. Carr, D. Hotz, J. C. Balda, H. Alan Mantooth, and A. Ong, "Assessing the Impact of SiC MOSFETs on Converter Interfaces for Distributed Energy

Resources," in *Industry Applications Conference, 2007. 42nd IAS Annual Meeting. Conference Record of the 2007 IEEE*, 2007, pp. 336-341.
[62] M. Savaghebi, A. Jalilian, J. C. Vasquez, and J. M. Guerrero, "Selective compensation of voltage harmonics in an islanded microgrid," in *Power Electronics, Drive Systems and Technologies Conference (PEDSTC), 2011 2nd*, 2011, pp. 279-285.
[63] L. Tzung-Lin, L. Chia-Tse, and P. T. Cheng, "An autonomous harmonic filtering strategy for distributed energy resources converters in microgrid," in *Power Electronics Conference, 2009. COBEP '09. Brazilian*, 2009, pp. 19-25.
[64] R. M. Moreno, J. A. Pomilio, L. C. P. da Silva, and S. P. Pimentel, "Mitigation of harmonic distortion by power electronic interface connecting distributed generation sources to a weak grid," in *Power Electronics Conference, 2009. COBEP '09. Brazilian*, 2009, pp. 41-48.
[65] K. Sung-Hun, S. R. Lee, H. Dehbonei, and C. V. Nayar, "Application of voltage- and current-controlled voltage source inverters for distributed generation systems," *Energy Conversion, IEEE Transactions on*, vol. 21, pp. 782-792, 2006.
[66] Y. P. a. H. Hosseinzadeh, "Comparison of Voltage Control and Current Control Methods in Grid Connected Inverters," *Journal of Applied Sciences*, vol. 8, pp. 648-653, 2008.
[67] A. J. von Appen, B. C. Marnay, C. M. Stadler, D. I. Momber, E. D. Klapp, and F. A. von Scheven, "Assessment of the economic potential of microgrids for reactive power supply," in *Power Electronics and ECCE Asia (ICPE & ECCE), 2011 IEEE 8th International Conference on*, 2011, pp. 809-816.
[68] H. Asano and S. Bando, "Economic evaluation of microgrids," in *Power and Energy Society General Meeting - Conversion and Delivery of Electrical Energy in the 21st Century, 2008 IEEE*, 2008, pp. 1-6.
[69] A. G. Madureira and J. A. Peças Lopes, "Ancillary services market framework for voltage control in distribution networks with microgrids," *Electric Power Systems Research*, vol. 86, pp. 1-7, 2012.
[70] A. Kargarian, B. Falahati, and F. Yong, "Stochastic active and reactive power dispatch in electricity markets with wind power volatility," in *Power and Energy Society General Meeting, 2012 IEEE*, 2012, pp. 1-7.
[71] E. Ela, B. Kirby, N. Navid, and J. C. Smith, "Effective ancillary services market designs on high wind power penetration systems," in *Power and Energy Society General Meeting, 2012 IEEE*, 2012, pp. 1-8.
[72] H. S. Rauschenbach. (1980). *Solar cell array design handbook : the principles and technology of photovoltaic energy conversion*.
[73] R. A. Messenger. (2010). *Photovoltaic systems engineering (3rd ed.)*.
[74] M. G. Villalva, J. R. Gazoli, and E. R. Filho, "Comprehensive Approach to Modeling and Simulation of Photovoltaic Arrays," *Power Electronics, IEEE Transactions on*, vol. 24, pp. 1198-1208, 2009.
[75] M. A. Vitorino, L. V. Hartmann, A. M. N. Lima, and M. B. R. Correa, "Using the model of the solar cell for determining the maximum power point of photovoltaic

systems," in *Power Electronics and Applications, 2007 European Conference on*, 2007, pp. 1-10.

[76] J. A. Gow and C. D. Manning, "Development of a model for photovoltaic arrays suitable for use in simulation studies of solar energy conversion systems," in *Power Electronics and Variable Speed Drives, 1996. Sixth International Conference on (Conf. Publ. No. 429)*, 1996, pp. 69-74.

[77] L. M. T. Y.Xu, J.N. Chiasson, F.Z. Peng, J.B. Campbell, "Generalized instantaneous nonactive power theory for STATCOM," *IET Electric Power Applications*, vol. 1, pp. 853-861, 2007.

[78] H. Chihchiang and S. Chihming, "Study of maximum power tracking techniques and control of DC/DC converters for photovoltaic power system," in *Power Electronics Specialists Conference, 1998. PESC 98 Record. 29th Annual IEEE*, 1998, pp. 86-93 vol.1.

[79] J. L. Santos, F. Antunes, A. Chehab, and C. Cruz, "A maximum power point tracker for PV systems using a high performance boost converter," *Solar Energy*, vol. 80, pp. 772-778, 2006.

[80] X. Liu and L. A. C. Lopes, "An improved perturbation and observation maximum power point tracking algorithm for PV arrays," in *Power Electronics Specialists Conference, 2004. PESC 04. 2004 IEEE 35th Annual*, 2004, pp. 2005-2010 Vol.3.

[81] T. Tafticht, K. Agbossou, M. L. Doumbia, and A. Chériti, "An improved maximum power point tracking method for photovoltaic systems," *Renewable Energy*, vol. 33, pp. 1508-1516, 2008.

[82] O. T. a. L. A. Dessaint, "Experimental Validation of a Battery Dynamic Model for EV Applications," *World Electric Vehicle Journal*, vol. 3, 2009.

[83] Y. X. S. Adhikari, F. Li, et. al, "Utility-Side Voltage and PQ Control with Inverter-based Photovoltaic Systems," presented at the 18th World Congress of International Federation of Automatic control (IFAC), Milan, Italy, August 28-Sept. 2, 2011, 2011.

APPENDIX

PUBLICATIONS DURING PHD STUDY

Journal:

[1] Huijuan Li, Fangxing Li, Yan Xu, D. Tom Rizy, and **Sarina Adhikari**, "Autonomous and Adaptive Voltage Control using Multiple Distributed Energy Resources," *IEEE Transactions on Power Systems*, accepted, 2012.

[2] Fangxing Li, Yanli Wei, and **Sarina Adhikari**, "Improving an Unjustified Common Practice in Ex Post LMP Calculation," *IEEE Transactions on Power Systems*, vol. 25, no. 2, pp. 1195-1197, May 2010.

[3] **Sarina Adhikari**, Fangxing Li, Yan Xu, and Huijuan Li, "PQ and PV Control of photovoltaic generator in three-phase distribution system": submitted to *IEEE Transactions on Power Systems (under revision).*

[4] **Sarina Adhikari** and Fangxing Li, "Coordinated V-f and P-Q Control of Solar Photovoltaic Generators with MPPT and Battery Storage in Microgrids," submitted to *IEEE Transactions on Smart Grid (under revision).*

Book Chapter:

[5] Fangxing Li, Pei Zhang, **Sarina Adhikari**, Yanli Wei, Qinran Hu, "Vision of Future Control Centers in Smart Grids," *Smart Grid Infrastructure & Networking*, McGraw-Hill Professional, ISBN-10: 0071787747, June 2012.

Conference:

[6] Philip Irminger, D. Tom Rizy, Huijuan Li, Travis Smith, Keith Rice, Fangxing Li, **Sarina Adhikari**, "Air Conditioning Stall Phenomenon – Testing, Model Development, and Simulation," IEEE PES T&D Conf. and Expo. 2012, Orlando, FL, May 7-10, 2012.

[7] Huijuan Li, Yan Xu, **Sarina Adhikari**, D. Tom Rizy, Fangxing Li, Philip Irminger, "Real and Reactive Power Control of a Three-Phase Single-Stage PV System and PV Voltage Stability," IEEE PES General Meeting 2012, San Diego, CA, July 22-26, 2012.

[8] **Sarina Adhikari**, Fangxing Li, Qinran Hu, and Zhenyuan Wang, "Heuristic optimal restoration based on constructive algorithms for future smart grids," *16th International Conference on Intelligent System Application to Power Systems (ISAP)*, Crete, Greece, Sept. 25-28, 2011.

[9] **Sarina Adhikari**, Yan Xu, Fangxing Li, et al, "Utility-Side Voltage and PQ Control with Inverter-based Photovoltaic Systems," *18th World Congress of International Federation of Automatic Control (IFAC),* Milan, Italy, August 28 - Sept. 2, 2011.

[10] D. Tom Rizy, Huijuan Li, Fangxing Li, Yan Xu, **Sarina Adhikari,** "Impacts of Varying Penetration of Distributed Resources with & without Volt/Var Control: Case Study of Varying Load Types," *IEEE PES General Meeting 2011,* Detroit, MI, July 24-29, 2011.

[11] Fangxing Li, Yanli Wei, and **Sarina Adhikari**, "Improving an Unjustified Common Practice in Ex Post LMP Calculation: An Expanded Version," *IEEE PES General Meeting 2010*, Minneapolis, MN, July 25-29, 2010.

[12] D. Tom Rizy, Fangxing Li, Huijuan Li, **Sarina Adhikari**, John D. Kueck, "Properly Understanding the Impacts of Distributed Resources on Distribution Systems," *IEEE PES General Meeting 2010*, Minneapolis, MN, July 25-29, 2010.

[13] Huijuan Li, Fangxing Li, **Sarina Adhikari**, Yan Xu, D. Tom Rizy, and John D. Kueck, "An Adaptive Voltage Control Algorithm with Multiple Distributed

Energy Resources," *North American Power Symposium (NAPS) 2009*, Starkville, MS, October 04-06, 2009.

[14] **Sarina Adhikari**, Fangxing Li, and Zhenyuan Wang, "Online Restoration for Distribution Automation using Constructive Back-Feed Algorithm," *(invited panel paper) IEEE PES General Meeting 2009,* Calgary, Canada, July 26-30, 2009.

[15] Ming Chen, Clinton Nolan, Xiaorui Wang, **Sarina Adhikari**, Fangxing Li, Hairong Qi, "Hierarchical Utilization Control for Real-Time and Resilient Power Grid," *21st Euromicro Conference on Real-Time Systems (ECRTS 09),* Dublin, Ireland, July 1-3, 2009.

[16] **Sarina Adhikari**, Fangxing Li, Huijuan Li, Yan Xu, John D. Kueck, and D. Tom Rizy, "Modeling Stalled Induction Motors with Voltage-Regulating Distributed Energy Resources," *PowerTech Conference 2009,* Bucharest, Romania, June 28-July 02, 2009.

[17] Arif Karakas, Fangxing Li and **Sarina Adhikari**, "Aggregation of Multiple Induction Motors using MATLAB-based Software Package," *IEEE PES Power Systems Conf. and Expo. (PSCE) 2009*, Seattle, WA, March 15-18, 2009.

Technical Reports:

[18] John Kueck, Tom Rizy, Fangxing Li, Yan Xu, Huijuan Li, **Sarina Adhikari**, and Phil Irminger, *Local Dynamic Reactive Power for Correction of System Voltage Problems*, DOE Technical Report, Oak Ridge, TN, November 2008.

VITA

Sarina Adhikari joined University of Tennessee at Knoxville in January 2008 for a PhD degree in Electrical Engineering. She completed her Bachelor's degree in Electrical Engineering from Institute of Engineering (IOE), Pulchowk, Lalitpur, Nepal and her Master's degree with a major in Electric Power System Management from Asian Institute of Technology (AIT), Pathumthani, Thailand in December 2005. She worked as a Research Associate in Renewable energy based project at AIT for two years after completion of her Master's degree. Her current research interests include Distributed energy resources (DERs) integration to the power systems, Solar Photovoltaic (PhV) integration in microgrids and inverter/converter controls.